



DIPLOMARBEIT

High-Dosage Neutron Dosimetry with TLDs

Study of the thermoluminescence properties and the tritium build-up effect in
 ${}^6\text{LiF}(\text{Mg,Ti})$ dosimeters as a result of irradiation with high neutron dosages in a
TRIGA Mark II reactor

Ausgeführt am

Atominstitut

der Technischen Universität Wien

unter der Anleitung von

Betreuung: Ao.Univ.Prof. Dipl.-Ing. Dr.techn. Christina Strelj

Mitwirkung: Ing. Manfred Fugger

Dipl.-Ing. Dr. Andreas Musilek

Dipl.-Ing. Dr. Johannes Sterba

durch

Eva Maria Lindner, BSc

Elterleinplatz 1/9a, 1170 Wien

Wien, 11.09.2014

(Unterschrift Verfasserin)

MASTER'S THESIS

High-Dosage Neutron Dosimetry with TLDs

Study of the thermoluminescence properties and the tritium build-up effect in ${}^6\text{LiF}(\text{Mg,Ti})$ dosimeters as a result of irradiation with high neutron dosages in a TRIGA Mark II reactor

Undertaken at the
Institute for Atomic and Subatomic Physics
at Vienna University of Technology

under the supervision of

Advisor: Ao.Univ.Prof. Dipl.-Ing. Dr.techn. Christina Strelt
Assistance: Ing. Manfred Fugger
Dipl.-Ing. Dr. Andreas Musilek
Dipl.-Ing. Dr. Johannes Sterba

by

Eva Maria Lindner, BSc
Elterleinplatz 1/9a, 1170 Wien

Abstract

The aim of this study was to investigate the performance of LiF(Mg,Ti) dosimeters during high-dosage neutron measurements in the mixed radiation field within the TRIGA Mark-II research reactor at the Institute of Atomic and Subatomic Physics, Vienna. For this purpose both TLD-600 (^6LiF) and TLD-700(^7LiF) chips were irradiated within the reactor at different powers and for different irradiation times. In subsequent thermoluminescence (TL) measurements first the primary TL signal acquired directly after irradiation was studied. Next the secondary TL signal (tritium build-up) caused by self-irradiation of the chips through tritium produced within the TLD-600 dosimeters during irradiation ($^7\text{Li}(n,\alpha)^3\text{H}$) was measured at weekly intervals. Finally some of the TLD-600 chips were dissolved and measured in a liquid scintillation analyser.

Due to a variety of correction factors (supra-linearity, saturation effects, sensitivity loss etc) needed to account for the high dosages within the reactor, it was clear that this would be a very complex task. Therefore the main aim of this thesis was to test and find the limits of thermoluminescence dosimetry in the radiation field of the reactor through the use of these three measurement methods. In addition we aimed to find a correlation between the results of all three techniques.

Only inconclusive results were found for the (primary) net neutron TL-signal as the high dosages within the reactor were mostly outside of the dosimeter's linear response range. The secondary TL-signal - the tritium build-up - was found to stay relatively stable over the course of several weeks. A good relationship between the tritium build-up and the reactor power was found between 1 and 10 kW. At higher reactor powers the tritium build-up showed a deviation from the expected results. In LSC measurements annealed dosimeters also showed a remarkable correlation with the tritium build-up. A comparison of the tritium activities within non-annealed dosimeters showed that only about 13 % of the calculated activity was actually measured. One possible reason for this could be the loss of tritium during the chemical dissolution of the dosimeters. Furthermore the neutron flux on which our calculations were based could have been too high as a result of a recent change in the reactor core configuration. At the time of this work measurements of the neutron flux at different irradiation positions within the reactor were still under way.

Kurzfassung

Das Ziel dieser Diplomarbeit war es die Messeigenschaften von LiF(Mg,Ti) Thermolumineszenz(TL)-Dosimetern für Hochdosis-Neutronenmessungen im gemischten Strahlenfeld des TRIGA Mark-II Forschungsreaktors am Atominstitut Wien zu untersuchen. Zu diesem Zweck wurden sowohl TLD-600 (^6LiF) als auch TLD-700 (^7LiF) Thermolumineszenz-Chips bei verschiedenen Reaktorleistungen und mit unterschiedlichen Bestrahlungszeiten im TRIGA Mark-II bestrahlt.

Mit der ersten Thermolumineszenz-Messung nach der Bestrahlung wurde der primäre TL-Messeffekt untersucht. Danach wurde wöchentlich der sekundäre TL-Messeffekt (Tritium-Build-up) gemessen, welcher durch die Betastrahlung von Tritium in TLD-600 Dosimetern entsteht. Tritium wird während der Neutronenbestrahlung im Reaktor durch $^6\text{Li} (n,\alpha)^3\text{H}$ Reaktionen produziert. Schließlich wurden noch einige der TLD-600 Chips chemisch aufgelöst und mit Hilfe von Flüssigszintillation gemessen.

Aufgrund von verschiedensten Korrekturfaktoren (Supralinearitäten, Sättigung, Empfindlichkeitsverluste, etc), die für den Hochdosis-Bereich angewendet werden mussten, war klar, dass dies eine sehr komplexe Aufgabe sein würde. Daher war das Hauptziel dieser Diplomarbeit, die Grenzen der Thermolumineszenz-Dosimetrie im Strahlenfeld des Reaktors durch die Anwendung dieser drei Methoden auszutesten. Darüber hinaus sollte auch eine Korrelation zwischen der Neutronenfluenz im Reaktor und den Messergebnissen der drei Methoden gefunden werden.

Die Messung des (primären) Netto-Neutronen TL-Messeffekts lieferte keine eindeutigen Ergebnisse, da die Dosimeter mit Dosen weit außerhalb ihres linearen Ansprechverhaltens bestrahlt wurden. Die durch Neutronenbestrahlung hervorgerufene Eigenaktivität der Dosimeter bewirkte den sekundären TL-Messeffekt (Tritium-Build-up), welcher auch nach wiederholtem Tempern relativ stabil blieb – nur ein leichter Abwärtstrend war über mehrere Wochen hinweg erkennbar. Eine gute Korrelation des Tritium-Build-ups mit der Reaktorleistung konnte nur im Bereich von 1 bis 10 kW gefunden werden. Bei höheren Reaktorleistungen wurde eine Abweichung vom Erwartungswert festgestellt. Ein unerwartet guter Zusammenhang wurde zwischen dem Tritium-Build-up und der in der Flüssigszintillation gemessenen Tritiumaktivität von getemperten Dosimetern gefunden. Beim Vergleich der mit Flüssigszintillation gemessenen Tritiumaktivitäten mit

den berechneten Werten wurde jedoch festgestellt, dass nur ca. 13 % der erwarteten Aktivität auch tatsächlich gemessen wurde. Dies war ein Hinweis, dass, abhängig von der chemischen Prozedur des AuflöSENS und der Probenaufbereitung, ein gewisser Teil an Tritium verloren geht. WeitERS gab es aufgrund der Neukonfiguration des Reaktor-kerns eine Unsicherheit bei der Neutronenfluenz, die für die Berechnungen herangezogen wurde. Die Vermessung der Neutronenflüsse an den verschiedenen Bestrahlungspositionen am Reaktor war zum Zeitpunkt dieser Arbeit Gegenstand diverser Projekte.

Danksagung

Zuallererst möchte ich mich bei Manfred Fugger bedanken, der diese Diplomarbeit vorgeschlagen und ermöglicht hat. Vielen, vielen Dank für deine ausführlichen Erklärungen, die Unterstützung bei der Organisation der Bestrahlungen und der Messdurchführung, die vielen aufschlussreichen Diskussionen und deine konstruktive Kritik, was den Inhalt dieser Diplomarbeit anging. Ohne dich wäre diese Arbeit nicht möglich gewesen! Danke!

Ein großes Dankeschön gebührt auch Frau Professor Christina Streli, für die laufende Betreuung während der letzten Monate und die Verbesserung meiner Diplomarbeit in Rekordzeit.

Weiters möchte ich mich bei Andreas Musilek für die Vermittlung der Diplomarbeit, das Interesse an deren Fortschritt und die vielen lustigen und hilfreichen Gespräche bedanken. Vielen Dank auch an Johannes Sterba für die Bedienung der schnellen Rohrpost während unserer Bestrahlungen und die Hilfe mit der Flüssigszintillation und der Berechnung der Neutronenaktivierung. Ein großes Dankeschön geht auch an Jan Welch für die tatkräftige Unterstützung im Chemielabor beim Auflösen meiner Dosimeter. Auch bei Michaela Foster, die immer für Fragen im Chemielabor zur Verfügung stand, möchte ich mich bedanken. Zuguterletzt möchte ich mich bei den Herren der Reaktorleitung Mario Villa, Robert Bergmann und Ernst Klapfer für ihre Flexibilität und die Überstunden beim Stufenbetrieb des Reaktors bis zum 'Badeschluss' bedanken.

In addition I would also like to thank Beata Ostachowicz and her colleagues from the AGH University of Science and Technology in Kraków for their help with the chemical dissolution of our dosimeters. Special thanks also go to Wladyslaw Pohorecki at the AGH who very patiently answered all my questions regarding neutron activation.

Das größte Dankeschön gilt natürlich meinen Eltern, die mir das Studium ermöglicht haben und mich bei meinen vielen Reisen und außeruniversitären Aktivitäten immer geduldig unterstützt haben. Meinem Bruder Simon möchte ich dafür danken, dass er mich schon in jungen Jahren für die Wissenschaft begeistert hat und dadurch einen

großen Teil dazu beigetragen hat, wer und was ich heute bin. Und 'last but not least' möchte ich mich bei Kieran Leschinski für die allumfassende Unterstützung während der letzten Wochen und Monate bedanken - Tara-chans!

Contents

Abstract	i
Kurzfassung	iii
Danksagung	v
Contents	vii
1 Introduction	1
1.1 Motivation	1
1.2 Literature Review	2
1.3 Aim of this study	5
2 Theoretical Background	7
2.1 Radio-Luminescence	7
2.2 Thermoluminescence	10
2.2.1 Physical Background	10
Energy Bands	10
Localised Levels and Crystallographic Defects	12
Traps and Recombination Centres	13
A simple theoretical model	16
2.2.2 Thermoluminescence Dosimetry	19
Glow Curve Structure, Thermal Fading and LET-Dependence	19
Reference Measurements - Calibration	21
Non-Linearity Effects	24
Annealing Procedure	24
TLD Materials	25
Practical Applications	25
2.3 Liquid Scintillation	26
2.4 Neutron Radiation	27
2.4.1 Neutron Sources and Neutron Spectrum	28
	vii

2.4.2	Neutron Interactions	29
	Neutron Cross Sections	29
	Types of Interactions	29
2.4.3	Neutron Detection with TLDs - Pair Method	30
2.4.4	Neutron Activation Analysis	32
3	Method	33
3.1	Instrumentation	33
3.1.1	Irradiation	33
	TRIGA Mark-II, Vienna	34
	Fast Pneumatic Transfer System	36
3.1.2	Thermoluminescence Dosimetry	38
	Thermoluminescence Dosimeters	38
	Read-out device - TL DAT-III	39
	Annealing Oven	43
3.1.3	Liquid Scintillation Counting	44
	Chemical dissolution of TL-dosimeters	44
	Liquid Scintillation Counter	46
3.2	Calibration	46
3.2.1	Thermoluminescence Dosimeters	46
3.2.2	Liquid Scintillation Counting	48
3.3	Data Analysis	50
3.3.1	Thermoluminescence Read-out	50
	Black Body Background and Photomultiplier Noise	51
	The Filter Attenuation Factor	52
	Non-linearity Effects	54
3.3.2	LSC Measurement - Estimate of Tritium Activity	61
4	Results and Discussion	63
4.1	Primary TL Measurement	64
4.1.1	Correlation with irradiation time	64
4.1.2	Correlation with reactor power	66
4.2	Secondary TL Measurement - Tritium Build-Up	69
4.2.1	Correlation with irradiation time	69
4.2.2	Correlation with reactor power	71
4.3	LSC Measurement	74
4.3.1	Comparison with predicted tritium activity	75
4.3.2	Comparison between non-annealed and annealed dosimeters	76
4.3.3	Correlation between the LSC and tritium build-up measurements	78
5	Summary and Future Outlook	81

Bibliography	87
Appendices	90
A	91
A.1 Technical Data - TRIGA Mark-II, ATI Vienna	91
A.2 TLD Calibration Data	94
A.2.1 TLD Set No. 1	94
A.2.2 TLD Set No. 2	96

Introduction

1.1 Motivation

Thermoluminescence dosimetry of neutron radiation is especially challenging inside mixed radiation fields of high intensity like those found in nuclear reactors. Many different factors have an impact on the signal read out from thermoluminescence (TL) dosimeters exposed to such a radiation field. These include non-linearity and saturation effects in the thermoluminescence signal as well as the superposition of both gamma and neutron induced measurement effects. As a result of high dosages TL dosimeters may experience persistent radiation damage. Therefore the dosimeters need to be continuously monitored with reference measurements to correct for this effect. In addition the strong light intensities caused by high-dosage radiation push the limits of the electronics within the thermoluminescence measurement device.

A research project previously carried out by Marko Mayr for his bachelor thesis dealt with non-linearity effects that occur in the signal structure of TLD-700 thermoluminescence dosimeters made from ${}^7\text{LiF}(\text{Mg},\text{Ti})$ after exposure to high-dosage gamma radiation [12]. These effects are generally well known - the aim of this project, however, was to reconfirm the effect for a particular charge of dosimeters with slightly altered attributes taken from the MATROSHKA and RADIS projects. As part of this work both TLD-600 made from ${}^6\text{LiF}(\text{Mg},\text{Ti})$ and TLD-700 dosimeters were irradiated to obtain dosage measurements from inside the TRIGA Mark-II nuclear research reactor at the

Institute of Atomic and Subatomic Physics of Vienna University of Technology. Due to the high neutron fluxes and gamma radiation levels within the reactor the results obtained from the primary thermoluminescence (TL) signal were inconclusive.

Thus, we decided to have a more detailed look at thermoluminescence dosimetry in high-intensity gamma and neutron radiation fields. We wanted to test the limits of this measurement technique by studying both primary and secondary effects after irradiation of LiF(Mg,Ti) dosimeters at different neutron fluences within the reactor. Apart from the non-linearity effects in the primary measurement of the TL signal tritium atoms are also produced within the dosimeter material via the $\text{Li}^6(\text{n},\alpha)\text{T}^3$ reaction. Since the half-life of tritium is approximately 12.3 years the TLD-600 dosimeters become radioactive for a long period of time. Due to this self-irradiation of the dosimeters the so called tritium build-up can be observed as a secondary effect caused by the β^- decay of tritium within the dosimeter material.

As the thermoluminescence measurement of this combination of high dosage radiation had not been previously studied at our institute a thorough literature review was done to assess what current research had to say about this topic and to see which direction our research should take. As a result we aimed to find a correlation between the three different neutron detection methods presented in the next two sections. In addition we also wanted to find an estimate for the neutron fluence-dependent limits of these measurement techniques.

1.2 Literature Review

Non-linearity effects due to high dosages of gamma radiation have long been studied for all different kinds of thermoluminescence dosimeters. The non-linearity reduces the ability to calculate accurate dosages from the TL-signal. Furthermore the exposure to high dosages of radiation has a long term impact on a dosimeter's properties as its sensitivity changes. These problems have already been addressed in the literature numerous times and will thus be discussed in section 2.2.2 of this thesis' theory chapter.

Every TL-dosimeter accumulates a certain amount of natural background radiation which can be easily accounted for. Neutron radiation, however, causes the production of tri-

trium within the dosimeter material. The β^- radiation from decaying tritium adds to the natural background and can have a significant long-term impact on dosimeter measurements. This phenomenon of self-irradiation apparent in the thermoluminescence read-out is called 'tritium build-up'. Especially in the case where TLD-600 dosimeters are used for the radiation exposure monitoring of personnel. Here it may lead to an artificial increase in a person's accumulated long-term dosage. Thus the limit for when the tritium build-up has an actual impact on a person's dosimetry reading must be found. This limit varies between different TL-dosimeter types and has been the topic of numerous publications. In an article by Romanyukha et.al concerning ${}^6\text{LiF:Mg,Cu,P}$ (TLD-600H) dosimeters 'the maximum neutron dose limit for the reuse of the TLD-600H was estimated to be 0.11 Gy for dosimeters exposed to reactor generated neutrons' [22]. Burgkhardt and Piesch found this value to be about 100-200 times higher for the TLD-600(${}^6\text{LiF:Mg,Ti}$) dosimeters used in this thesis [5].

Much of the literature on the tritium build up concerns itself with this effect. It is, however, not part of our particular area of research.

A further review of the available literature showed that the tritium build-up has mainly been studied in the context of fusion reactors like ITER(International Thermonuclear Experimental Reactor). The ITER is an experimental fusion reactor of the Tokamak type with a magnetic confinement in a doughnut shaped vacuum container, where fusion reactions with deuterium and tritium in plasma form take place. As a result of this reaction neutrons are also released:



The necessary strong magnetic fields are produced with a combination of superconducting coils surrounding the vessel and an electric current through plasma. While there is an almost unlimited supply of deuterium, tritium must be bred to obtain a sufficient number of atoms. This tritium self-sufficiency is obtained through a breeding process with Li contained within the reactor blanket, taking advantage of the following two reactions: ${}^6\text{Li}(\text{n},\alpha)\text{T}$ and ${}^7\text{Li}(\text{n},\text{n}'\alpha)\text{T}$.

In this context the tritium build-up can be used to obtain a measure of the tritium production within the reactor blanket. The thermoluminescence signal from this build-up,

however, does not give an absolute value for the amount of tritium contained within the dosimeter. Therefore a technique first proposed by Dierckx [7] is used for calibrating the observed tritium build-up through liquid scintillation counting (LSC) of the dissolved TL-dosimeters. This way an absolute tritium activity measurement can be correlated with the relative thermoluminescence signal. In their article Pohorecki et al. describe how they implemented this method [17]. The horizontal channel of the thermal column of a research reactor was used to only irradiate the TL-dosimeters with thermal neutrons. After a special dissolution procedure the dosimeters were measured in a liquid scintillation counter. For the MTS-N dosimeters (LiF:Mg,Ti - with natural abundance of lithium: 7.6% ^6Li , 92.4% ^7Li) used in this experiment a good correlation was found between the tritium activity measured by LSC [Bq/mg] and the observed tritium build-up signal [mGy/h].

In 1976 McKlveen and Schwenk used ^6LiF and ^7LiF dosimeters to determine the neutron flux within a sub-critical reactor and a TRIGA reactor. They were able to obtain accurate measurements for thermal neutron fluxes between 10^2 and $10^{12}\text{n cm}^{-2}\text{s}^{-1}$ [14]. In their study they compared their thermoluminescence measurements to results from BF_3 detection, foil activation and fission chambers. This enabled them to calculate an empirical exposure rate to flux conversion factor. They were not able to obtain conclusive results for higher neutron fluxes as the TL read-outs became increasingly unreliable in that range.

Another study done by Torkzadeh and Manouchehri tried to correlate the neutron flux within a nuclear research reactor with the tritium build-up measured after annealing of the dosimeters [25]. Bare and cadmium covered TLD-600 dosimeters were used to get a measure of both the thermal and epithermal neutron fluence (only epithermal neutrons can overcome the cadmium layer).

After irradiation within the reactor core at thermal neutron fluences between $2.25 \cdot 10^{11}$ and $2.25 \cdot 10^{13}\text{n cm}^{-2}$ an almost linear dependence between the thermal fluence and the TL read-out of the tritium build-up was found. Comparing the TL readout of the bare dosimeters with the cadmium covered ones showed that the ratio between them stayed the same at all fluences. This method can, however, only be used for obtaining a correlation when the thermal neutron flux within the reactor is known in detail.

1.3 Aim of this study

None of the techniques mentioned in the previous section have been implemented for the purpose of dosage measurement within the TRIGA Mark-II nuclear research reactor at the Institute for Atomic and Subatomic Physics, Vienna.

First of all we aimed to reproduce and test the limits of the method used by McKlveen and Schwenk in 1976, where TLD-600 and TLD-700 dosimeters were used to analyse the **primary TL-signal** after irradiation within the reactor [14]. It should be noted, however, that the authors only mentioned neutron fluxes but did not state any exact irradiation times. As a result the neutron fluence is unknown and exact comparisons of their results with ours were not possible. We planned to expand on this method by also investigating the secondary TL-signal caused by the tritium build-up.

Therefore in addition, we aimed to implement a method similar to the one outlined in the article by Torkzadeh and Manouchehri, where the **tritium build-up** was used as **a measure of the thermal neutron flux** the dosimeters had been exposed to. In our study we only used the bare ${}^6\text{LiF:Mg,Ti}$ dosimeters, though, as we were not interested in the epithermal part of the spectrum. Furthermore, as opposed to their study we did not irradiate our samples within the core of the reactor where the neutron flux is well known, rather, we used the fast pneumatic transfer system to transport our dosimeters into the reactor. However, the exact neutron flux at the position of the transport system was not known for certain. Thus, a method for the calibration of the tritium build-up induced TL-signal was necessary. This brought us to the third part of our experiment.

To be able to quantify the TL signal gained from the tritium build-up, thirdly, we aimed to implement the **LSC calibration technique** described by Pohorecki et al. Using a similar chemical procedure the dosimeters were dissolved and afterwards measured in a liquid scintillation counter. By doing so, we obtained an absolute value for the tritium activity within the dosimeters.

Combining all three of these methods we aimed to find an empirical correlation between the actual tritium activity, the tritium build-up, the primary TL-signal and the thermal neutron fluence within the TRIGA Mark-II at our institute. After reviewing the

literature we found no examples of all three of these methods having ever been implemented at once. Hence we intended to test these techniques at different thermal reactor powers and times to verify that the relationship between the neutron fluence, the primary TL-signal, the TL signal of the tritium build-up and the tritium activity measured with LSC is linear.

To summarise: the three main methods that were implemented to measure the high-dosage neutron flux within the TRIGA Mark-II were:

1. Analysis of the **primary neutron induced TL-signal** obtained through measurement of both TLD-600 ($\gamma + n$ component) and TLD-700 (only γ component). The net neutron signal obtained with this method was expected to be proportional to the neutron flux within the reactor. By exposing the dosimeters to different neutron fluences and irradiation times we wanted to find the limits of this technique.
2. Analysis of the **secondary TL-signal(tritium build-up)** induced by the β^- radiation of the tritium atoms produced within the TLD-600 dosimeter material. This signal was also expected to be proportional to the neutron flux within the reactor.
3. Measurement of the **absolute tritium activity** within the TLD-600 dosimeters through **liquid scintillation counting**. This measurement was meant to give us a quantitative value to which both method 1 and 2 could be correlated.

Theoretical Background

The first section of this thesis aims to give an overview of the basic physical concepts underlying the methods and phenomena discussed in later sections.

Firstly we give an introduction to radio-luminescence - the basic physical phenomenon upon which both detectors we used rely. Next a detailed description of both thermoluminescence and liquid scintillation is given. In section 2.4 we discuss different neutron interactions as well as the possibility of detecting neutrons with certain types of thermoluminescence dosimeters. In the following section tritium production within the thermoluminescence dosimeter material is presented as one of the side effects induced by neutron irradiation. Direct and indirect Tritium detection methods with both TLDs and LSC is explained as well.

2.1 Radio-Luminescence

Thermoluminescence Dosimeters (TLD) as well as a Liquid Scintillation Counter (LSC) were used for data acquisition in this thesis. Both detection systems belong to the group of luminescence detectors. In this first part of the theory section the basic physics behind these detectors is introduced and their main differences is explained.

When energy is absorbed by an atom and electrons are excited to a higher energy state, light can be observed when the electrons relax and fall back into their ground states.

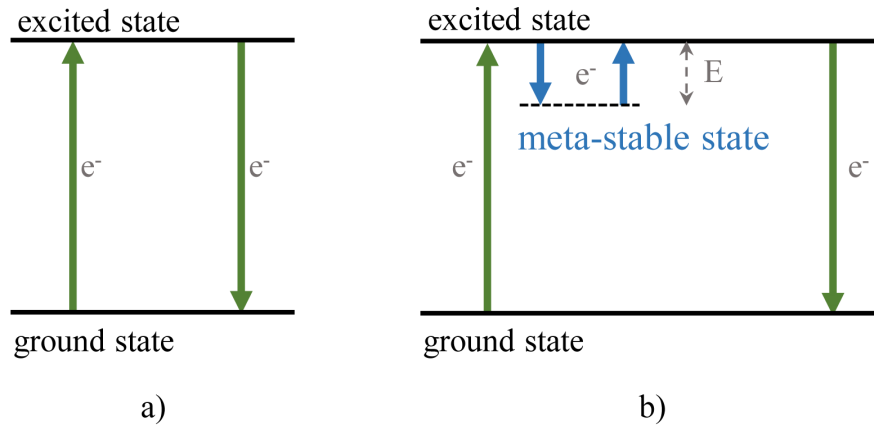


Figure 2.1: Energy transitions that cause a) fluorescence and b) phosphorescence, where E is the energy an electron requires to escape the meta-stable energy state

This phenomenon is called luminescence. Luminescence should not be confused with incandescence, which is the light emitted from a hot body due to its temperature as opposed to the absorption of external energy. Different types of luminescence can be distinguished by their causes and by the time it takes for the absorbed energy to be re-emitted as light. Among the causes for luminescence are chemical reactions, electric currents, sound as well as the absorption of photons, mechanical energy and ionising radiation. Accordingly, they are named chemi-, electro-, sono-, photo-, mechano- and radio-luminescence.

Another important distinguishing characteristic is time. Depending on the time difference, τ , between the absorption of energy and its re-emission in the form of light either fluorescence ($\tau < 10^{-8}$ s) or phosphorescence ($\tau > 10^{-8}$ s) is observed. Phosphorescence can be explained through the existence of meta-stable energy states, which lie between the ground and the excited level (see figure 2.1). These meta-stable states can trap electrons and will only release them after a time τ has passed. Thermodynamically this can be described by

$$\tau = s^{-1} \exp(E/kT) \quad (2.1)$$

where k is Boltzmann's constant, T is temperature, s is a constant and E is the trap depth - the difference between the energies of the meta-stable and the excited state. Thus, for phosphorescence the time τ is dependent on temperature, which also leads to

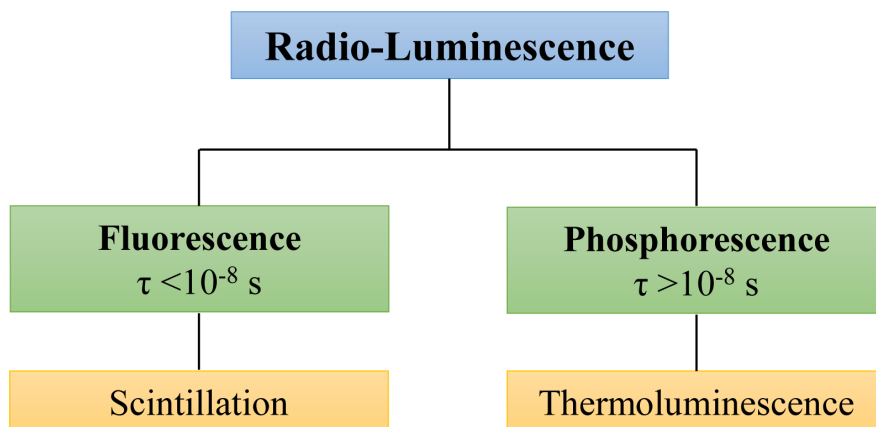


Figure 2.2: The different types of radioluminescence may be distinguished by the time τ that passes between the irradiation and the emission of light

the phenomenon of Thermoluminescence.

Thermoluminescence belongs to the group of long period phosphorescence with τ ranging from a few minutes to 4.6×10^9 years - the age of our solar system [13]. Just from looking at the mentioned time scales it is obvious that this process must be heavily reliant on temperature. Thermoluminescence dosimetry takes advantage of this fact. A measurement of the absorbed radiation is obtained by heating up the dosimeter. This is possible even if a long time has passed since the material was exposed to radiation (see section 2.2.2). Scintillation on the other hand belongs to the group of fluorescent processes. Light is emitted within 10^{-8} s after the absorption of ionising radiation and cannot be observed when the source of the radiation is removed.

As only scintillation and thermoluminescence are of importance in the context of this thesis, figure 2.2 only shows where these two types of radiation induced luminescence are located in the overall picture.

Therefore the main difference between scintillation and thermoluminescence is the time τ at which light is emitted. While a radioactive source must be present to be able to observe scintillation, thermoluminescence can be observed a long time after exposure by simply heating up the dosimeter.

2.2 Thermoluminescence

The 17th-century natural philosopher, chemist, physicist and inventor Robert Boyle was probably the first person to write down a scientific record on the observation of thermoluminescence. He described a diamond that would glow faintly when ‘placed upon a warm part of his naked body’ [4]. What Boyle observed was the accumulated natural background radiation which the diamond had absorbed.

The first researchers to artificially induce thermoluminescence were Trowbridge and Burbank in 1898 [26]. They first ‘cleared’ fluorite of natural thermoluminescence by heating it and then exposed that same fluorite crystal to radiation in the x-ray part of the spectrum.

The effect was also described by Marie Curie in her doctoral thesis on ‘Radio-active Substances’. She explained that ‘certain bodies, such as fluorite, become luminous when heated; they are thermo-luminescent.’ [11] Her work raised interest in that particular field of research and led to many subsequent publications on the topic of radioactivity induced thermoluminescence.

2.2.1 Physical Background

To better understand thermoluminescence and its underlying physical concepts this section outlines the basic physics behind the band structure of crystalline materials and the impact of traps and recombination centres on their radiative/photon emitting properties.

Energy Bands

The electrons of a crystalline material, such as the materials used for thermoluminescence dosimeters, are under the influence of the periodically varying potential of the atoms contained in the crystal’s lattice. Solving the single-electron Schrödinger equation for the ‘nearly free electron model’ gives ‘allowed’ and ‘forbidden’ regions as the solution. Forbidden regions are completely empty as there are no ‘allowed’ electron energies in that zone.

This picture can also be described with ‘energy bands’ and ‘band gaps’ as the allowed

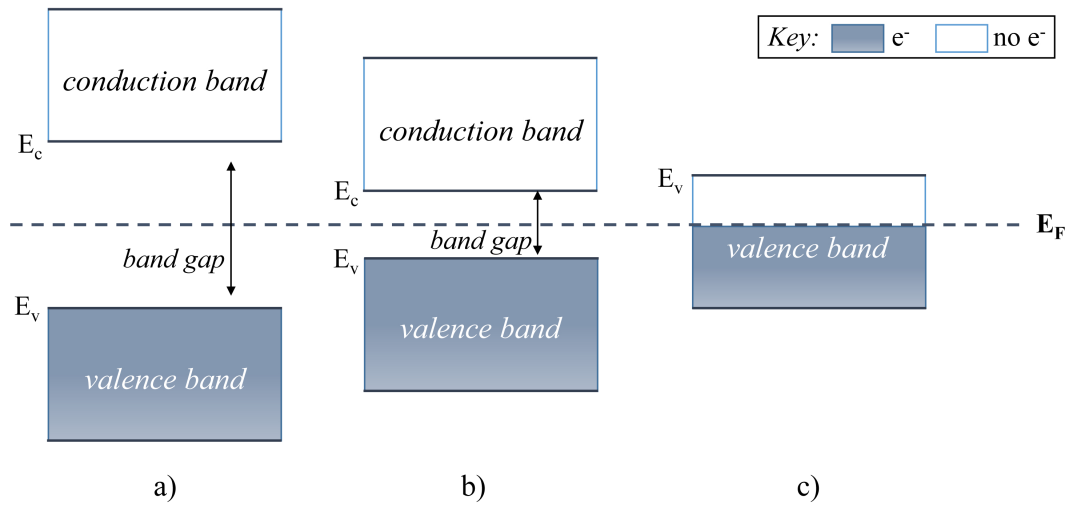


Figure 2.3: The band structure with respect to the Fermi energy E_F at absolute zero of a) insulators, b) semi-conductors and c) metals; with E_v the energy at the top of the valence band and E_c the energy at the bottom of the conduction band

and forbidden zones respectively, with the valence band below and the conduction band on top of the band gap. The electron occupancy of these bands is given by

$$N(E) = Z(E)f(E), \quad (2.2)$$

where $N(E)$ is the density of the occupied energy states and $Z(E)$ the density of the available energy levels. $F(E)$ is the Fermi-Dirac distribution which gives the probability of an electron occupying a state with the energy E :

$$f(E) = \frac{1}{\exp \frac{E-\mu}{kT} + 1} \quad (2.3)$$

with the temperature T , the Boltzmann constant k and the chemical potential μ , which is dependent on the temperature and equal to the Fermi energy E_F at absolute zero.

'The Fermi energy E_F is defined as the energy of the topmost filled level in the ground state of the N electron system. The ground state is the state of the N electron system at absolute zero.' [10]

Looking at where the Fermi Energy E_F lies with respect to the band structure makes

it possible to determine whether the material is a metal, semi-conductor or insulator.

If the valence band is completely full at absolute zero, i.e. the Fermi energy lies within the band gap, it will not exhibit conductivity when an external electrical field is applied. This is the case for insulators and semi-conductors as can be seen in figure 2.3 a) b). With the lower edge of the conduction band E_c and the top of the valence band E_v the energy gap E_g can be described as:

$$E_c - E_v = E_g \quad (2.4)$$

In perfect insulators and semi-conductors $Z(E) = 0$ for $E_c > E > E_v$ at absolute zero. These materials are only able to conduct if some of the valence electrons are able to overcome the band gap and enter the conduction band. This process shows an exponential dependence on both the temperature T and the width of the band gap E_g namely $\exp \frac{E_g}{kT}$

Metals on the other hand have a half-empty valence band even at absolute zero, which allows the electrons to move if an electric field is applied and therefore metals exhibit conductivity(see figure (2.3 c)). In addition to that they either only have a small or no band gap, which means that their valence and conduction bands overlap. This prevents metals from showing thermoluminescence as a band-gap is needed to 'store' ionising radiation, which will be explained in further detail in the following paragraphs.

Localised Levels and Crystallographic Defects

Defects and impurities within the crystal structure of insulators and semi-conductors affect the periodical potential of the lattice discussed in the previous section. These changes in the periodicity enable the electrons to have energy levels within the band gap which would otherwise be forbidden. These energy states are **localised energy levels** as opposed to the allowed energy states within the bands which extend throughout the lattice.

There are many different kinds of **crystallographic defects** that may occur during the production and/or lifetime of a crystal. From a geometrical point of view four different

dimensions of defects can be identified. Please note that when talking about atoms in the context of the following defects depending on the specific crystal either atoms, ions or molecules are implied.

- **Point defects (zero-dimensional):** Point defects are defects that only concern one particular lattice position. They can either be intrinsic or extrinsic defects depending on whether the defect can occur within the perfect crystal or is caused by an external force.
 - *Intrinsic point defects:* Vacancies (Schottky defects): A vacant lattice position that should usually be occupied by a certain type of atom according to the standard structure of the crystal. Interstitial atoms: Atoms that are located somewhere between the standard lattice sites of the perfect crystal structure. Frenkel defects: This type of defect is a combination of the first two intrinsic point defects mentioned. It is caused by an atom moving from its standard position within the lattice to an interstitial position leaving a vacancy behind.
 - *Extrinsic point defects:* Substitutional or interstitial impurities: This defect occurs when an atom which is completely foreign to the perfect crystal structure replaces an atom on its standard lattice position or is added at an interstitial site. This defect may happen during the melting process or the natural growth of the crystal but can also be introduced into the lattice structure later on through diffusion processes. It is caused intentionally in the case of dopant atoms.
- **One or more dimensional defects** such as line, planar and bulk defects can also lead to the formation of localised levels.

Defects may also occur due to radiation damage at high dosages of ionising radiation. This may lead to non-linearity effects within thermoluminescence dosimeters. As the practical implications of these effects are very important in the context of this thesis they will be discussed in a separate section (2.2.2).

Traps and Recombination Centres

Any luminescence process is caused by transitions of electrons between different energy states. Also in the case of thermoluminescence ionising radiation excites electrons into the conduction band. In the conduction band these electrons are then able to freely move

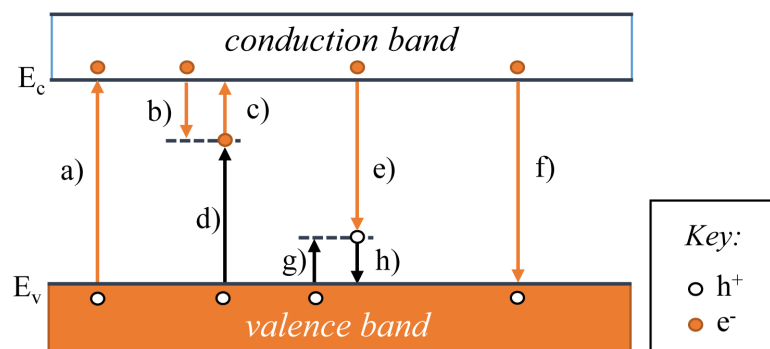


Figure 2.4: Transitions between bands and localised energy levels: a) direct transition of an e^- from the valence band to the conduction band; b) a free e^- becomes trapped at a defect centre and c) is released again; d) and e) indirect recombination of e^- and h^+ ; f) direct recombination of an e^- and h^+ ; g) a free h^+ gets trapped at a defect centre and h) is released again

around the crystal's lattice. However, as a result of defects in the crystal structure the electrons may become trapped and can subsequently only be released if thermal energy is supplied to the crystal. This section discusses the different possibilities for transitions and how probable they are.

Whenever an electron transitions to the conduction band it leaves a hole behind in the valence bands. These holes can also be described as positive charge carriers. Just like electrons holes can also be trapped within the band gap if defect centres are present. Again looking at the band structure of crystalline insulators and semi-conductors at absolute zero we can see that within the band gap the localised energy levels of holes are located below the Fermi energy level E_F while those of the electrons can be found above (Figure 2.5).

Figure 2.4 shows the different transitions between the bands and defect centres electrons and holes may go through. Transitions a) and f) show the direct transitions of electrons between the valence and conduction band. In the case of thermoluminescence transition a) is caused by ionising radiation. While the electron is now in the conduction band a hole is created within the valence band. Transition f) shows the direct recombination of the electron from the conduction band with a hole in the valence band. The free electron-hole pairs created in transition a) may also wander through their respective

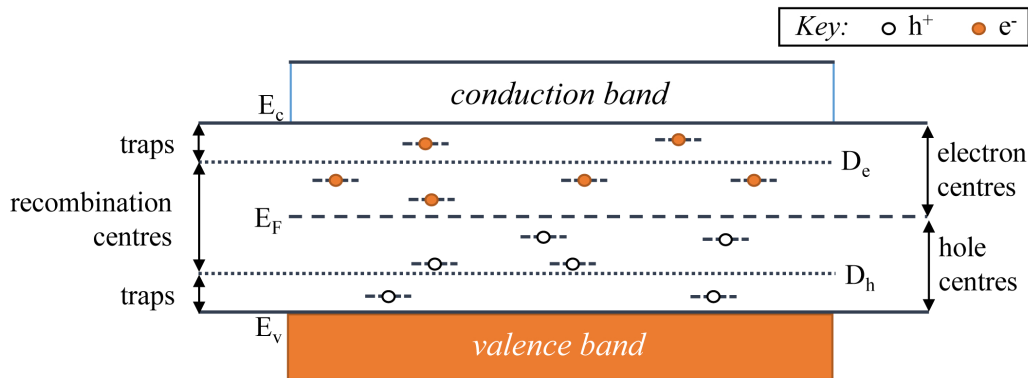


Figure 2.5: The e^- are located above and the h^+ are located below the Fermi energy level E_F at absolute zero. D_e and D_h mark the border between trapping and recombination centres for e^- and h^+ respectively.

energy bands and become trapped at localised defect centres as shown in transitions b) and g). Once electrons/holes are trapped at localised energy levels within the band gap they may be freed through thermal or optical stimulation as shown in transitions c) and h). As a second option the trapped electrons and holes may also recombine with each other as can be seen in transitions d) and e). These are the so-called indirect recombination processes.

During the direct and indirect recombination processes h), d) and e) light may be emitted and as a result luminescence can be observed. While direct recombination is always radiative the probability of indirect recombinations being radiative is again dependent on temperature and varies from material to material.

Looking at the above mentioned transitions the localised energy levels within the band gap may be grouped into two categories: traps and recombination centres. If localised energy levels act as traps the electrons/holes are more likely to be released back into the energy band they came from (transitions c) and h)) rather than recombine with a charge carrier of opposite sign. In the case that they act as recombination centre the opposite is true and they are more likely to recombine through transitions d) and e).

Now the question is: which factors make one process more likely than the other? As previously discussed in section 2.1 the likelihood of an electron transitioning from one en-

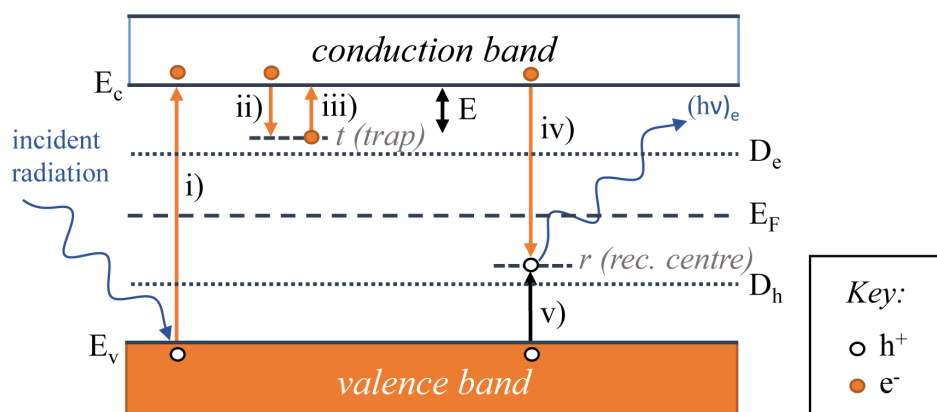


Figure 2.6: A simple theoretical model for thermoluminescence: i) an e^- is ionised by incident radiation and then ii) becomes trapped indefinitely until it is iii) released again by an increase in temperature - after that iv) the e^- recombines with a h^+ that had previously been caught v) in a recombination centre - during this recombination light $(h\nu)_e$ is emitted and thermoluminescence can be observed.

ergy level to another is proportional to the following exponential function: $\exp(E/kT)$ (see equation 2.1), where E corresponds to the ‘energy gap’ or ‘depth’ of the localised energy level. Thus release of the electrons/holes through transitions c) and f) becomes increasingly unlikely the deeper the gap is. From a certain depth onwards recombination is more probable. Figure 2.5 shows how electron and hole traps are located at the edges of the band gap whereas recombination centres can be found at its centre.

The energy depth D where both trapping and recombination are equally likely marks the border between the traps and recombination centres. In figure 2.5 D_e and D_h represent these borders for electrons and holes respectively. Due to the temperature dependence of the above mentioned exponential equation D_e and D_h shift to the centre of the band gap with increasing temperature as the release of the charge carriers becomes more likely.

A simple theoretical model

To apply the physical concepts discussed in the previous section to thermoluminescence dosimetry a simple theoretical model is needed to explain what is happening within the band structure when thermoluminescence occurs.

This model, which was first developed and discussed in the 1940s by Garlick & Wilkins [9] as well as Randall & Wilkins [19] [20], looks at just two localised energy levels within the band gap of a semi-conductor or insulator crystal. As shown in figure 2.6 the first of these two levels, t , is located just above the border D_e between the electron trapping and recombination centres and is thus a trap. The second one, r , is located between D_h - the same border just for holes - and the Fermi energy level which separates the electron defect centres from the hole centres. Therefore r is a recombination centre.

Through energy absorbed from incident radiation $E_{abs} > E_c - E_v$ electrons from the valence band become ionised and transition into the conduction band. As a consequence free holes are created in the valence band. These free charge carriers will now either recombine with each other or get trapped in a defect centre. Thermoluminescence crystals usually have a wide band gap which makes the direct recombination of free electrons with free holes less likely than indirect recombination in localised energy levels. Thus, for recombination to occur the free holes need to first be caught at localised recombination centres (see figure 2.6 v)). Through transition iv) a free electron then combines with the trapped hole and as a result light $(h\nu)_e$ is emitted.

However, free electrons within the conduction band are also likely to become trapped at a localised energy level such as t . This way the recombination process is delayed until such a time as the electron is supplied with enough energy to escape the trap. The probability of that escape per unit time is given by

$$p = \tau^{-1} = s \exp -\frac{E}{kT} \quad (2.5)$$

where E is the trap depth, k the Boltzmann constant, T the temperature and s a constant that varies between different thermoluminescence materials. If the temperature T during irradiation is low so that $E \gg kT$ the electron will become trapped indefinitely. As free holes are created together with free electrons an equal amount of both charge carriers will be trapped. If the crystal is heated up the electrons will be freed and luminescence can be observed. This fact is taken advantage of in thermoluminescence dosimetry where the light intensity of this heat induced luminescence is measured.

The intensity $I(t)$ of the light is proportional to the rate of recombinations between

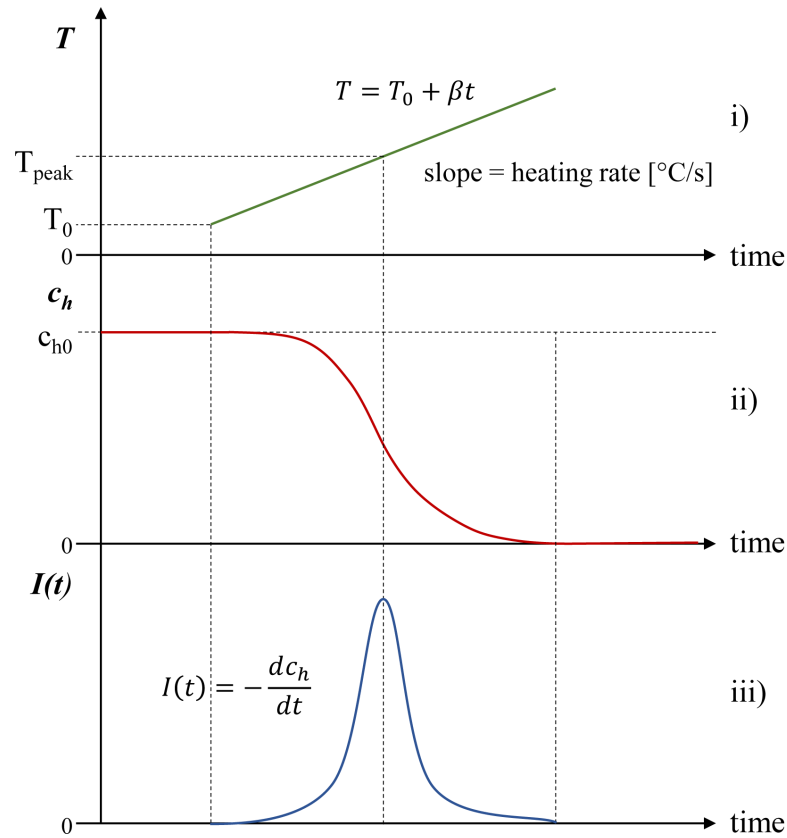


Figure 2.7: The process of thermoluminescence dosimetry: The thermoluminescent material is i) heated at a linear heating rate β and ii) as the concentration of holes c_h decreases iii) the intensity of the light emission $I(t)$ increases until it reaches the maximum at the temperature T_{peak} .

electrons and holes at the recombination centre r (Figure 2.6):

$$I(t) = -\frac{dc_h}{dt} \quad (2.6)$$

Here c_h is the concentration of trapped holes - its change over time gives the recombination rate.

Figure 2.7 shows that an increasing temperature (i) due to a constant heating rate causes a decrease in the concentration of holes (ii). The corresponding light intensity curve (iii) peaks when the temperature equals T_{peak} . In practical thermoluminescence dosimetry this intensity curve is called a 'glow curve' and is the result of the measurement of thermoluminescence using a photo-multiplier.

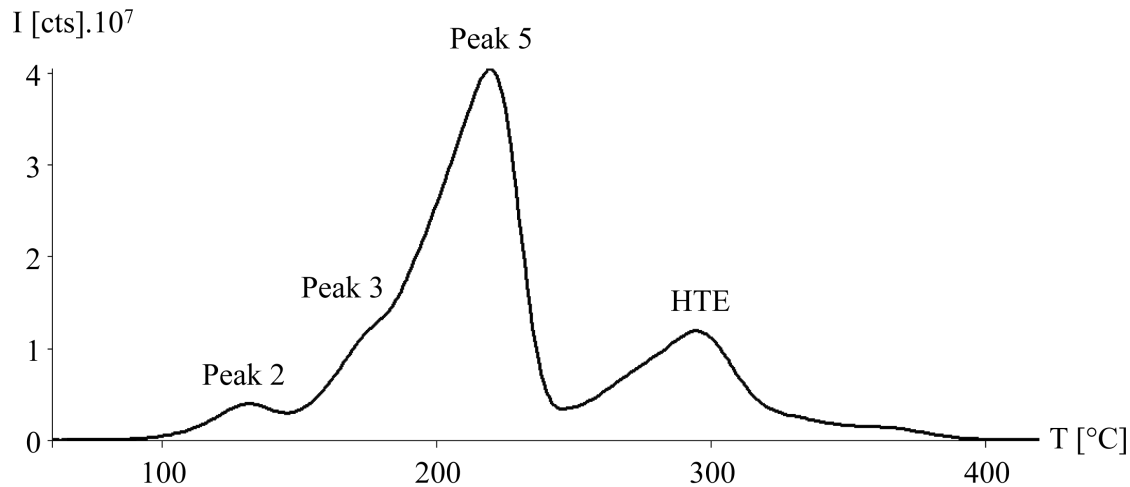


Figure 2.8: A glow curve of a TLD-700 thermoluminescence dosimeter showing several overlapping peaks at different temperature ranges. The dominant peak 5 with a maximum at 220 °C is used for thermoluminescence dosimetry. The high temperature emission (HTE) is a measure of the linear energy transfer (LET) of the absorbed radiation.

2.2.2 Thermoluminescence Dosimetry

This section gives a short theoretical overview of the different steps involved in thermoluminescence dosimetry. More details on the actual method used in this project are given in chapter 3.1.2 where our experimental methods are presented.

To begin with the reference measurements (calibration), annealing, read-out and analysis process are introduced. Next the different properties of thermoluminescence materials and the types of dosimeters available are discussed. At the end the various possibilities for the application of thermoluminescence dosimetry are reviewed.

Glow Curve Structure, Thermal Fading and LET-Dependence

The intensity curve corresponding to the thermoluminescence emission measured by a photo-multiplier in a TL read-out device is called a ‘**glow curve**’. The glow curves’ peaks and structure vary between different thermoluminescence materials.

As previously discussed in simple terms thermoluminescence is caused by defects within

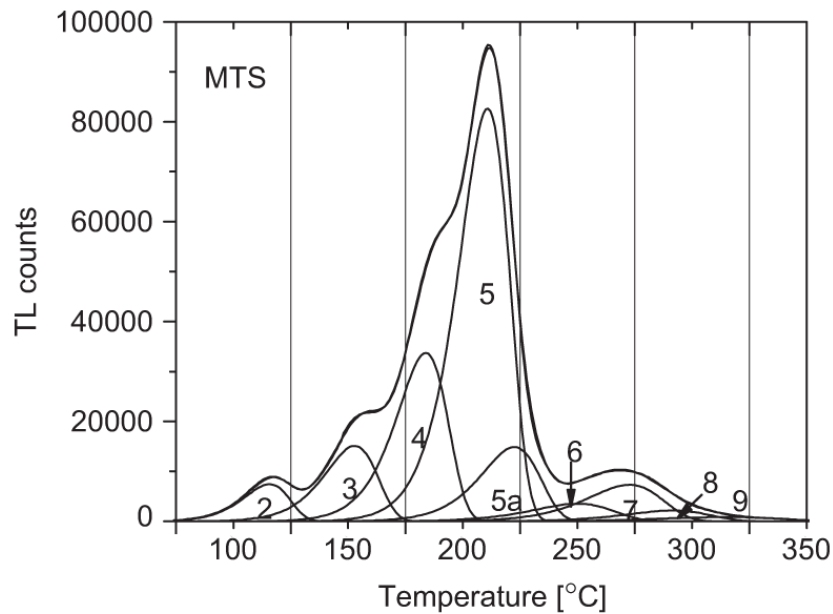


Figure 2.9: Deconvolved glow curve of a LiF(Mg,Ti) dosimeter of the MTS type showing peaks 2 to 9. Peaks 2 and 3 are subject to thermal fading. Peak 5 is the most stable peak and therefore used as the 'dosimetric peak' in TL dosimetry. The high temperature peaks 6 to 8 have been shown to have a functional correlation with the LET of the absorbed radiation. Source: [18]

the crystal lattice of the material. In thermoluminescence dosimeters these defects are artificially created by introducing impurities into the crystal i.e. dopants. Different dopant elements cause different kinds of defect centres and thus, even if the same basic material is used the peak maxima and properties of the dosimeters' glow curve can differ greatly.

For all types of thermoluminescence materials several glow curve peaks can be observed during read-out. Figure 2.8 shows an example of a typical LiF(Mg,Ti) glow curve - several overlapping peaks are visible at different temperatures. Deconvolving these peaks is a very complex matter and still a topic of research. For the LiF(Mg,Ti) dosimeters used in this study 9 different peaks can be resolved (see figure 2.9). Depending on the time between irradiation and read-out some of the peaks change in intensity or disappear completely over time. This is caused by the so-called **thermal fading** process. As shown in equation 2.5 the probability for a trapped electron to escape is exponentially

dependent on the temperature T as well as the trap depth E :

$$p = \tau^{-1} = s \exp -\frac{E}{kT}$$

For low trap depths the probability of an electron escaping is relatively high even at room temperature. Thus, low temperature peaks, such as peak 2 and 3 in figure 2.9, which correspond to traps with lower energy depths E , fade over time. As this escape is made possible by the thermal energy of the temperature around the dosimeter this process is called thermal fading.

Even though other peaks are not subject to thermal fading they may still show unstable behaviour as their intensities can depend on a number of different factors. Up to an energy dosage of about 1 Gy the glow curve structure stays the same. Above 1 Gy different peaks do, however, show varying degrees of non-linearity.

Other peaks' structure is highly **dependent on the Linear Energy Transfer(LET)**. The LET is directly proportional to the density of the absorbed ionising radiation, so these peaks can be used as an indicator of the microscopic radiation density in case the source of the radiation is not known. For LiF(Mg,Ti) dosimeters the high temperature emissions (HTE) between 250 and 350 °C (see figure 2.8) have a functional correlation with the LET of the absorbed radiation. [3] [2] [23] Figure 2.10 shows the HTE's response to different kinds of ionising radiation with varying degrees of LET.

In the face of all these unpredictable dependencies it is clear that only stable peaks which are not influenced by external factors other than the absorbed energy dosage can be used for thermoluminescence dosimetry. *The most stable peak of the TLD-600 and TLD-700 dosimeters is the dominant peak number 5 at 220 °C visible in figure 2.8. This peak was used for all thermoluminescence measurements presented in this work.*

Reference Measurements - Calibration

Unfortunately the analysis of a TL dosimeter's glow curve alone does not yield an absolute value for the dosage of ionising radiation that was absorbed within the material. Depending on the material the glow curve shape changes and several different glow

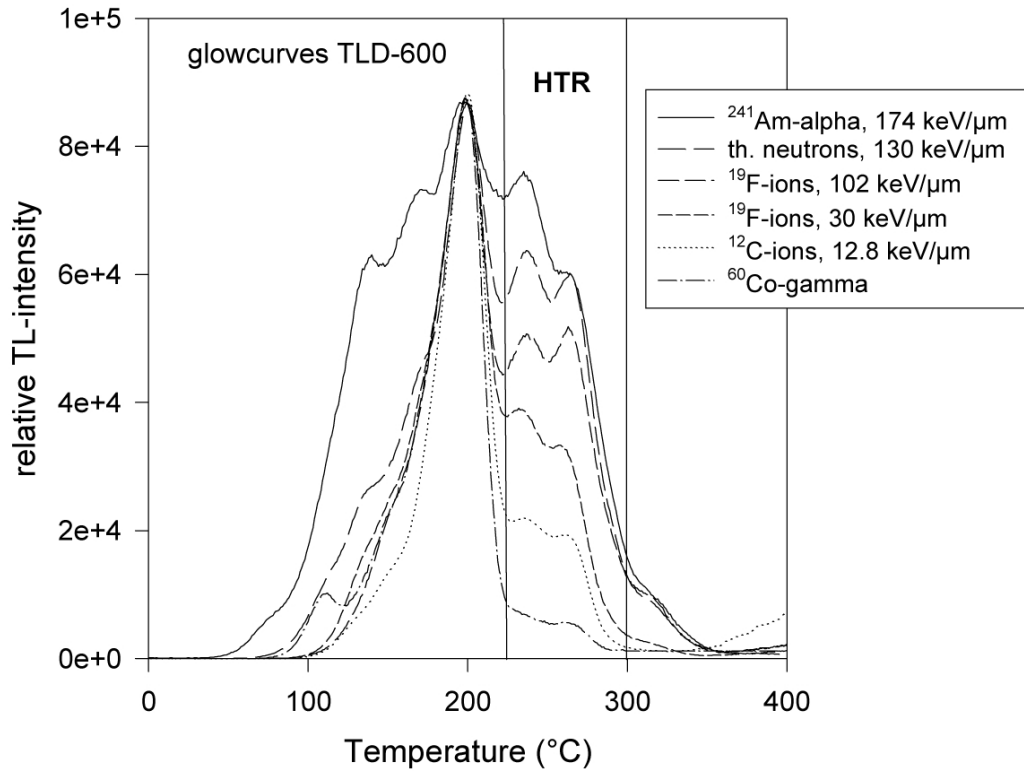


Figure 2.10: LET dependence of the high temperature emission of a TLD-600 dosimeter. The HTE increases with the microscopic ionisation density of the absorbed particle. Peak 5 is normalised to equal height. Source: [23]

curve peaks can be observed. Some of these peaks are, however, known to have a linear correlation with the absorbed dosage. It is important to note, though, that this linearity is only stable for a certain dosage range. The non-linearity effects that occur outside of this dosage range are discussed at a later point in this section.

To be able to correlate the observed thermoluminescence intensity of a glow curve peak a reference measurement with a known source of radiation is necessary. This way a calibration factor can be obtained that allows for the calculation of an actual dosage value from the glow curve's intensity.

If the activity of a radioactive source and the geometrical structure of the irradiation setup is known the dose rate \dot{D} received by a TL dosimeter a certain distance away can

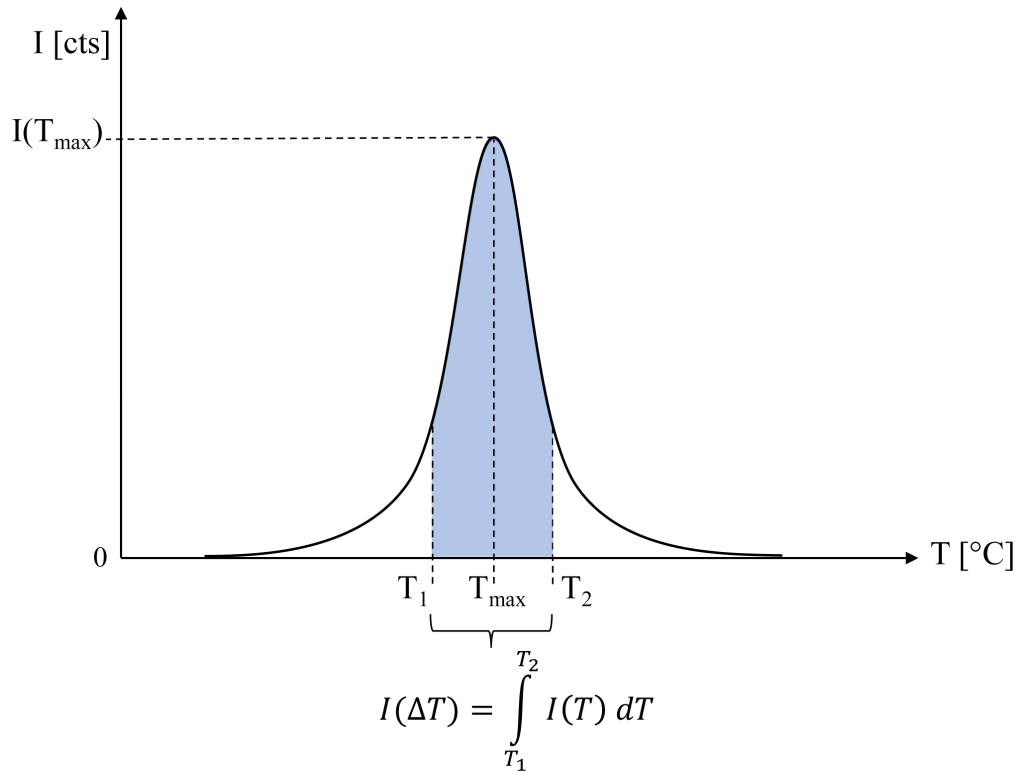


Figure 2.11: Intensity maximum $I(T_{max})$ and intensity integral $I(\Delta T)$ of a stable peak

be calculated. Multiplied by the exposure time t_{exp} the accumulated energy dosage D the dosimeter was subjected to can be worked out:

$$D = \dot{D} \cdot t_{exp} \quad (2.7)$$

From the intensity read-out after this irradiation either the maximum $I(T_{max})$ or integral value $I(\Delta T)$ of a stable peak may be used as a reference as shown in figure 2.11. *All measurements presented in later sections are based on the read-out of the maximum of peak 5 $I(T_{max})$ at $T_{max} = 220$ °C.*

If the absorbed dosage D_{cal} is known, the calibration factor f_{cal} can be calculated in the following manner:

$$f_{cal} = \frac{I(T_{max} \text{ or } \Delta T)}{D_{cal}} \quad (2.8)$$

Due to the glow curve intensity being proportional to the number of photons read-out by the photomultiplier its dimension is given in counts [cts]. Thus the calibration factor f_{cal}

has the dimension of [cts/Gy]. This way any further intensity read-out I of an unknown radioactive source can be correlated with an actual absorbed energy dosage D_{abs} by dividing it with the calculated calibration factor:

$$D_{abs} = \frac{I}{f_{cal}} \quad (2.9)$$

Non-Linearity Effects

High amounts of dosage outside of the linear dosage range can change the response of the glow curve peaks due to damage inflicted by the ionising radiation. While the first read-out after absorption of such a high dosage usually shows **supra-linear behaviour** - an overestimation of the absorbed dosage - or **saturation** - an underestimation is observed. For high radiation intensities these effects can ultimately lead to a **loss of sensitivity** during subsequent read-outs.

This loss of sensitivity can be observed if another reference measurement is done after the absorption and read-out of high-dose radiation. Depending on the specific thermoluminescence material and the extent of the dosage the sensitivity loss compared to the response during the initial calibration can be up to 50% or sometimes even higher.

Due to these non-linearity effects during the exposure to high energy dosages reference measurements have to be undertaken in regular intervals to be able to evaluate the obtained glow curves.

Some of this radiation damage has been shown to be repaired [25] during long annealing procedures of around 20 hours at 400°C as recommended by Burgkhardt and Piesch [5].

Annealing Procedure

Even if they are not irradiated directly any thermoluminescence dosimeter will accumulate a certain amount of dosage if left untouched for a period of time. This dosage corresponds to the natural background radiation and can be quite substantial if dosimeters are stored for a long time. In addition the last read-out process performed on the dosimeter may not have emptied all the traps sufficiently which could affect the results

of the next measurement.

To counteract these two factors so-called ‘annealing procedures’ are used before irradiation and after read-out to reset the dosimeters to their initial untouched state and prepare them for the next usage. Standard annealing procedures can vary between different dosimeter materials and types. The most common one includes annealing the dosimeters at 400°C for one hour and letting them cool down inside the oven for the following 20 hours. This initialising process defines the sensitivity and glow curve structure of TL dosimeters. Thus, it needs to be carried out in the exact same manner each time for the dosimeter results to be consistent.

TLD Materials

From all that has been discussed so far it is possible to see how a material used for thermoluminescence dosimetry has to have certain properties that are essential for the process. The material’s glow curve needs to have at least one peak that has a linear relationship with the absorbed dosage over the range that the dosimeter is intended to be used for. That peak also has to be stable and should not be subject to thermal fading.

Such materials can be produced by doping LiF or CaF₂ with certain other elements to produce defect centres. Lithium-fluoride is the most widely used thermoluminescence dosimeter material. LiF TLDs are available with different ⁶Li and ⁷Li isotope ratios and various dopant elements. The most common type uses Mg and Ti as dopants and its stable peak (number 5) is linear between dosages of 10⁻⁶ Gy and 10 Gy. Thermal fading is relatively small with a loss of 5-10% per year. This type was also used in this work.

Practical Applications

There are a number of applications thermoluminescence dosimetry is perfectly suited for. This section aims to give a brief overview of the different possibilities.

The most common and probably most important application of thermoluminescence dosimetry is the **monitoring of personnel** exposed to radiation. Small badges are worn directly on the body and the dosimeters are exchanged and read out at regular intervals to give an estimate of the accumulated dosage a person was exposed to.

Another wide-spread application is **thermoluminescence dating** - here advantage is taken of the thermoluminescence properties of materials by measuring and calculating the age of certain structures or objects (e.g. bricks, clay items, etc.) from the accumulated natural background radiation.

Thermoluminescence dosimeters are also used in **environmental monitoring** of the natural background radiation. This method can be used to monitor elevated levels of radiation in certain geological zones or for example close to nuclear power plants. Air crews may also be monitored as radiation from cosmic rays at high altitudes can cause a significantly higher natural background.

This study is, however, concerned with one of the lesser known applications where thermoluminescence dosimeters are used to do **reactor dosimetry**. A more detailed explanation can be found in the following sections.

2.3 Liquid Scintillation

As liquid scintillation counting(LSC) was only used to confirm the results of the main detection method of this thesis - thermoluminescence dosimetry - only a brief introduction to this measurement technique will be given in this section.

Liquid scintillation counting is the standard technique used for the detection of beta-radiation. It relies on the phenomenon of fluorescence which was explained in section 2.1 of this work. In this case fluorescence is induced by adding scintillating/fluorescent elements to a radioactive sample. Usually the radioactive sample is mixed with a so-called scintillation cocktail consisting of a solvent and scintillators. The beta radiation from the radioactive material is absorbed within the cocktail and transferred through the liquid until it reaches a scintillator and photons are emitted. This light is then detected by two photomultiplier tubes connected to a coincidence circuit, which ensures that only the actual light pulses that reach both photomultiplier tubes are counted. Thus, it is important that the samples together with the cocktail are measured in transparent/translucent glass or plastic containers.

Counting efficiencies vary depending on the energy of the beta particles emitted by the radioactive isotope and the amount of quenching that occurs. Quenching is an efficiency loss that can be caused by a sample's colour and certain chemical compounds within the sample. So-called quench curves are determined to correct for this effect.

2.4 Neutron Radiation

The most important thing to note about neutron radiation is that neutrons of course do not carry a charge. As opposed to gamma and x-rays neutrons do, however, have a mass and they are 2000 times heavier than electrons. Furthermore free neutrons themselves aren't stable particles, they have a half life of 10.25 minutes and decay into protons via β^- emission.

As neutrons are not charged, no interactions with charged particles involving the coulomb force and subsequent energy loss can occur. Thus neutrons are able to pass through many centimetres of matter without ever interacting, which makes them difficult to detect.

Yet, if neutrons do interact with matter it is only with the nucleus as it is the heaviest part of the atom and electrons are very small and light-weight compared to it. Due to this fact neutrons cannot be classed as directly ionising radiation. Electrons may only be influenced by neutrons indirectly through the directly ionising radiation resulting from neutron interactions with the nuclei. Neutrons are therefore termed indirectly ionising radiation.

In the following sections we first discuss different neutron sources and the various energy levels of the neutron spectrum. Next an overview of the possible neutron interactions is given and we explain how their probabilities are closely connected to their cross section and the neutron energy. In the following section neutron detection with the TLD pair method are explained, which the results presented in later sections partially rely on. In the last section a brief review of the neutron activation analysis is given as a means to compare the results obtained from both TLD and LSC measurements to a theoretically predicted value.

Energy Range	Name
0–0.025 eV	Cold
0.025 eV	Thermal
0.025–0.4 eV	Epithermal
0.4–0.6 eV	Cadmium
0.6–1.0 eV	Epicadmium
1–10 eV	Slow
10–300 eV	Resonance
300 eV–1 MeV	Intermediate
1–20 MeV	Fast
>20 MeV	Relativistic

Table 2.1: Neutron energy spectrum [6]

2.4.1 Neutron Sources and Neutron Spectrum

Free neutrons occur as a product of both fission and fusion but may also be produced as a result of other nuclear reactions.

The (α, n) reaction for example is a common reaction taken advantage of in neutron sources. In many cases long-lived, heavy radioactive isotopes that emit alpha-radiation are used to induce this reaction in lighter elements such as ^9Be and ^7Li . Also for example (d, n) , (p, n) and (γ, n) reactions result in the emission of neutrons.

An example of a fusion reaction resulting in the production of free neutrons was briefly outlined in section 1.2. Here deuterium and tritium are fused and as a result neutrons are emitted: $^2\text{D} + ^3\text{T} \rightarrow ^4\text{He} + n + 17.6 \text{ MeV}$.

Also during the fission of heavy radioactive isotopes such as uranium or plutonium neutrons are created. In this case the resulting free neutrons are essential for the up-keep of the fission reaction.

According to their energy neutrons may be classified as thermal, fast or relativistic neutrons. An overview of the complete neutron energy spectrum can be found in table 2.1. The neutron energy has a great impact on which type of neutron interaction is most likely to occur. This is discussed in detail in the next section.

2.4.2 Neutron Interactions

To be able to properly understand how neutron interactions work the concept of cross sections needs to be introduced first.

Neutron Cross Sections

The probability for the interaction of a neutron and a nucleus is given by its neutron cross section. From a classical point of view this concept can be imagined as ‘the probability of a single neutron attempting to pass through a thin layer of material that has an area A and contains N target nuclei, each of cross-sectional area d . The sum of all the areas of the nuclei is Nd . The probability of a single neutron hitting one of these nuclei is roughly the ratio of the total target area Nd to the area of the layer A . In other words, the probability of a single neutron having a collision with a nucleus is Nd/A .’ [21] Therefore it is plausible why the neutron cross section has the SI unit of cm^2 . From a quantum mechanical standpoint, however, the actual cross section σ differs from this geometrical concept. Therefore the actual values of σ need to be viewed as the effective area of the neutron cross section. As neutron interactions were in the beginning mainly investigated in the context of heavy fissionable elements another cross-sectional unit was introduced - the barn. A barn, b , is defined as 10^{-24} cm^2 , which is on the order of magnitude of the geometrical cross section of heavy nuclei. Effective neutron interaction cross sections can, however, be much higher. Furthermore it is important to note that cross sections are different for every individual interaction and also heavily dependent on the energy of the neutron. Each possible interaction has its own independent cross section and probability. A list of neutron cross sections can be found online at: [16] and [15]. The total cross section is the sum of all individual cross sections and gives the probability of any of these interactions occurring.

Types of Interactions

Two main ways in which neutrons interact are absorption and scattering. Figure 2.12 gives an overview of all the possible interactions and their respective cross sections. σ_t denotes the total neutron cross section, σ_s that of the cross-sectional sum of all scattering interactions and σ_{abs} that of all absorption possibilities.

- **Scattering:** The general structure of the nucleus stays the same during scattering, the nucleons do not change and generally no radiation is emitted. For the neutron only its speed and direction may change as kinetic energy is transferred to the nucleus. The scattering process can either occur elastically or inelastically.

During elastic scattering some of the neutron's kinetic energy is transferred to the nucleus. The overall kinetic energy of both particles does, however, stay the same as no energy gets converted in this process. The nucleus is sped up by the recoil velocity, while the neutron is slowed down.

While the total kinetic energy stays the same for elastic scattering it decreases during inelastic scattering as some of the energy is transferred to the nucleus. Through this process the neutron is again slowed down. However, instead of absorbing kinetic energy the nucleus gets excited to a higher energy level, which will eventually lead to the release of gamma radiation.

- **Absorption:** a variety of radiation is emitted during the different absorption interactions. According to the type of radiation emitted four kinds of absorption can be distinguished: electro-magnetic (n, γ), charged ($n, \text{charged particle}$) and neutral (n, n) absorption as well as fission.

The neutron interaction that is most important for this study is the ${}^6\text{Li}(n, \alpha){}^3\text{H}$ reaction. It has a high cross section for thermal neutrons ($\sigma = 940 \text{ b}$ [16]), which allows for the production of significant amounts of tritium within the TLD-600 dosimeter material. This tritium is the cause of the phenomenon termed '**tritium build-up**', where an elevated background is observed in a thermoluminescence signal due to the low energy beta-radiation emitted by tritium within the TL dosimeters.

2.4.3 Neutron Detection with TLDs - Pair Method

Because neutrons only interact with the nucleus it is difficult to detect them through the measurement of ionised electrons. A number of different indirect methods have, however, been developed for their detection. One of these methods is the so-called pair method, which relies on the use of the neutron detecting capabilities of TLD-600 thermoluminescence dosimeters and will be explained in the following paragraphs.

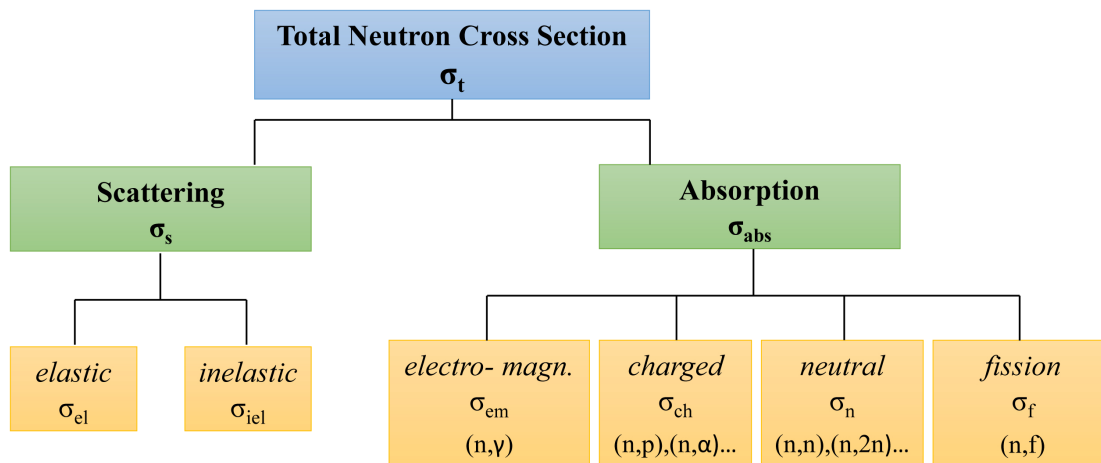


Figure 2.12: An overview of the possible neutron interactions with their respective cross-sections. The total neutron cross section is comprised of the sum of all scattering and absorption cross-sections.

As the TLD-600 chips are made from ${}^6\text{LiF}$ the following reaction takes place if they are exposed to thermal neutrons: ${}^6\text{Li}(n, \alpha){}^3\text{H}$. As tritium is produced also radiation is also emitted within the dosimeter material. These alpha particles are then able to ionise electrons within the chip. This leads to a higher primary TL measurement within TLD-600 dosimeters compared to TLD-700 chips exposed to the same radiation field. Depending on the thermal neutron fluence the TL signal can be significantly higher and, due to the high ionising density of the alpha particles, the glow curve structure is altered as well.

Figure 2.13 shows an example of a TLD-600 and a TLD-700 glow curve after exposure to a mixed radiation field of gamma radiation and neutrons. While the TLD-700 curve only represents the gamma-part of the absorbed dosage the TLD-600 glow curve has a much higher intensity and a significantly different structure.

The pair method takes advantage of this fact. The peak 5 read-out of the TLD-700 chip is subtracted from that of the TLD-600 dosimeter. The remainder is the net neutron TL signal - a measure of the neutron radiation the dosimeters were exposed to. If a TL signal calibration is done with a known neutron source the net neutron signal can be translated into an exact measurement of the neutron fluence.

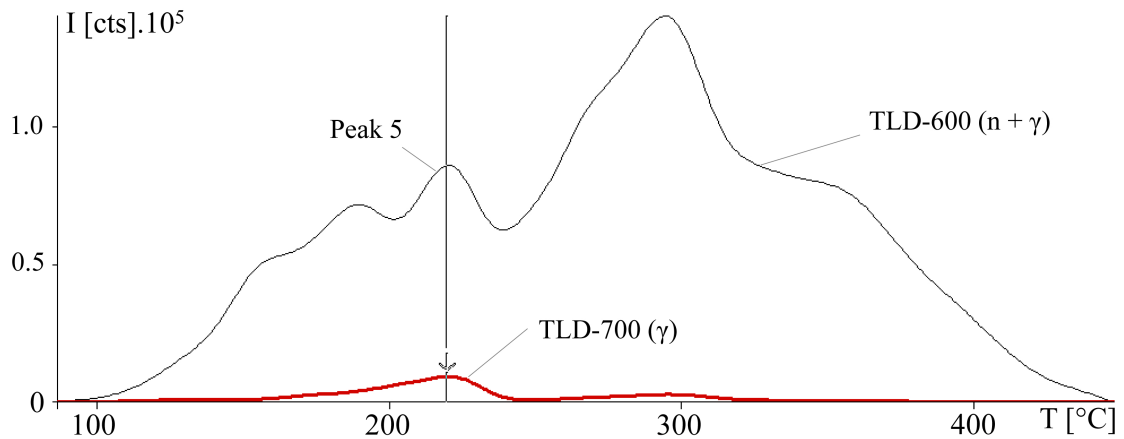


Figure 2.13: Glow curves of a TLD-600 and TLD-700 dosimeter after irradiation in a mixed field of both gamma and neutron radiation. The neutron-sensitive TLD-600 chip shows a significant increase in TL-light intensity and has a very different glow curve structure compared to that of the TLD-700 chip.

2.4.4 Neutron Activation Analysis

Neutron activation analysis can be used to determine the amount of a certain element within a material. Through exposure to neutron radiation well known activation and decay processes are triggered, which can then be measured using spectrometry. Depending on the energy of the produced radioactive elements different kinds of techniques such as gamma spectrometry or liquid scintillation counting may be employed.

To calculate the activity of a specific element produced through neutron activation the following equation is used:

$$A(t) = N \cdot \phi \cdot \sigma(1 - e^{-\lambda t}) \quad (2.10)$$

where $A(t)$ is the activity of the element produced through the neutron interaction with the cross section σ and a number N of atoms available for interaction. The target material is exposed to a neutron flux ϕ for an irradiation time t . This technique was employed to estimate the amount of tritium produced within the thermoluminescence dosimeters during irradiation in the reactor. This made it possible to compare the results from the LSC measurement of tritium to a predicted value.

CHAPTER 3

Method

This section first gives an overview of the different instruments used to obtain the data presented in section 4 of this thesis. Next their calibration is discussed and the subsequent analysis of the acquired data is explained in detail.

3.1 Instrumentation

Here, two types of thermoluminescence dosimeters which constitute the basis for this work are introduced. The following section covers the research reactor and transfer systems used to irradiate the above mentioned dosimeters. Next the instruments and processes needed for thermoluminescence dosimetry as well as liquid scintillation counting are explained in detail.

3.1.1 Irradiation

For the irradiation of the dosimeters in a mixed radiation field with a high flux of neutrons and high doses of gamma radiation a research reactor, such as the TRIGA Mark-II reactor in Vienna was necessary. Furthermore it was also essential to have a way of irradiating the dosimeters for an exact length of time at a stable and known position within the reactor core. The use of the fast pneumatic transfer system which had been installed at this reactor a few years ago allowed for both of these things.

TRIGA Mark-II, Vienna

The TRIGA Mark-II research reactor at the Institute of Atomic and Subatomic Physics of Vienna University of Technology was used to irradiate the thermoluminescence dosimeters with high dosages of both gamma and neutron radiation.

TRIGA reactors were initially designed between the years of 1956 and 1958 by General Atomics. TRIGA stands for Training, Research, Isotopes, General Atomic. A team of scientists led by Dr. Edward Teller was aiming to design a reactor with “inherent safety” - ‘a safety guaranteed by the laws of nature’ [8]. The inventors intended to make the reactor ‘safe even in the hands of a young student.’

The final design was a pool-type reactor with uranium zirconium hydride (UZrH) fuel, which would make a nuclear meltdown impossible due to its large negative fuel temperature coefficient of reactivity. In addition UZrH also has a superior retention of fission products - more than 99% of all volatile fission products would be retained even if all the cladding were to be removed [1]. Nowadays TRIGA reactors are the most widely used research reactor type in the world.

The TRIGA Mark-II reactor in Vienna has been in operation since 1962. It was first fuelled with highly enriched uranium, but as a result of the Reduced Enrichment for Research Test Reactors programme the fuel rods have recently been changed to the high density low-enriched type with a uranium enrichment of 19.8%. It consists of 74 fuel elements with a maximum thermal power of 250kW and a neutron flux of $1.10^{13} \text{ n cm}^{-2}\text{s}^{-1}$ in the central irradiation tube [28]. More technical data of the reactor can also be found in the appendix A.1.

For research purposes the reactor is equipped with several irradiation devices. A schematic diagram of the TRIGA Mark-II reactor and some of its irradiation devices are shown in figure 3.1. A complete list can be found in table 3.1.

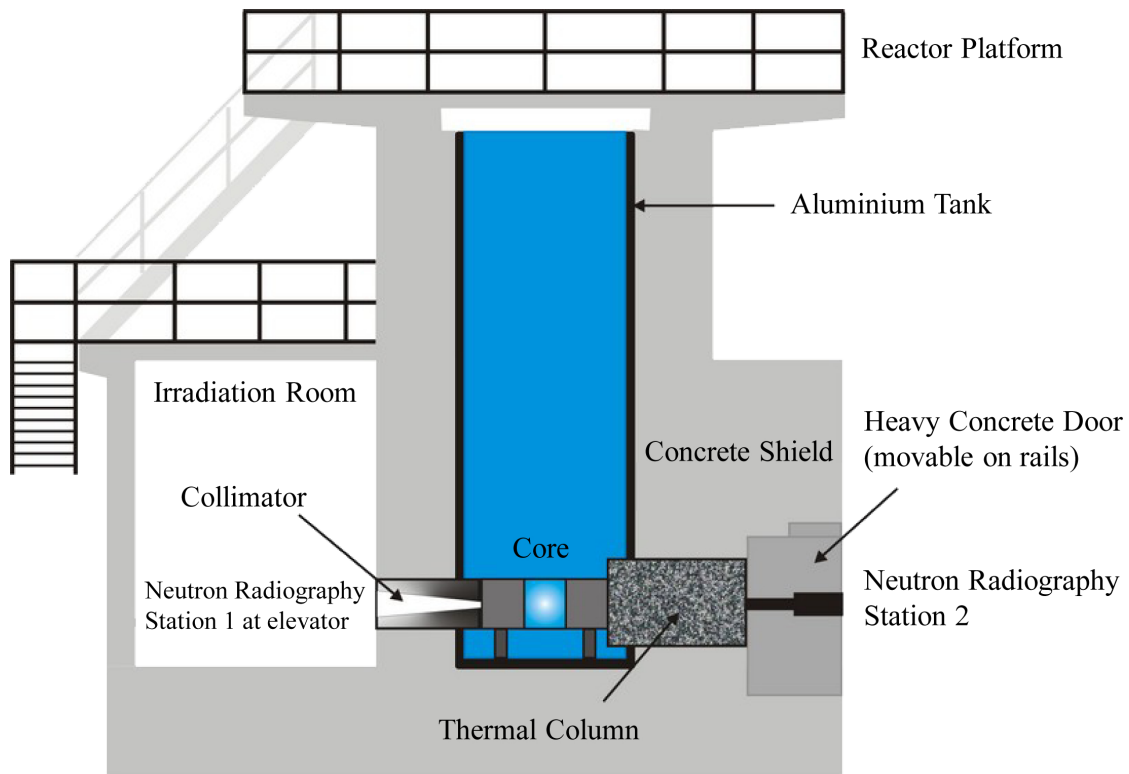


Figure 3.1: Schematic representation of the TRIGA Mark-II nuclear research reactor at the Institute of Atomic and Subatomic Physics, Vienna. Source: [28]

No.	Type
5	reflector irradiation tubes
1	central irradiation tube
1	pneumatic transfer system (transfer time 3 s)
1	fast pneumatic transfer system (transfer time 20 ms)
4	neutron beam holes
1	thermal column
1	neutron radiography facility

Table 3.1: Irradiation devices at the TRIGA Mark-II nuclear research reactor



Figure 3.2: Dosimeter container for use during irradiation able to hold 6 dosimeters

Fast Pneumatic Transfer System

The fast pneumatic transfer system (FPTS) is a pneumatic tube system that makes the transport of small samples into the reactor core possible. It uses pressure to propel samples into the reactor core and back. The transfer takes about 300 ms each way [24]. The irradiation takes place at the end of the transfer pipe which is located at the edge of the reactor core next to the rotary specimen rack (see figure 3.3). At the reactor's maximum thermal power output of 250 kW this position is subject to a thermal ($E_n = 0.025$ keV) neutron flux of approximately $2 \cdot 10^{12}$ n cm⁻² s⁻¹. This transfer system permits a quick and precise transport of samples into the reactor core. Samples get irradiated for an exact period of time that can be adjusted easily.

In previous attempts to irradiate thermoluminescence dosimeters within the reactor the dosimeter packages had been hooked to a string and lowered down into the central irradiation tube for a certain number of minutes [12]. In contrast to this method irradiating the samples with the fast pneumatic transfer system reduces the transport time and all the uncertainties connected to a manual transfer of the samples. In addition the FPTS allows for the samples to be irradiated at exactly the same position each time, which makes the irradiation geometry reproducible. Therefore this system was found to be the ideal method of irradiating thermoluminescence dosimeters and all the reactor exposures discussed in the following chapters were carried out this way.

For the transfer the dosimeters were placed into small plastic cases, which would not produce any long-lived radioactive isotopes when subjected to neutron radiation. The cases were put together in-house using old dosimeter containers. Each plastic case is able to hold up to 6 dosimeters (Figure 3.2). This also enabled the use of the pair method discussed in section 2.4.3 where three TLD-600 and three TLD-700 could be placed into one polystyrene case and irradiated together.

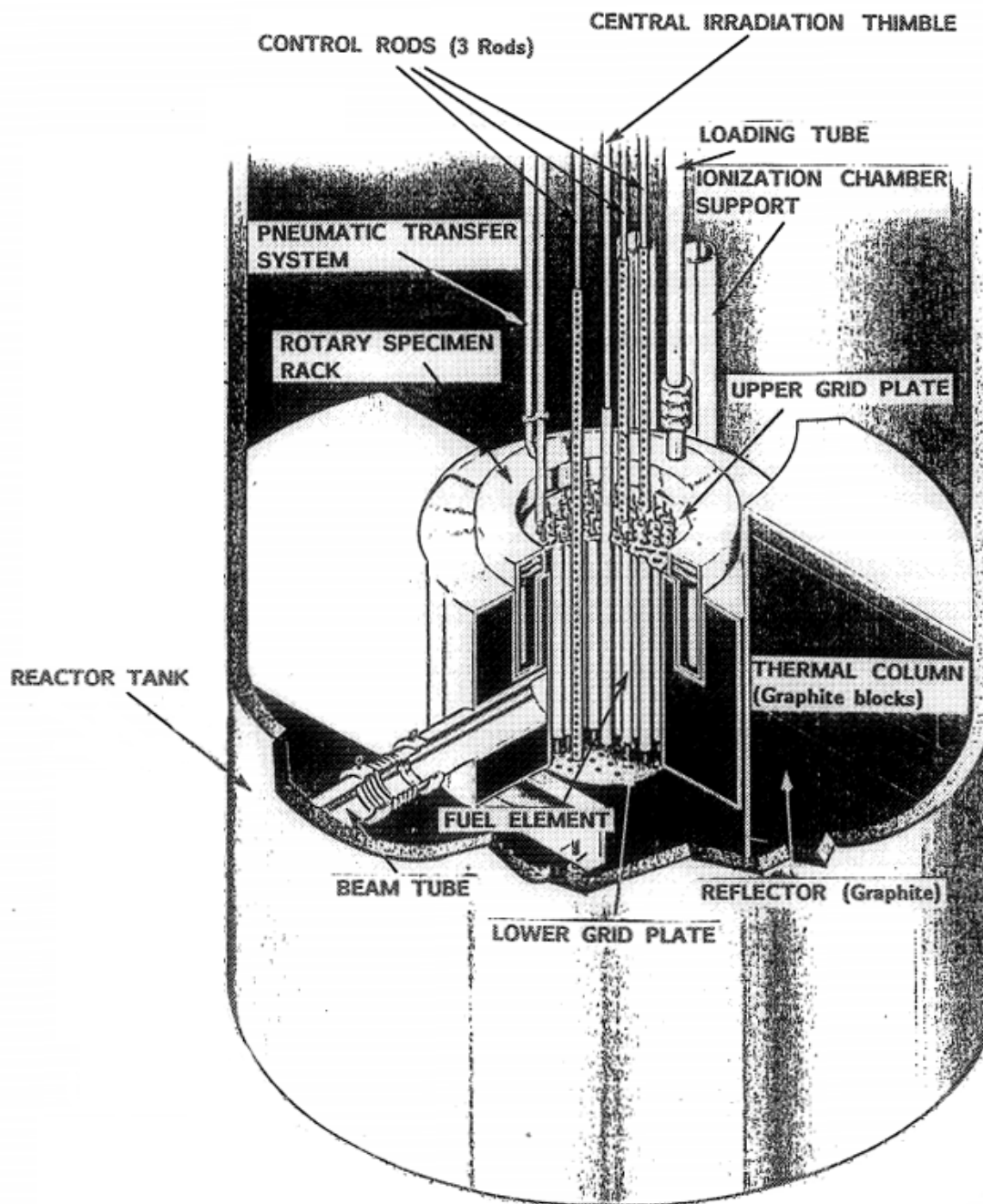


Figure 3.3: A schematic view of the different parts of the TRIGA Mark-II, Vienna. The Fast Pneumatic Transfer System is located next to the rotary specimen rack. Source: [28]

3.1.2 Thermoluminescence Dosimetry

Thermoluminescence Dosimetry was the main measurement method used in the course of this Master's project. This section will explain all the necessary instruments and steps for the practical implementation of this type of dosimetry.

Thermoluminescence Dosimeters

For the measurements in this thesis leftover dosimeters from previously undertaken thermoluminescence projects were used.

58 leftover TLD-700 and 67 leftover TLD-600 chips from the MATROSHKA project were used. Both types of dosimeters were produced by the company Harshaw(ThermoScientific) and are made from Mg and Ti doped LiF . Their detailed specifications can be found in tables 3.2 and 3.3.

TLD-600	
Composition	${}^6\text{LiF:Mg,Ti}$
Li-Content	95.62% ${}^6\text{Li}$, 4.38% ${}^7\text{Li}$
Chip dimensions	3.2 x 3.2 x 0.89 mm
Dosimetric Glow Peak	220°C (Peak 5)
Mass	23 mg

Table 3.2: Data of the TLD-600 dosimeters produced by Harshaw

TLD-700	
Composition	${}^7\text{LiF:Mg,Ti}$
Li-Content	0.001% ${}^6\text{Li}$, 99.999% ${}^7\text{Li}$
Chip dimensions	3.2 x 3.2 x 0.89 mm
Dosimetric Glow Peak	220°C (Peak 5)
Mass	23 mg

Table 3.3: Data of the TLD-700 dosimeters produced by Harshaw

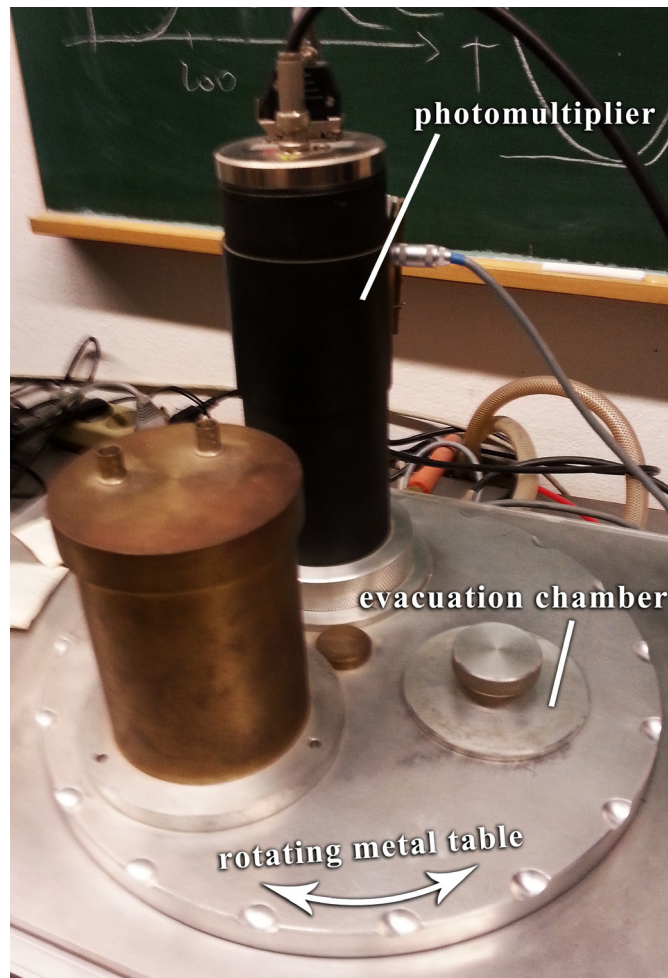


Figure 3.4: Setup of the TL-DAT-III: A rotating metal table sits atop the evacuation chamber which enables the photomultiplier tube to be placed on top of the chamber for measurements. A lid protects the evacuation chamber from being polluted - it can be removed to access the chamber.

Read-out device - TL DAT-III

The freshly irradiated dosimeters need to be read out in a thermoluminescence dosimetry unit. The unit we used for our measurements was the TL DAT-III read-out device which was designed and built by Ing. Manfred Fugger at the Institute of Atomic and Subatomic Physics, Vienna and completed in 1994. It is an improved version of the TL DAT-II, which was also developed at our institute. [27] The most important components, filters and the software of the TL DAT-III will be outlined in the following paragraphs.

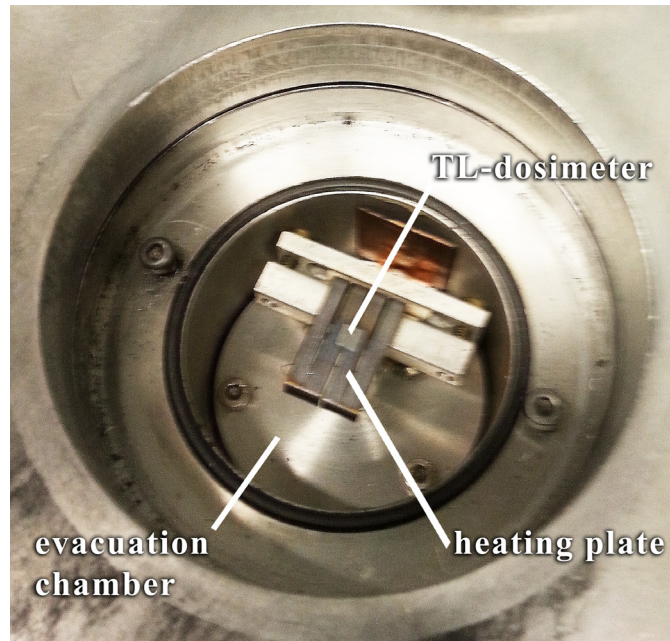


Figure 3.5: The evacuation chamber of the TL-DAT-III and the heat conducting plate within that chamber with a TL-dosimeter sitting on top of it.

Components

The three most important components of the TL-DAT-III are the evacuation chamber, the heat conducting plate within that chamber and the photomultiplier on top of it. A picture of this setup can be seen in figure 3.4.

- The **evacuation chamber** is connected to both an evacuation pump and a nitrogen gas cylinder. This way the chamber can be evacuated prior to heating and flooded with highly pure (5.0 grade) nitrogen gas during the measurement. This helps to minimise parasitic luminescence effects that would otherwise falsify the read-out.
- The **heating plate** is located at the centre of the evacuation chamber and is made from a Nikrothal resistance plate on top of which the dosimeters are placed (see Figure 3.5). A NiCr-Ni thermocouple is attached to the bottom of the plate using an electrically insulating ceramic adhesive. The heating plate itself was constructed in such a way that it follows a meandering pattern. The electrical current's change in direction due

to this pattern reduces the magnetic field induced during the heating process, which could otherwise have an adverse effect on the performance of the photomultiplier.

A negative effect of this pattern is, however, that it is not possible to achieve a homogeneous temperature distribution on top of this type of heating plate. The thermal contact resistance between the plate and the TL-dosimeter as well as the temperature gradient within the dosimeter cause the actual temperature to 'lag behind' the temperature of the thermocouple during the heat-up process. As a result a temperature shift would occur within the observed glow curve. This effect can be minimised by using slow heating rates that allow the dosimeter to adapt to the new temperature. In this work a heating rate of 2.8 °C/s was chosen and all dosimeters were heated to a maximum temperature of 450 °.

- The most important piece of equipment of every thermoluminescence read-out unit is its **photomultiplier**. In this case a photomultiplier of the type 9235QA from THORN EMI is used to detect the light emitted from the dosimeters during the heating process. The photomultiplier sits on top of a rotating metal table so that it can be moved above the evacuation chamber once the dosimeter has been placed onto the heat conducting plate.

In general photomultipliers can be operated in one of two different modes: The continuous current mode and the single photon counting mode. The former is an analogue method where the photomultiplier output is processed electrically. A photon induced current is amplified and measured. Due to all the electrical components involved in this process a lot of background noise is accumulated. Therefore a continuous stream of multiple photons is required to stay above the detection limit. The single photon counting mode on the other hand is a digital method where photons are processed individually with the gain of the photomultiplier set so high that an 'avalanche' of electrons is created by each photon. Therefore each incident photon is counted separately and the detection limit of the photomultiplier is very low. The photomultiplier tube is, however, faster than the digital converter it is followed by. Here each 'avalanche' of electrons is translated into a pulse. As each pulse comes with a certain width only photon counts up to a certain number can be resolved - at higher numbers individual counts will start to overlap. Thus, if too many photons arrive at the same time they

will not be detected. Up to a certain light intensity this 'dead time' can, however, be digitally corrected.

For our purposes the photomultiplier of the TL-DAT-III is set to single photon counting mode. For this set-up dead time effects have been found to be negligible for light intensities below 400,000 cts/°C. For higher intensities losses do occur and are dependent on the counting rate. As these losses can only be corrected digitally up to a certain threshold (between 400,000 and 2,100,000 cts), it was necessary to use optical light filters for the measurement of dosimeters that were exposed to higher dosages of radiation. These filters will be discussed in the following section.

Filters

Two different types of filters were used for the measurements presented in later chapters. First of all infrared glass filters (Type: BG24, thickness: 1 mm) were inserted for all measurements to reduce the background caused by black body radiation, especially at high temperatures. Two infrared filters were placed into the filter housing, which was then fixed on top of the evacuation chamber (see figure 3.6). In addition to that for the reasons outlined in the previous paragraphs on photomultipliers it was necessary to insert optical grey filters between the TL-dosimeter and the photomultiplier tube when measuring TL-dosimeters that were exposed to high-dosage radiation. This way the light emitted from the TL-dosimeters during the heating process first passed through the filters and only a reduced amount reached the photomultiplier. To this end different combinations of optical glass filters can be used to gain a variety of light attenuation factors - a measure of the amount the incident light intensity is weakened by a set of filters. Filters and their impact on the thermoluminescence read-out will be discussed in section 3.3.1 on the data analysis of TL measurements.

Software

The software used for data acquisition with the TL DAT-III was first developed in 1985 at the Institute of Atomic and Subatomic Physics in Vienna and has been refined over the years. Its name is 'MDA - Measuring & Data Acquisition' (Copyright 1985-2014 WEGS Data) and the current version is V03.87. This version of MDA was used for the

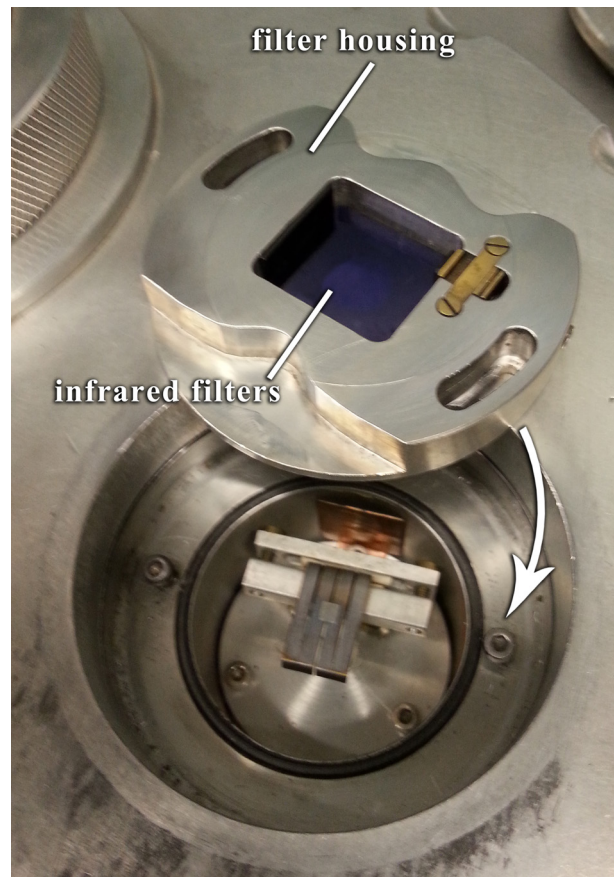


Figure 3.6: Two infrared filters located within the filter housing which can be fixed on top of the evacuation chamber.

data acquisition of all thermoluminescence read-outs presented in this work.

Annealing Oven

A Heraeus KM 170 oven (Heraeus Instruments GmbH, Hanau, Germany) was used for the preparation of the TL-dosimeter chips. The annealing procedure described in the next paragraph was performed on all dosimeters before irradiation as well as after the TL-read-out.

First the Heraeus oven was pre-heated to 400 °C. Once the oven had reached the desired temperature the chips were placed on a plate made from quartz-glass and inserted into the oven. After the dosimeters had been exposed to a temperature of 400 °C for one

hour the heat was turned off and the chips were left to cool for at least 10 hours until they reached room temperature.

3.1.3 Liquid Scintillation Counting

We tried to obtain an absolute value for the amount of tritium produced within the dosimeter material through the measurement of beta-radiation in a liquid scintillation counter. To this end the chips had to be dissolved first and then mixed with a scintillator. The chemical process involved in this procedure, the scintillation cocktail and the liquid scintillation counter will be outlined in the following paragraphs.

Chemical dissolution of TL-dosimeters

After irradiation with thermal neutrons some of the TLD-600 dosimeters contained significant amounts of tritium. In order to be able to measure the low energy beta radiation emitted by tritium with LSC the ${}^6\text{LiF}(\text{Mg,Ti})$ chips had to be dissolved. The chemical process we applied for this purpose was very similar to the one outlined by Pohorecki et. al in their paper on the measurement of tritium production [17].

First of all a 1:4 mixture of nitric acid and hydrogen peroxide was used to dissolve the TLD-600 chips. With the help of pipettes 0.5 ml of HNO_3 ($\geq 65\%$, p.a., ISO, M 63.0 g/mol) and 2 ml of H_2O_2 (30 %, p.a., ISO, stabilised, M 34.01 g/mol) were transferred into a 20 ml LSC plastic container. Next a stir bar was added, which would later enable the liquid inside the container to be mixed properly. After the dosimeter chip was inserted into the mixture the lid of the container was closed to prevent tritium from escaping during the dissolution.

Next the LSC container was fixed inside a metal clamp above a water bath in such a way that the acidic mixture was surrounded by water (see figure 3.7). A magnetic mixer was used to stir the liquid at 300 rpm and heat it at 75°C for approximately 20 minutes. To make this dissolution process more time efficient four plastic containers were fixed together with rubber bands and heated at the same time. It is assumed that most of the tritium bound within the dosimeter material forms water with the oxygen from H_2O_2 and thus remains within the solution.



Figure 3.7: A metal clamp holds the four LSC bottles containing the $\text{HNO}_3 + \text{H}_2\text{O}_2$ mixture and the TLD-600 dosimeters above a water bath. The bottles are dipped in far enough for the acidic mixture to be surrounded by water. The magnetic mixer is set to 75 °C and 300 rpm.

Once the 20 minutes had passed the dosimeters were no longer visible and had been completely dissolved. After a cooling period of about 10 minutes 0.5 ml were extracted from this 'parent solution'. This aliquot was then dissolved in 49.5 ml of distilled water to ensure the pH of the solution would not be too acidic for the scintillation cocktail. Next a 10th of this solution, i.e. 5 ml, was removed with a syringe and transferred to a 20 ml LSC glass container, which were used to keep the quenching of the LSC measurement as small as possible. Finally 5 ml of the UltimaGold scintillation cocktail produced by PerkinElmer was added and the samples were ready for liquid scintillation counting.

Liquid Scintillation Counter

The Tri-Carb 2910 TR Liquid Scintillation Analyser (PerkinElmer) at our institute was used to obtain liquid scintillation measurements.

3.2 Calibration

To be able to correctly analyse the data obtained in this study both the thermoluminescence dosimeters and the liquid scintillation counter had to be calibrated. This chapter gives an overview of the calibration techniques used and their respective results.

3.2.1 Thermoluminescence Dosimeters

Two sets of both TLD-600 and TLD-700 chips were used for the purpose of this thesis. The first set of dosimeters consisted of 37 TLD-600 and 35 TLD-700 dosimeters. They were intended to be used for measurements within the reactor. The second set was comprised of 29 TLD-600 and 19 TLD-700 chips. Here the TLD-700 groups were used for the determination of the filter attenuation factors described in section 3.1.2. The TLD-600 chips were first used for the determination of non-linearity effects outlined in section 3.3.1, followed by an irradiation and subsequent dissolution for use in the LSC.

The dosimeters intended for use in thermoluminescence dosimetry had to be calibrated several times during the course of this work to check their response and account for high-dosage induced sensitivity loss. An initial calibration was done for all of the above mentioned dosimeters except for the TLD-600 chips for which a reference measurement was unnecessary as they were going to be dissolved for LSC measurements. A Cs-137 calibration facility at the Institute of Atomic and Subatomic Physics, Vienna was used for all reference measurements.

The maximum of the dominant peak 5's intensity at 220 °C (described in section 2.2.2) was used for all thermoluminescence measurements presented in this thesis.

The TLD-700 chips of the second set of dosimeters were also irradiated at a distance of 1.5 m from the Cs-137. The irradiation period was 69 hours, which lead to an accumulated energy dose of 26.86 mGy. The results of this calibration can be found in

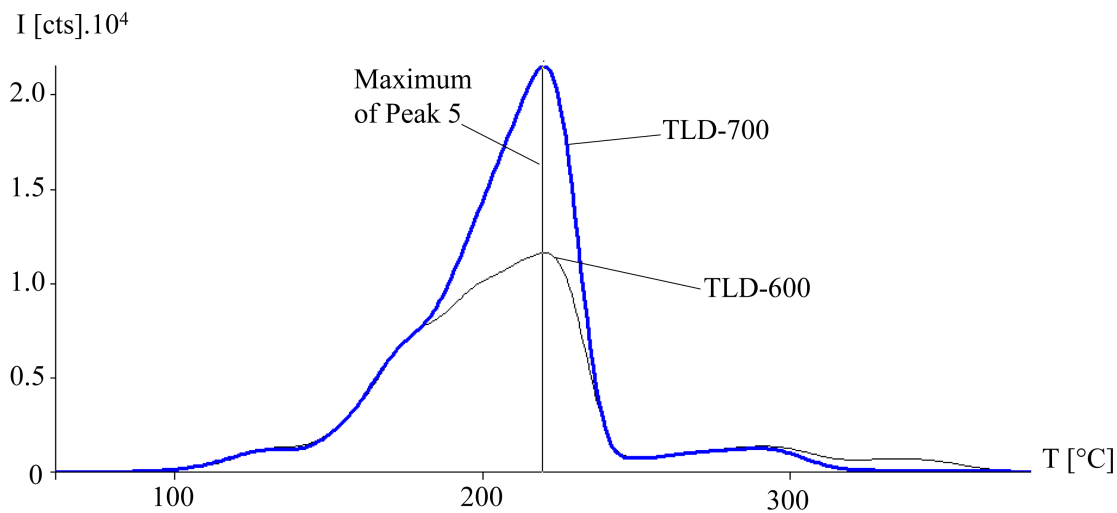


Figure 3.8: Results of the reference measurement of a TLD-600 and a TLD-700 chip. Peak 5's maximum intensity at 220 °C was used as a reference. Irradiation with a Cs-137 source at a distance of 1.5m for 44 hours - resulting energy dosage: 17.34 mGy. A significant difference in the glow curve shape of the TLD-600 chip is visible.

appendix A.2.2.

For the initial reference measurement the first set of TL-dosimeters was irradiated at a distance of 1.5 m for 44 hours resulting in an absorbed energy dose of 17.23 mGy. After the TL read-out the chips were sorted into 12 different groups according to their calibration factor. Each group consisted of 3 TLD-600 and 3 TLD-700 chips, the specific results for the initial calibration can be found in appendix A.2.1.

From these results for the height of the dominant peak 5 an average for the initial calibration factors of both TLD-600 and TLD-700 was found. At 674.70 cts/mGy \pm 3.31 % the average of the TLD-600 calibration factors was found to be significantly lower than that of the TLD-700 chips at 1,188.57 cts/mGy \pm 7.83 %. This fact is also apparent when comparing the glow curves of the two dosimeter types. For the same dosage the TLD-600 and TLD-700 show a significant difference in glow curve shape (see figure 3.8).

For normal dosimeter charges of this type the glow curves as well as the calibration

factors should be the same. It seems that due to some anomalies during their production the glow curves of the whole charge of TLD-600 dosimeters differ from their expected shape. This problem can, however, be compensated by regular reference measurements.

3.2.2 Liquid Scintillation Counting

As was briefly outlined in section 2.3 the efficiency of liquid scintillation counting depends on the 'quench' of the sample that is measured. As radiation is emitted within the sample the scintillation cocktail inside the sample allows for the energy to be transferred and emitted as light which is measured by photomultiplier tubes. Quenching occurs if the energy transfer within the solution is inefficient or a part of the emitted photons is absorbed and does not reach the photomultiplier tubes. There are two types of quench: colour quench and chemical quench. Colour quench occurs if the photons produced by the radiation get absorbed or scattered by the colour within the sample, which results in a reduced amount of light available for detection. Chemical quench occurs if a part of the electrons used for the transfer within the solution is captured, as a result the transfer efficiency decreases. Both effects cause a reduction in the number of photons produced and counted by the liquid scintillation analyser.

To account for this effect the quench of each sample is determined through spectral analysis by the liquid scintillation analyser. In the case of the Tri-Carb 2910 TR, which was used for our measurements, the quench is a function of the t-SIE value. This value is calculated inside the Tri-Carb 2910 TR from the Compton spectrum induced in the sample by an external gamma source. The t-SIE value is a relative value on a scale between 0 (most quenched) and 1000 (no quench). The Tri-Carb 2910 TR automatically measures and calculates the t-SIE value for each sample. Quench curves are used to determine the absolute activity (dpm - decays per minute) of a sample from the counts per minute (cpm) that were measured. The quench curve shows the counting efficiency as a function of the t-SIE value for a particular isotope (see figure 3.9). Thus, the counting efficiency for each sample can be determined and the actual activity can be calculated:

$$\text{Activity [dpm]} = \frac{\text{Measured Value [cpm]}}{\text{Efficiency [\%]}} \quad (3.1)$$

A factory stored tritium quench curve was provided by the Tri-Carb 2910 TR (PerkinElmer).

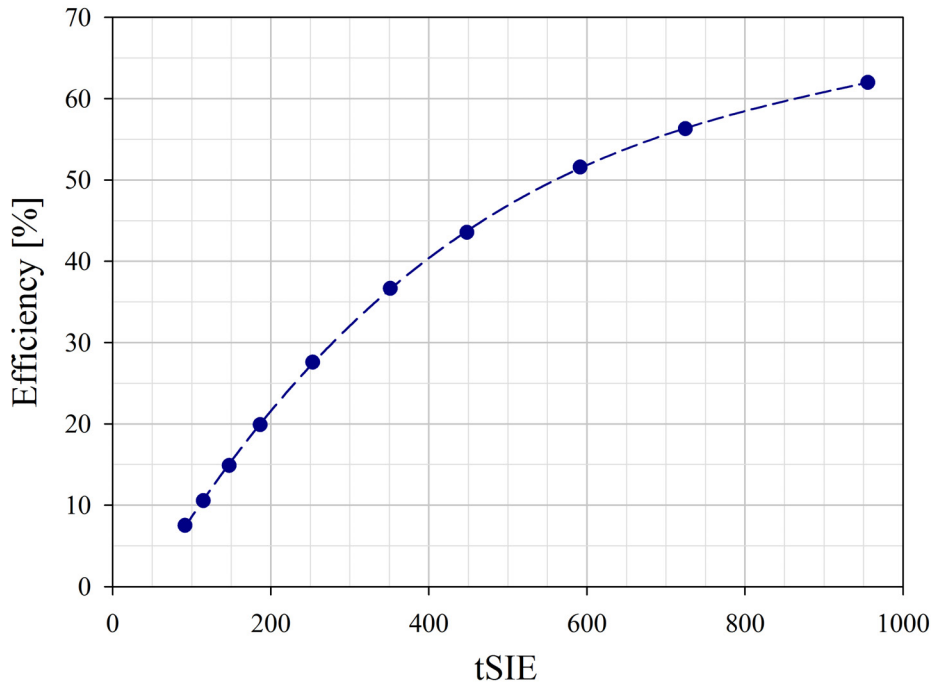


Figure 3.9: The H-3 quench curve shows the relationship between the quench indicator tSIE and its corresponding counting efficiency of tritium samples with LSC.

It can be seen in figure 3.9. To test the validity of this H-3 quench curve a tritium standard solution was used. We prepared two 20 ml LSC samples with 100 and 200 μl of the H-3 solution respectively. The H-3 standard had a known activity of 183,350.0 dpm/ml $\pm 1.5\%$ equal to 3,055.8 Bq $\pm 1.5\%$ in April 2005. From this data the expected activities of the two samples for the time of the measurement (26/05/2014) were calculated and found to be 183.0 Bq for the 100 μl H-3 sample and 365.9 Bq for the 200 μl one. An LSC measurement of these samples gave the results shown in table 3.4. The efficiencies were calculated using the following function which was fitted to the H-3 quench curve:

$$y = -7.2571 + 0.1734.x - 0.0002.x^2 + 5.4077.10^{-8}.x^3 \quad \text{with } R^2 = 1.00 \quad (3.2)$$

A good correlation between the calculations and the measurement of the samples was found for the pure H-3 samples. Another two samples with 100 μl of the H-3 standard mixed with a dissolved and inactive TLD-700 chip each was prepared. The TLD-700 chip had been dissolved according to the procedure outlined in section 3.1.3. The results of the measurement of these samples can be found in table 3.4. Due to the addition of

H-3 Std [μl]	Count Rate [cpm]	tSIE	Efficiency	Activity [dpm]	Activity [Bq]	Expected Activity [Bq]	Relative Error
100	4919	486.24	46.1 %	10,677	177.9	183.0	2.8 %
200	9600	473.38	45.3 %	21,191	353.2	365.9	3.5 %
100 (diss. TLD-700)	3054	287.88	30.9 %	9,881	164.7	183.0	10.0 %
100 (diss. TLD-700)	2982	283.04	30.4 %	9,797	163.3	183.0	10.8 %

Table 3.4: LSC measurement results for the 100 and 200 μl H-3 standard samples and 100 μl H-3 sample combined with a dissolved TLD-700 chip. Evaluated channel: 0 - 18.6 keV, count time: 120 min, count rate was corrected for background; efficiency calculated from tSIE value given by the Tri-Carb 2910 TR.

the dissolved chip the samples had a much lower quench indicator of approximately 285 and thus a much lower corresponding counting efficiency than the pure H-3 samples. At a value of 164 Bq the measured activity was 10.4 % lower than the expected value of 183 Bq. These results were reproduced with another independent sample. Therefore it can be concluded that the H-3 quench curve's accuracy seems to decrease at lower tSIE values. All samples measured for the purpose of this research contained the same amount of dissolved dosimeter material resulting in a tSIE value of around 285. Therefore equation 3.2 was modified to incorporate a correction factor accounting for this 10.4 % loss.

3.3 Data Analysis

To be able to interpret the data correctly and produce useful results with thermoluminescence dosimetry and liquid scintillation counting several influencing factors had to be accounted for beforehand. These effects will be discussed in the following sections.

3.3.1 Thermoluminescence Read-out

There are several parameters that can have an impact on the dosage measurement with TL-dosimeters, such as the black body background and the type of filter used during the TL read-out as well as non-linearity effects due to high dosage radiation. All these factors need to be taken into account when the dosage D_{abs} absorbed within the dosimeter

is read-out and calculated:

$$D_{abs} = I_{net} \cdot f_{cal} \cdot f_a \cdot f_{sl} \quad (3.3)$$

Here I_{net} describes the net TL-signal, f_{cal} the individual dosimeter's calibration factor, f_a the filter attenuation factor and f_{sl} the supra-linearity factor. The following sections will discuss the different correction factors in detail and explain when and how they need to be applied.

The read-out from the maximum of peak 5's intensity at 220 °C (described in section 2.2.2) was used for all thermoluminescence measurements presented in the following sections.

Black Body Background and Photomultiplier Noise

Especially for low-dosage read-outs where only 2 infrared filters and no grey filters are inserted the background induced by black body radiation and photomultiplier noise can have a significant impact on the glow curve structure. Figure 3.10 shows an example of such a TL read-out - it is evident that the black body radiation adds a notable contribution to the thermoluminescence signal, especially at high temperatures. The photomultiplier noise is fairly low and apparent at all temperatures. During a standard procedure both phenomena are corrected by simply fitting a curve to the high temperature part of the glow curve around 380 - 450 °C and subtracting said curve from the rest of the

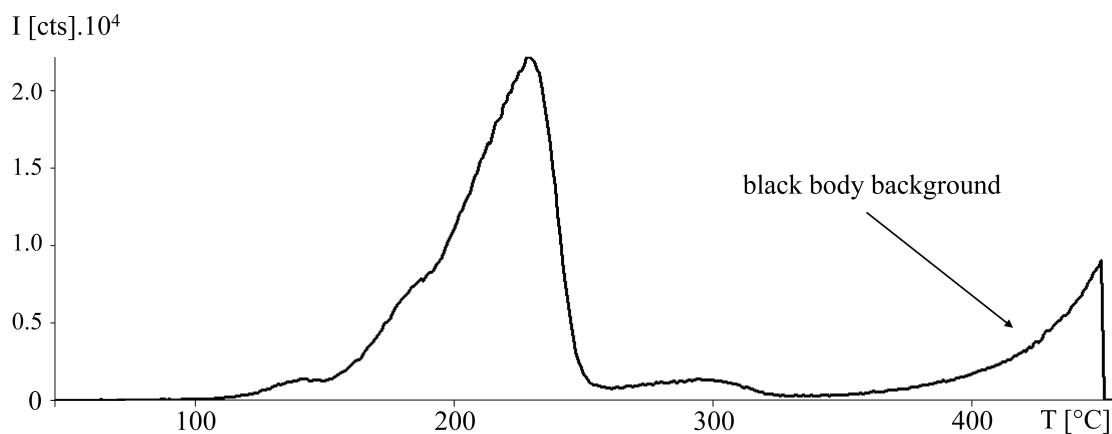


Figure 3.10: A glow-curve without any correction of the black body radiation - especially at high temperatures the background is significant.

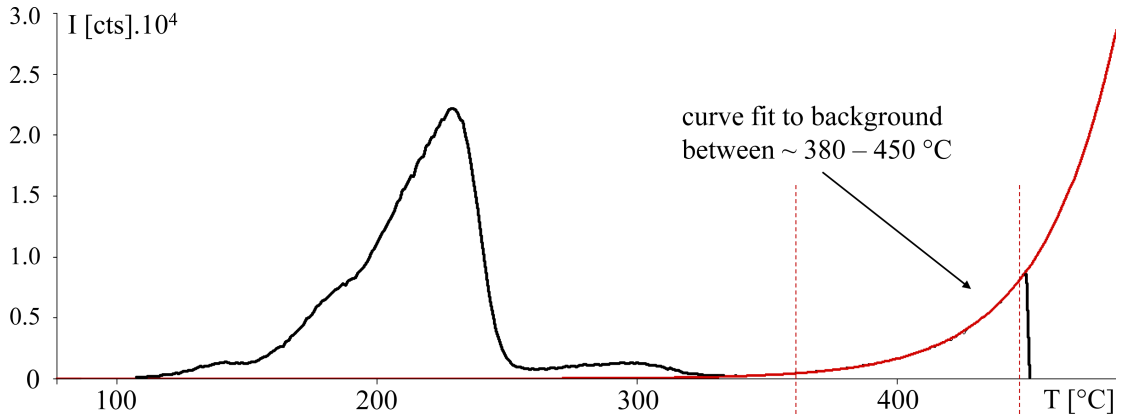


Figure 3.11: A curve is fit to the black body background between around 380 - 450 °C and the photomultiplier noise. To obtain the background corrected net signal this curve is subtracted.

read-out. In this manner a background corrected net TL-signal can be obtained. The net glow curve is then used to read-out the maximum of peak 5 I_{net} at 220 °C, which is needed for the calculation of the dosage in equation 3.3. This standard procedure is especially important for low intensity TL signals.

The Filter Attenuation Factor

By taking the photon count from a filtered TL-readout of a peak-maximum I_f and multiplying it with the attenuation factor f_a the actual, unfiltered photon count I_{unf} of the peak can be calculated:

$$I_{unf} = I_f \cdot f_a \quad (3.4)$$

Two types of neutral glass filters produced by the company 'Schott' were used for the measurement of high-dosage radiation. By definition neutral glass filters have a mostly stable transmission factor τ over a desired wave-length range. LiF(Mg,Ti) TL dosimeters mainly emit light between 300 and 500 nm with a maximum at 380 nm. Therefore we used NG3 ($\tau \sim 10\%$ at $\lambda = 500$ nm) and NG10 ($\tau \sim 0.85\%$ at $\lambda = 500$ nm) filters (Thickness: 1 mm) produced by the company Schott in this study because of their mostly stable transmission coefficients in this wavelength range.

Filter Combination	Attenuation Factor f_a	Absolute Error	Relative Error
1 x NG3	28.9	0.3	1.1%
2 x NG3	504	23	4.5%
3 x NG3	4,410	556	12.6%
2 x NG3 + 1 x NG10	9,571	1,961	20.5%
2 x NG3 + 3 x NG10	40,062	11,238	28.1%

Table 3.5: Attenuation factors for different combinations of the filters NG3 and NG10, data taken from Marko Mayr's bachelor thesis [12]

Eventhough the transmission coefficients for these filters are known they can, however, not be used to calculate the light attenuation factor in this particular case. The reason for this is that the filter strength is affected by diffuse light reflected off the aluminium wall of the filter housing, which is able to reach the photomultiplier. While this is a statistically constant and reproducible effect, it makes the calculation of the attenuation factor of a specific filter combination impossible. Thus, an empirical approach was necessary to find the attenuation factors for the different filter combinations.

Some of these factors had already been determined by Marko Mayr [12] and can be found in table 3.5. We were mainly interested in the last filter combination shown in this table as its attenuation factor would have been high enough for the radiation dosages found in the TRIGA Mark-II. This filter combination was, however, not available anymore as the third NG10 filter had broken. Hence, it was necessary to find new filter combinations that would serve our needs.

To this end 16 TLD-700 chips were irradiated with a Sr-Y-90 beta radiation source at the Institute of Atomic and Subatomic Physics, Vienna for 8 minutes. At a dosage rate of 2.7 Gy/min the dosimeters were subjected to a total dosage of approximately 21.6 Gy. Without using a filter (and assuming no dead time limitations for the photomultiplier) this dosage would theoretically cause a peak 5 TL-read-out of about 25,000,000 photon cts for a TLD-700 chip. In practice, using the well known filter combination '3 x NG3' with a filter attenuation factor of 4.409.5 a peak 5 read-out of about 5600 cts would be obtained. We assumed that the attenuation factor of the new filter combinations would lie about halfway between that of '3 x NG3' and '2 x NG3 + 3 x NG10' at around

Filter Combination	Attenuation Factor f_a	Absolute Error	Relative Error
4 x NG3	11,692	1,494	12.8%
3 x NG3 + 2 x NG10	16,865	2,401	14.2%
4 x NG3 + 1 x NG10	18,462	2,349	12.7%

Table 3.6: Results for the attenuation factors of three new sets of combinations between the filters NG3 and NG10

18,000. This allowed an estimate for the peak 5 read-out of around 1,400 cts, which would be at the lower end of statistically significant detectability. As dosage rates much higher than 21.6 Gy were expected from the irradiations within the reactor these new filter combinations would lie in the optimum range for our future measurements.

A maximum of 5 glass filters can be placed on top of the two infrared filters within the filter housing. We had four NG3 and two NG10 filters available. The 16 TLD-700 chips were split into 4 groups of 4 and were measured with the three new filter combinations ‘4 x NG3’, ‘3 x NG3 + 2 x NG10’ and ‘4 x NG3 + 1 x NG10’. To be able to obtain absolute values for their attenuation factors the fourth group of dosimeters was measured with the known combination ‘3 x NG3’ in place. The results of these measurements were in good agreement with our estimates and can be seen in table 3.6. The relative errors of around 13 % are probably caused by the diffuse background mentioned above. A calibration was done for all 16 TLD-700 dosimeters that were used in this measurement series and the results in table 3.6 were adjusted accordingly.

Non-linearity Effects

As has already been described in section 2.2.2 two different non-linearity effects can be distinguished when doing high-dosage thermoluminescence dosimetry. The first one is apparent during the primary TL read-out of a dosimeter after exposure to high-dosage radiation and leads to either supra-linear behaviour and saturation of peak 5. The second phenomenon is observed during all subsequent TL measurements of the same dosimeter as the high amounts of absorbed radiation lead to a loss of sensitivity in peak 5. These two effects will be discussed in the next paragraphs.

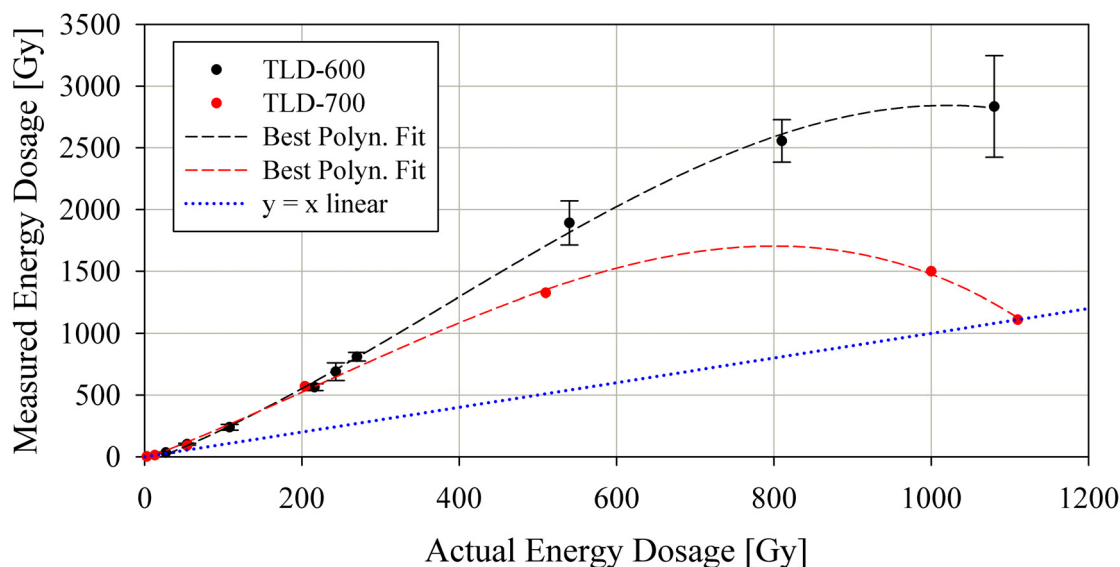


Figure 3.12: Supra-linear behaviour and saturation of TLD-600 and TLD-700 chips after exposure to high-dosage radiation. As a reference the dotted blue line represents the linear plot $y=x$. TLD-700 data taken from: [12] - no error values available.

Supralinearity

The supra-linear behaviour of LiF(Mg,Ti) dosimeters is generally well known and had also recently been reconfirmed in particular for the charge of TLD-700 dosimeters used in this project [12]. However, as was explained in section 3.2.1 of this work the batch of TLD-600 chips used for the purpose of this research do not conform to the standard glow curve structure. It was therefore necessary to determine whether their supra-linear (and saturation) behaviour differed from the norm as well.

To this end the 29 chips of the second set of TLD-600 dosimeters were irradiated with the Sr-Y-90 beta radiation source at the Institute of Atomic and Subatomic Physics, Vienna for different lengths of time. As the energy dosage rate of this source is well known the actual energy dosage absorbed by the dosimeters could be calculated and compared with their respective peak 5 TL read-outs. A comparison of the results for both TLD-600 and TLD-700 dosimeters is shown in figure 3.12. Unfortunately no error values were available for the data of the TLD-700 dosimeters taken from Marko Mayr [12] - a repetition of these measurements was not possible due to the limited

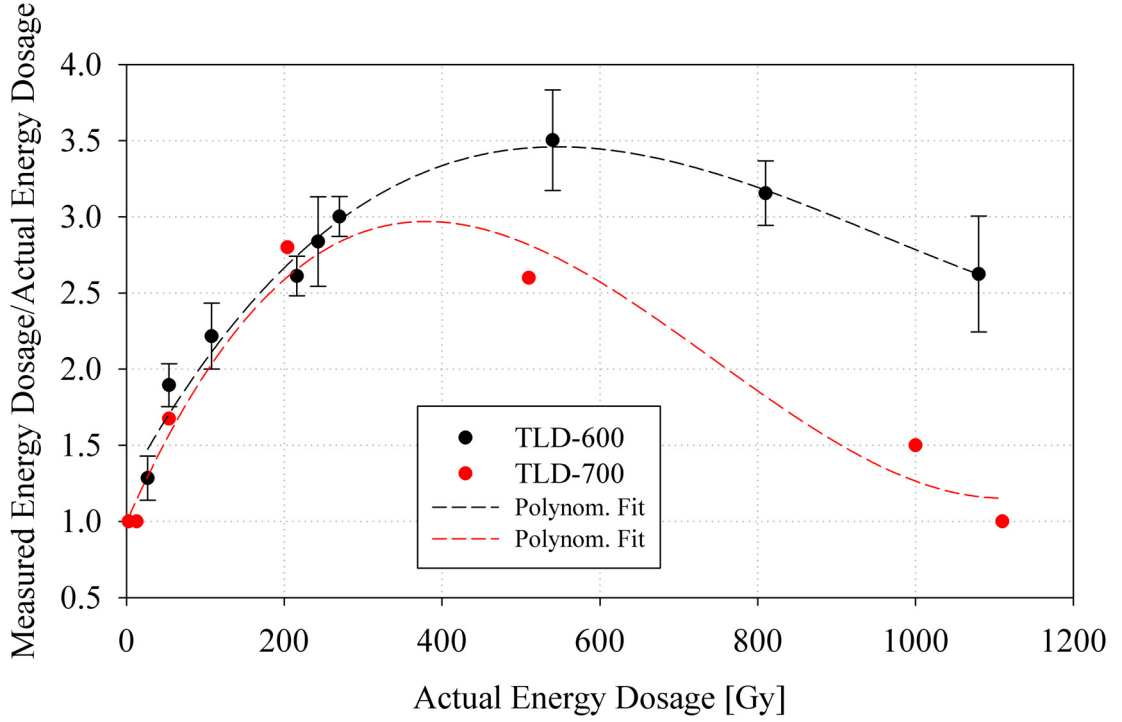


Figure 3.13: A comparison of the actual energy dosage to the quotient of the measured and actual dosage. The over-estimation of the LiF(Mg,Ti) dosimeters at high dosages is clearly visible. TLD-700 data taken from: [12] - no error values available.

amount of dosimeters available for our research project. The comparison of the available data does, however, show that the TLD-600 chips are more strongly supra-linear than their TLD-700 counterparts. In order to apply this information to subsequent high-dosage TL measurements third order polynomial curves were fitted to the data points. The resulting equations were used to determine the actual energy dosage D_a from the dosages measured D_{TL} with the TL-dosimeters. The equations for the TLD-600 and TLD-700 chips respectively are ($R^2 = 0.9993$ for both):

$$D_{TL} = -50.8226 + 2.4243.D_{act} + 0.0036.D_{act}^2 - 3.1347.10^{-6}.D_{act}^3 \quad (3.5)$$

$$D_{TL} = -15.8574 + 2.4017.D_{act} + 0.0021.D_{act}^2 - 2.9744.10^{-6}.D_{act}^3 \quad (3.6)$$

Once the actual dosage is known the quotient between the actual and measured dosage can be determined as:

$$f_{sl} = \frac{D_{act}}{D_{TL}}. \quad (3.7)$$

The factor f_{sl} is the supra-linearity/saturation factor needed for the determination of the correct energy dosage absorbed by the dosimeter in equation 3.3. Generally supra-linearity seems to start to take effect between 10 and 20 Gy. Thus, the necessary corrections need to be applied to the TL signal for measurements in this dosage range and upwards of it.

For comparison's sake this non-linearity effect can also be expressed as the quotient of the measured and actual energy dosage values, which makes the over-estimation of the dosage in the TL dosimeters even more apparent(see figure 3.13). While the maximum of the TLD-700 supra-linearity lies at a quotient of around 3 the TLD-600 chip's maximum goes up to a factor of around 3.5.

Sensitivity Loss

If dosimeters are used for high-dosage measurements repeatedly another non-linearity phenomenon occurs: peak 5 experiences a loss of sensitivity. The sensitivity loss of peak 5 manifests itself in the change of a TLD chip's response to radiation. This is an important effect that needs to be monitored and corrected for especially if dosimeters are to be reused after exposure to high dosages of radiation. To this end regular reference measurements are necessary to keep track of the individual change in each dosimeter's calibration factor.

For this purpose all our dosimeters were repeatedly checked through irradiation with a Cs-137 source and subsequent TL measurement. Figure 3.14 shows an example of such a repeated measurement. The dosimeter groups 2 to 5 contain 3 TLD-600 and 3 TLD-700 dosimeters each. After they had been exposed to low reactor powers once or twice a calibration measurement was done to check for sensitivity loss. Both dosimeter types in all groups had lost a certain amount of sensitivity and the new calibration factors were between 90 and 95 % of their initial values. This is apparent from the dark blue and black bars described as TLD-600 and TLD-700 *before* in figure 3.14.

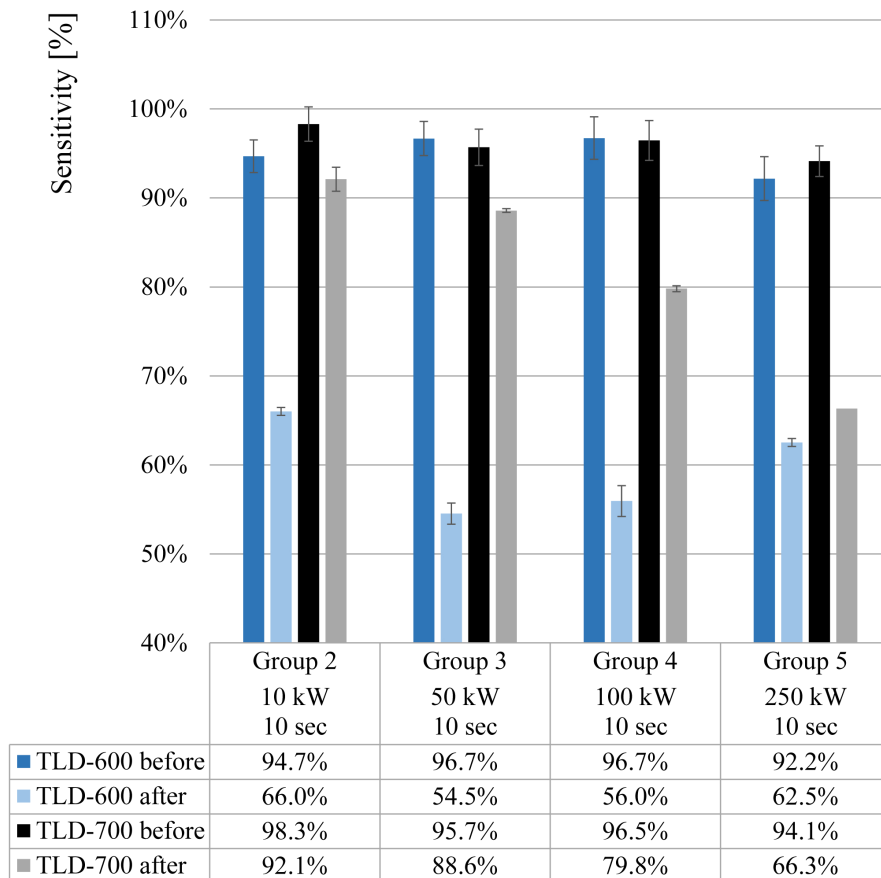


Figure 3.14: The dark blue (TLD-600 before) and black (TLD-700 before) bars show the sensitivity loss after one or two low power irradiations within the reactor, where 100 % represents the initial calibration factor. The light blue (TLD-600 after) and grey (TLD-700 after) bars represent the sensitivity after irradiation at reactor powers of between 10 and 250 kW. A significant loss of sensitivity is visible.

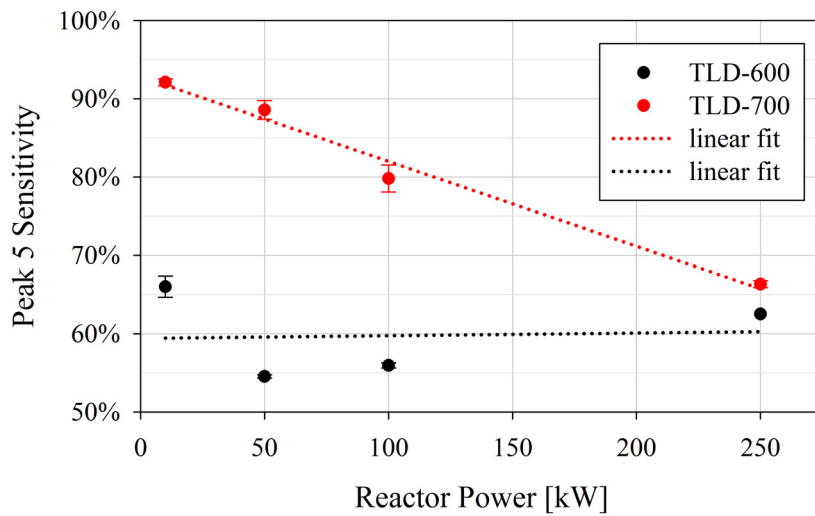


Figure 3.15: Peak 5 sensitivity after irradiation at different reactor powers. While the neutron- and gamma-sensitive TLD-600 chips show a significant loss at all wattages, the purely gamma-sensitive TLD-700 chips show an almost linear decrease with reactor power.

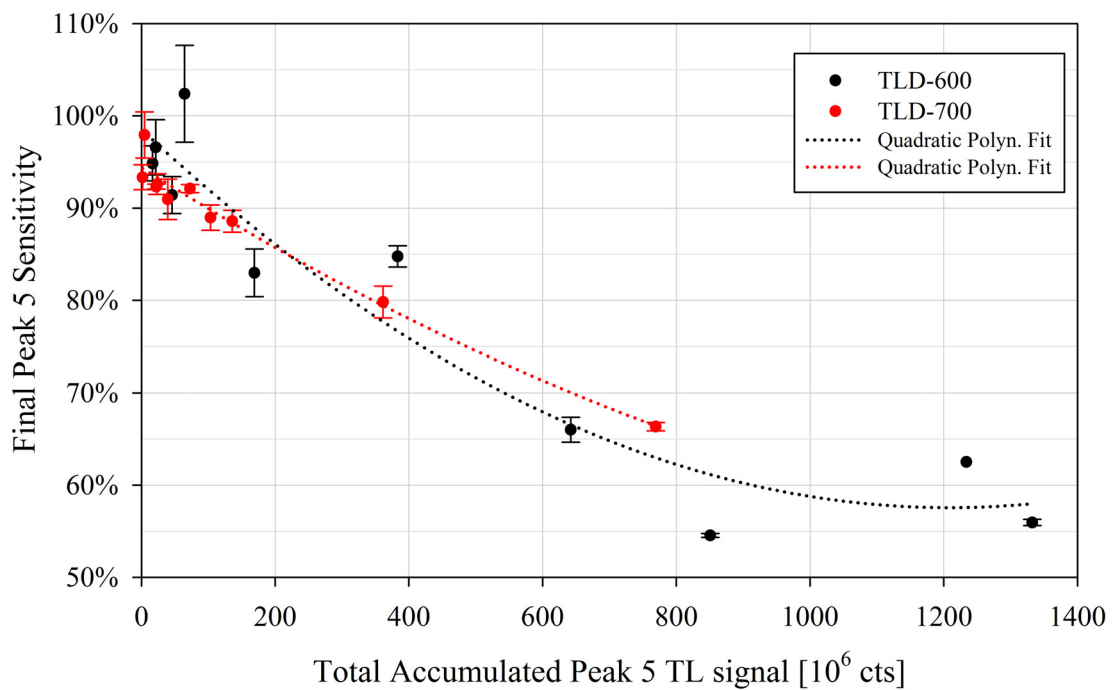
After this evaluation the same dosimeter groups were subjected to higher reactor powers of between 10 and 250 kW. After the initial TL signal was read out the dosimeters were annealed and another reference measurement was done to check their sensitivity. The results represented by the light blue (TLD-600) and grey (TLD-700) bars denoted as (after) in figure 3.14. Due to their neutron detection capabilities the TLD-600 chips had been damaged more severely and showed a higher loss of sensitivity than their TLD-700 counterparts. While the sensitivity loss of the TLD-600 dosimeters did not show any dependence on the reactor power, the TLD-700 chips showed an almost linear sensitivity decline with reactor wattage (see figure 3.15).

From these results it is obvious that it is important to know the exact history of each dosimeter to be able to acquire exact measurements. Looking at the history of 10 dosimeter groups used in this study and analysing the data it was possible to find the total amount of photon counts the peak 5 had accumulated over the course of this research. Plotting this lifetime TL signal count against the sensitivity of the dosimeter during the last reference measurement shows the relationship between high-dosage ra-

diation exposure and the dosimeters' response (Figure 3.16).

The integral TL-signal had to be used as a reference instead of an energy dosage as the exact determination of the same was impossible at the high neutron fluxes within the reactor. Quadratic polynomial functions were fit to the data point in order to estimate a dosimeter's loss of sensitivity assuming its thermoluminescence history is known.

Through the knowledge of a dosimeter chip's history and/or regular reference measurements it is, thus, possible to correct the calibration factor f_{cal} in equation 3.3 in such a way that a dosage measurement is still possible after the repeated use of a TL chip. All results presented in section 4 of this study were corrected for this effect.



3.3.2 LSC Measurement - Estimate of Tritium Activity

Apart from the efficiency/quench calibration outlined in section 3.2.2, no further corrections had to be accounted for in the data obtained from liquid scintillation counting. However, to be able to put the acquired data into context it was found to be useful to calculate an expected value for the activity of the tritium within the dosimeters. This was done using the equation for neutron activation (see section 2.4.4). It is assumed that after exposure most of the produced tritium bonds with fluoride atoms and thus remains within the dosimeter material.

Several parameters need to be known for the correct calculation of the expected tritium activity from equation 2.10. Firstly the amount of lithium-6 atoms within the dosimeter needs to be calculated. This can be done using the weight of the dosimeter and the ratio of the lithium isotopes within the TLD-600 chips. With 95.62 % ^6LiF and 4.48 % ^7LiF and a mass of 23 mg per chip the amount of ^6Li atoms N in a TLD-600 dosimeter was calculated to be $5.30 \cdot 10^{20}$. The pneumatic transfers system's end is located next to the rotary specimen rack within the reactor. Here the dosimeters are exposed to a neutron flux ϕ of approximately $1.73 \cdot 10^{12} \text{ n cm}^{-2}\text{s}^{-1}$ at 250 kW reactor power. The interaction responsible for the tritium production within the dosimeter $^6\text{Li}(n, \alpha)^3\text{H}$ has a cross section of $\sigma = 940 \text{ b}$ for thermal neutrons. Tritium has a half-life of 12.32 years, from which the corresponding λ may be calculated.

With all of this information it is possible to calculate an estimate for the tritium activity within a chip if the reactor power and irradiation time t are known. Assuming a linear relationship between the reactor power and its corresponding neutron flux the results in table 3.7 were obtained.

Reactor Power [kW]	Neutron Flux [n cm⁻² s⁻¹]	Mass of chip [mg]	Irradiation Time [s]	Activity [Bq/chip]	Activity [Bq/mg]
10	6.92E+10	23	10	615	26.7
50	3.46E+11	23	10	3,074	133.7
100	6.92E+11	23	10	6,148	267.3
250	1.73E+12	23	10	15,370	668.3

Table 3.7: Calculated tritium activities for dosimeters irradiated at different reactor powers and corresponding neutron fluxes.

Results and Discussion

In this chapter we present the results from the thermoluminescence and LSC measurements, which were done to acquire data on both the neutron flux inside the reactor and the tritium production within the dosimeter material. The following chapter is subdivided into three sections.

The first two sections discuss the results obtained with the thermoluminescence method. Primary and secondary thermoluminescence measurements will be presented in two separate sections. While primary measurements were acquired from the dosimeters directly after irradiation, secondary measurements concern themselves with the phenomenon of the tritium build-up. The tritium build-up is caused by the self-irradiation of the dosimeter through the tritium produced inside the material during neutron irradiation. It is termed ‘secondary’ measurement as it can only be observed after the initial/primary measurement and the subsequent annealing procedure are completed.

In the third section of this chapter we present the results for the tritium activity within the dosimeters. Measurements from TLD-600 chips were acquired through the dissolution and subsequent LSC measurement of said chips. Furthermore we discuss an attempt at finding a correlation between the obtained tritium activity and the secondary TL measurements presented in the second section of this chapter.

4.1 Primary TL Measurement

By measuring the primary thermoluminescence signal after irradiation within the TRIGA Mark-II reactor we were aiming to find a direct correlation between this measurement and the neutron flux within the reactor. A net neutron signal was obtained by irradiating both TLD-600 and TLD-700 dosimeters at the same time and subtracting the gamma component (TLD-700) of the measurement from the mixed gamma and neutron signal acquired with the TLD-600 chips. Like the neutron flux, the net neutron TL signal acquired was expected to have a linear correlation with both the reactor power and the irradiation time.

4.1.1 Correlation with irradiation time

To investigate the correlation of the net neutron TL signal with time four dosimeter groups were irradiated within the reactor in two separate sessions. During each session one dosimeter group was irradiated for 10 seconds and the other group was irradiated for 30 seconds at the same reactor wattage. A power of 1 kW was chosen as this reactor wattage had been found to deliver a sufficiently high TL signal without a strong influence from non-linearity effects. After correction of the non-linearity effects and the filter attenuation we expected to find a factor of 3 between the net neutron TL signals for the different irradiation times.

Figure 4.1 shows the results we obtained from this measurement. A factor of 5.1 was found between group 1 and 2, while a factor of 3.3 was found between group 5 and 7. The average total error for the measurements seemed to lie at around 7 %. Only group 1's measurement showed a much higher error of 15.88 %.

From these numbers the second set of dosimeters seems to have a much better correlation with time than the first. The poor result for group 1 and 2 can, however, be explained. While a total of 2 NG3 and 3 NG10 filters was used for the measurements of group 1 and 2, only 3 NG3 filters were inserted for the measurements of group 5 and 7. Hence, the signal from group 1, which had a low intensity to begin with, was decreased even further. This led to a low number of photon counts and poor statistics. The total error in figure 4.1 was calculated by taking the standard deviation of both the TLD-600 and TLD-700 measurements as well as the counting error \sqrt{N}/N into consideration.

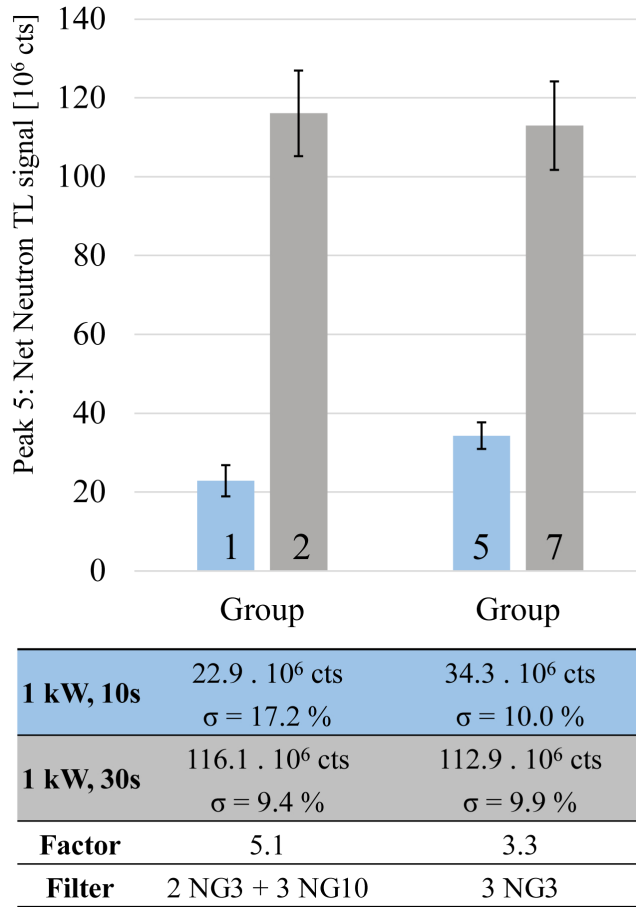


Figure 4.1: Groups 1, 2, 5 and 7 were irradiated at a reactor power of 1 kW. In the first session group 1 was irradiated for 10s and group 2 for 30s. The same irradiation times were used in a second session for group 5 and 7 respectively. During the measurements, however, two different sets of filters were in place.

Taking all of these points into account a decent correlation between the net neutron TL signal and irradiation time was found at a reactor power of 1 kW. The results have, however, also shown that the selection of a filter adequate for the expected neutron fluence is of utmost importance for good counting statistics. More measurement series are necessary to confirm the reproducibility of this correlation.

TLD Group	Net Neutron TL signal [10^3 cts]	Std. Dev.	Total Error	Reactor Power [kW]	Expected Factor	Measured Factor
7	1,608	49.0 %	49.7 %	0.01		
8	4,955	10.1 %	15.2 %	0.1	10	3.08
9	34,676	4.0 %	9.7 %	1	10	7.00
10	364,975	1.3 %	8.6 %	10	10	10.53
2	292,577	2.1 %	9.0 %	10		
3	798,193	3.3 %	10.0 %	50	5.0	2.73
4	1,199,697	3.1 %	10.3 %	100	2.0	1.50
5	797,236	12.0 %	19.5 %	250	2.5	0.66

Table 4.1: Peak 5 net neutron TL signals at different reactor powers. Results corrected for supra-linearity and sensitivity loss. Irradiation time: 10 seconds. Filters: '3 NG3' for 10 W - 10 kW, '4 NG3 + 1 NG10' for 50 - 250 kW.

4.1.2 Correlation with reactor power

Just like the neutron flux has a linear relationship with the reactor power, the same is expected of the net neutron TL signal obtained from the the TLD-600 and TLD-700 pairs. Thus, 8 dosimeter groups were separated into two sets. For all groups the irradiation time was 10 seconds. The first set including groups 7 to 10 was irradiated at low reactor powers between 10 W and 10 kW. The second set included the groups 2 to 5 and was irradiated at high reactor wattages of between 10 kW and 250 kW. Upon exiting the fast pneumatic transfer system the dosimeters emitted moderate levels of radiation in the μSv range. This was due to the activation of fluorine contained within the dosimeters. With a half life of 11 seconds fluorine-20 did, however, decay quickly and the radiation was back at low levels soon. Nonetheless, groups 2 to 5 were left at the exit position of the fast pneumatic transfer system overnight for safety reasons.

The results of these irradiations can be found in table 4.1. All net neutron TL signals were calculated using the pair method outlined in section 2.4.3. All results were corrected for supra-linearity effects and the sensitivity loss was accounted for with additional reference measurements. 3 NG3 filters were used for measurements of dosimeters irradiated at reactor powers between 10 W and 10 kW. For higher reactor wattages a configuration of '4 NG3 + 1 NG10' filters was used.

The factors that we expected to find between different reactor powers can be seen in the column next to the different wattages. When comparing these expected factors with

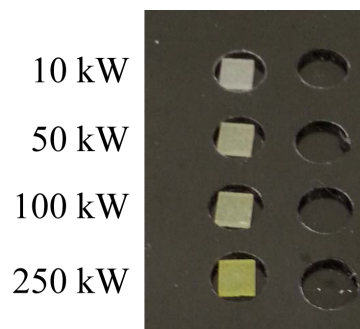


Figure 4.2: Due to radiation damage the dosimeters' optical properties change. The TLD-600 dosimeter chips turned a shade of green at reactor powers between 50 and 250 kW. The colour intensified as the wattage was increased.

the factors that were actually measured, it becomes apparent that good results can only be obtained for power ranges between 1 and 10 kW. Especially at very low and very high reactor powers the measurements do not fit together well and high total errors were found.

The extremely high total error of 49.7 % at 10 W is caused by the very low neutron flux at this power range. The neutron induced TL signal in the TLD-600 dosimeters is so very low that it can barely be resolved above the gamma background of the reactor. Therefore measurements at this power level are unusable due to poor statistics. This measurement did, however, help us in determining the lower limit of neutron detection within the TRIGA Mark-II.

In the high reactor power range upwards from 10 kW non-linearity effects became significant. The dosimeters irradiated at wattages of 50 kW and higher were severely damaged by the radiation. This is apparent in the change of their optical properties. The dosimeters turned a shade of green and the colour intensified with reactor power (see figure 4.2).

Apart from their colour the damage is also clear from the measurements. The measured factors deviate from the expected ones, especially the factor between 100 kW and 250 kW which unexpectedly is below 1. While the peak 5 of the TLD-600 dosimeters irradiated at 50 kW and 100 kW seems to be close to saturation their structure is still

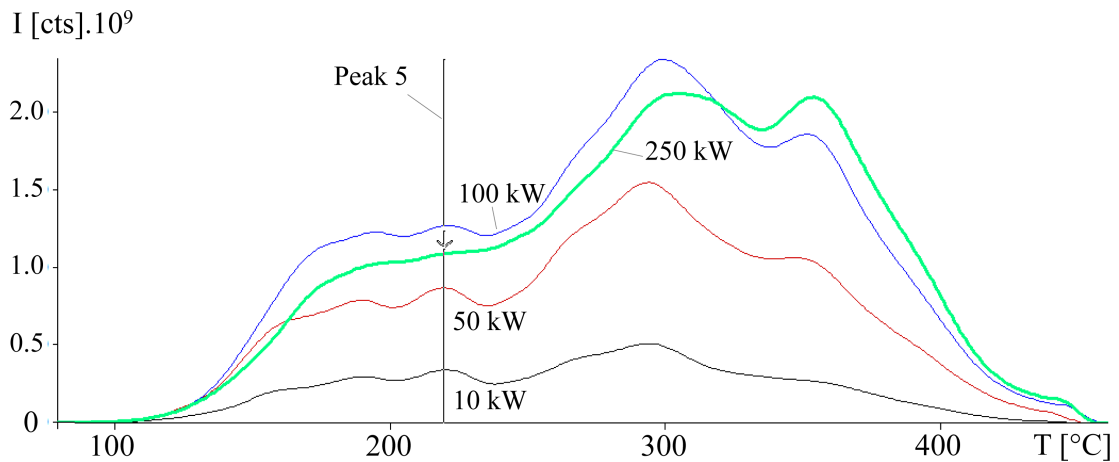


Figure 4.3: The TLD-600 TL signal after irradiation at different reactor powers. Irradiation time: 10 seconds. Glow curves corrected for filter factor. The intensity of the 250 kW signal is mostly smaller than that of the 100 kW. In addition the 250 kW glow curve does not have any visible peak 5 - the dosimeter was completely saturated.

similar to that of dosimeters irradiated at lower wattages (see figure 4.3). However, the TLD-600 chips irradiated at 250 kW seem to saturate completely. Their peak 5 is no longer visible and their intensity largely lies below that of the chips irradiated at 100 kW. Only the high temperature part of their glow curve is still higher than that of the other dosimeter groups. A second measurement with completely untouched TLD-600 dosimeters in the reactor power range between 10 kW and 250 kW showed the same results. Thus, a negative impact on the glow curve structure from previous low level irradiations can be ruled out.

Generally the primary TL signal seems to be a very unreliable source for the measurement of the mixed neutron and gamma field within the reactor. At low reactor powers the flux is not large enough to give rise to a viable TL signal. On the other hand at high reactor powers the non-linearity effects in the primary TL signal are so large that even with correction factors in place no usable measurements can be acquired. Reasonable results were only obtained at reactor powers between 1 kW and 10 kW. In this range primary TL measurements may be able to help determine the neutron flux inside the fast pneumatic transfer system. This is, however, only possible if a neutron calibration is available for the dosimeters, which is not the case for this particular charge of TLD-600 dosimeters. In general it is very difficult to estimate what impact the anomalous glow

curve structure of the TLD-600 chips had on these measurements. In addition we only had a limited amount of TL-dosimeters available for this study, which made a proper reproduction of all results impossible. In the future it would, thus, be prudent to repeat these measurements using a different charge of TL dosimeters with a well defined glow curve structure and a known neutron calibration.

4.2 Secondary TL Measurement - Tritium Build-Up

Tritium solely emits low level beta radiation with a maximum energy of around 18.5 keV. It has a half life of 12.3 years. Already after a few days the tritium produced within the TLD-600 dosimeters can cause a heightened background TL signal. The tritium within the dosimeters was produced by the neutron radiation inside the reactor. Thus, like the primary TL signal this secondary signal should have a linear relationship with the reactor power and its corresponding neutron flux for identical irradiation times. Likewise the TL signal of the tritium build-up should show a linear growth with irradiation time at identical reactor powers.

4.2.1 Correlation with irradiation time

As outlined in section 4.1.1 the dosimeter groups 1 and 2 had been irradiated at a reactor power of 1 kW for 10 and 30 seconds respectively. After the evaluation of the primary TL signal the dosimeters were annealed at 400°C and left to cool in the oven overnight. After this ‘reset’ the TLD-600 dosimeters of both groups were put aside and left to accumulate a tritium build-up for about 7 days. Once this period of time had passed the dosimeters were measured and a daily tritium induced energy dosage rate was calculated from read-outs of peak 5. Next the dosimeters were annealed again and the whole process was repeated several times to acquire a number of dosage rate measurements. We expected to find a factor of 3 between the TL signal read-outs for the two different times.

The results of consecutive weekly measurements over the course of two months are displayed in figure 4.4. An average (natural background corrected) energy dosage rate of $45.5 \mu\text{Gy/d} \pm 13.8 \%$ was found for the TLD-600 chips of group 1, which had been irradiated at 1 kW for 10 seconds. This rather large error is due to the low counting

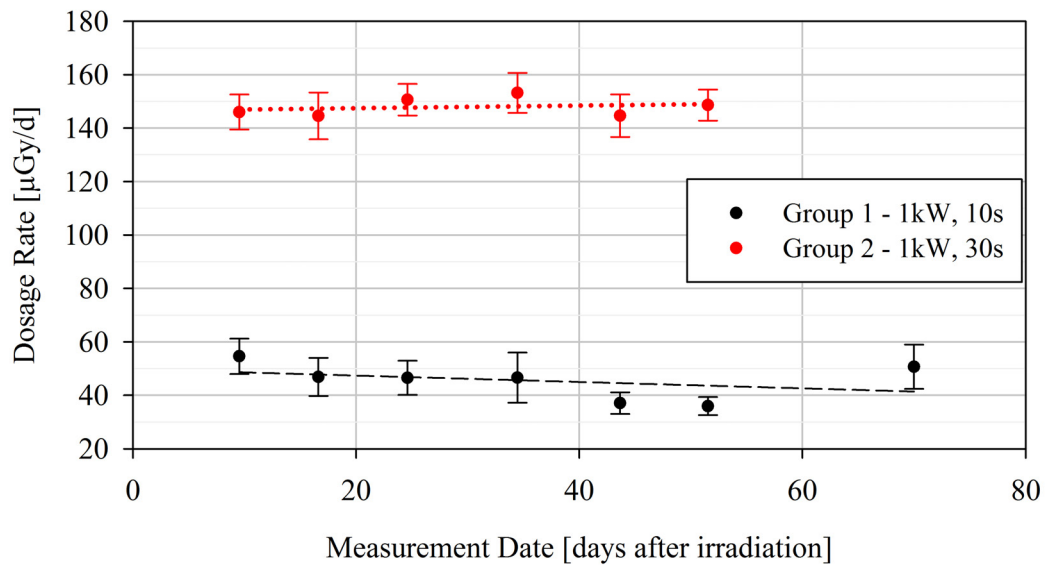


Figure 4.4: Dosage Rate measurements of the dosimeter groups 1 and 2 irradiated at a reactor power of 1 kW for 10 and 30 seconds respectively. All measurements were corrected for natural background radiation. Only infrared filters were used. The daily energy dosage rates were calculated by averaging the TL dosage measurement over the accumulation period.

statistics of the tritium build up after a short accumulation time of just one week. The average dosage rate of group 2, irradiated at 1 kW for 30 seconds, was determined to be $147.9 \mu\text{Gy/d} \pm 2.2 \%$. Thus, a factor of 3.25 was found between the two irradiation times, which was in good agreement with our expectations.

Within errors the measurements stayed stable for the monitored period of about two months. The slight downward trend of these and all subsequent tritium build-up measurements is probably caused by the annealing process. During the repeated heating of the dosimeters some of the tritium is lost due to diffusion processes within the LiF crystals. The individual dosimeter's crystal properties may also have an impact on this effect. Studies over longer periods of time need to be carried out to be able to confirm this hypothesis.

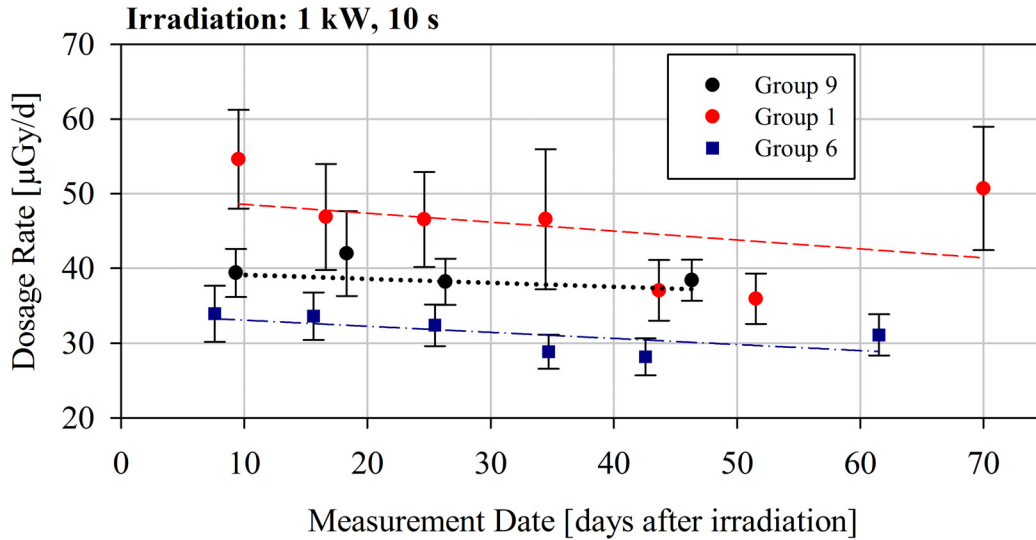


Figure 4.5: Dosimeter groups 1, 6 and 9 were irradiated at 1 kW for 10 s in three separate irradiation sessions. The subsequent tritium build-up was monitored over the course of several weeks. The measurements seem to be quite group dependent.

4.2.2 Correlation with reactor power

First of all it was important to check the reproducibility of a single tritium build up measurement. As several dosimeter groups had been irradiated separately at a reactor power of 1 kW for 10 seconds, secondary thermoluminescence measurements were carried out for these TLD-600 chips. The dosimeter groups 1, 6 and 9 were monitored for several weeks.

The results of these repeated tritium build-up read-outs are shown in figure 4.5. Again a moderate downward trend of the dosage rate is visible over time. As has been outlined previously this is probably due to tritium losses during the annealing process. The difference in the general trend of the groups may also have been caused by small variations of the dosimeter's position within the fast pneumatic transfer system inside the reactor during the separate irradiation sessions.

To check the tritium build-up's correlation with the neutron fluence irradiations at different reactor powers were necessary. As we outlined in section 4.1.2 the dosimeter groups 7 to 10 had been irradiated for 10 seconds at a reactor power of 0.01, 0.1, 1 and

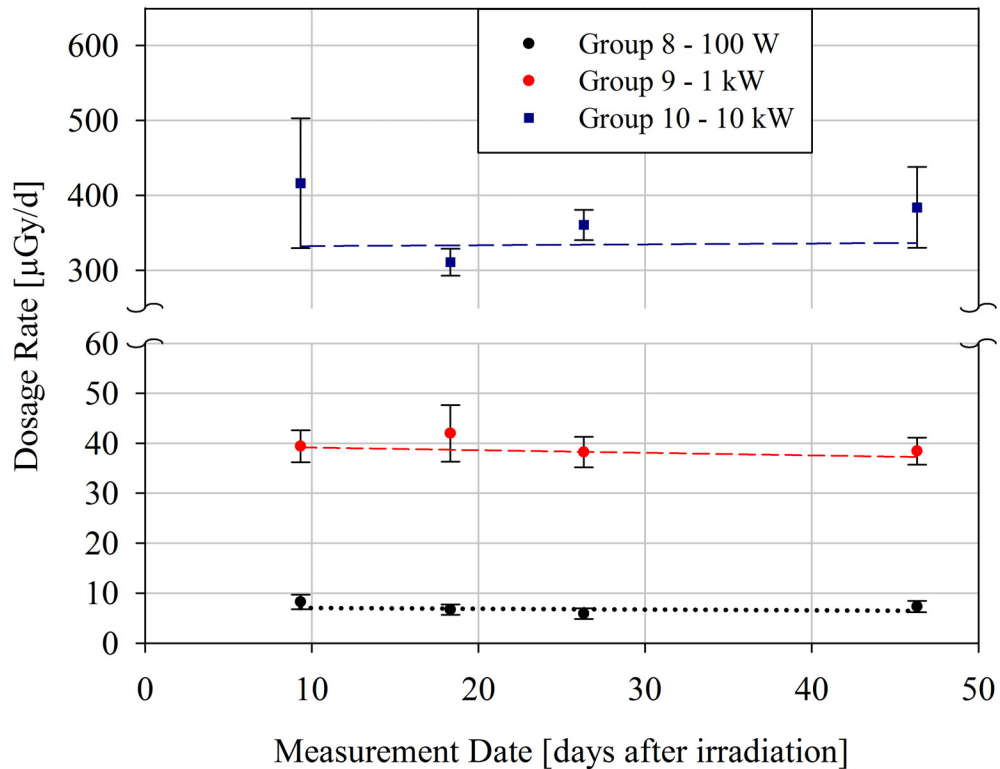


Figure 4.6: Dosimeter groups 8, 9 and 10 were irradiated at different reactor powers for 10 seconds each. The subsequent tritium build-up was monitored over the course of 6 weeks. Especially the results between 1 kW and 10 kW are in good agreement with the expected values.

10 kW respectively. After the measurement of the primary TL signal and the subsequent annealing these dosimeters were monitored for tritium build-up. According to the reactor powers we expected to find a factor of 10 between the respective energy dosage rates of the different dosimeter groups.

During the first secondary TL measurement no viable signal could be obtained from the TLD-600 chips of group 7 irradiated at 10 W reactor power. Thus, no subsequent measurements were made with this group. Groups 8, 9 and 10 were monitored weekly for 6 weeks and the results of their measurements are shown in figure 4.6.

Again it can be noted that the tritium build-up seems to only show a minor decrease

Reactor Power [kW]	Energy Dosage Rate [$\mu\text{Gy/d}$]	Error	Measured Factor	Expected Factor
0.1	7.0	19.7 %		
1	39.5	8.1 %	5.6	10
10	367.9	10.7 %	9.3	10
10	340.6	3.5 %		
50	1270.4	2.0 %	3.7	5
100	1639.5	1.7 %	1.3	2
250	3648.5	1.2 %	2.2	2.5

Table 4.2: Energy dosage rates corresponding to the tritium build-up of dosimeters irradiated at reactor powers of between 0.1 and 250 kW. Irradiation time: 10 seconds. Filters: only infrared. Error calculation: 0.1 - 10 kW: standard deviation + counting error; 10 - 250 kW: only counting error.

when exposed to repeated annealing. The average energy dosage rates that were found over the period of 4 weeks can be seen in the upper half of table 4.2. Just like with the net neutron TL signals obtained from the primary TL measurements the secondary measurements seem to also be in good agreement with the expected results in the range between 1 and 10 kW. Even though the tritium build-up could be resolved for the dosimeters irradiated at 100 W, the poor statistics of the photon count lead to a large error and sub-optimal results. In future longer dosage accumulation times should be observed for dosimeters irradiated at low reactor powers.

The lower half of table 4.2 shows the results for the measurement of the tritium build up of 4 TLD-600 chips irradiated for 10 seconds at 10, 50, 100 and 250 kW respectively. Only four dosimeters were available for this measurement as the rest was intended for immediate dissolution and subsequent measurement by LSC. Therefore, the errors shown in the second half of table 4.2 are solely based on the counting error as a standard deviation was not available. All measurements were also corrected for loss of sensitivity due to the high levels of radiation within the reactor in this range.

The measured factors do differ from the expected factors, however, the difference is not as significant as the deviation found for the net neutron signal of the primary TL measurement. The initial annealing procedure after irradiation could have had an impact on the amount of tritium preserved within the dosimeters. A comparison of the

LSC measurement of the tritium activity within annealed and non-annealed dosimeters is presented in section 4.3. In general, however, more measurements in this power range are necessary to further investigate this hypothesis.

A second set of tritium build-up measurements was done with dosimeter groups 2 to 5 that had previously been irradiated at the same reactor power range (see section 4.1.2). The results were, however, unusable for finding a correlation as some of the dosimeters had been exposed to neutron radiation beforehand. This had an unquantifiable impact on the amount of tritium inside the material.

4.3 LSC Measurement

By dissolving and measuring previously irradiated TLD-600 chips with a liquid scintillation counter we tried to obtain a quantitative value for the amount of tritium produced within the dosimeters. Through LSC measurements it was possible to determine the tritium activity corresponding to a certain irradiation time and reactor power. Using the neutron activation analysis method outlined in section 3.3.2 we were able to compare our results with predicted values. By studying both annealed and non-annealed dosimeters an estimate of the tritium loss during the heating process was obtained. At the end of this section we also compare the results of the tritium build-up to those of the LSC measurements.

The second set of TLD-600 dosimeters described in 3.2.1 consisted of 29 chips that were split into 5 groups and irradiated at different reactor powers for 10 seconds respectively. One dosimeter of each group was used for the determination of the primary and secondary TL signals outlined in the previous two sections. Two chips per group were directly dissolved after irradiation. Another pair of chips from each group was first annealed and then dissolved for measurement by LSC. Thus, for each of the reactor powers 10, 50, 100 and 250 kW the tritium activity of four dissolved TLD-600 dosimeters was measured. After the LSC measurements all acquired results were first corrected for their respective quench indicator. Next all values were multiplied by a factor of 50 to obtain the activity of the complete dosimeter rather than just the aliquot contained within the LSC sample.

Reactor Power [kW]	Chip 1 Activity [Bq/chip]	Chip 2 Activity [Bq/chip]	Average Activity [Bq/chip]	Std. Dev.	Measured Factor	Expected Factor	Predicted Activity [Bq/chip]	Percentage of Predicted Activity
10	97.7	90.6	94.2	3.7 %			615	14.7 %
50	421.9	477.7	449.8	6.2 %	4.78	5.00	3,074	15.5 %
100	625.9	675.7	650.8	3.8 %	1.45	2.00	6,148	11.0 %
250	1919.3	2015.3	1967.3	2.4 %	3.02	2.50	15,370	13.1 %

Table 4.3: Results from the LSC measurements of the H-3 activity of non-annealed TLD-600 chips irradiated at different reactor powers for 10 seconds respectively. On average only $13.6 \% \pm 1.7 \%$ of the predicted activity was actually measured.

Reactor Power [kW]	Chip 1 Activity [Bq/chip]	Chip 2 Activity [Bq/chip]	Average Activity [Bq/chip]	Std. Dev.	Measured Factor	Expected Factor	Predicted Activity [Bq/chip]	Percentage of Predicted Activity
10	73.5	72.7	73.1	0.5 %			615	11.8 %
50	265.6	279.2	272.4	2.5 %	3.73	5.00	3,074	9.1 %
100	358.8	340.5	349.6	2.6 %	1.28	2.00	6,148	5.5 %
250	783.1	837.1	810.1	3.3 %	2.32	2.50	15,370	5.4 %

Table 4.4: Results from the LSC measurements of the H-3 activity of annealed TLD-600 chips irradiated at different reactor powers for 10 seconds respectively. Only a low percentage of the predicted activity was actually measured.

4.3.1 Comparison with predicted tritium activity

The results for the tritium activities of non-annealed TLD-600 chips are shown in table 4.3 and those for the annealed dosimeters can be found in table 4.4. Dosimeters irradiated at the same reactor power were dissolved independently in order to check the reproducibility of the chemical procedure. Looking at the standard deviations that were found it seems that the results are reproducible within reasonable uncertainties.

First we compared the results for the tritium activity within the dosimeters with the values predicted (calculated) by neutron activation (see section 3.3.2). All the activities measured by LSC are significantly lower than expected. On average only $13.6 \% \pm 1.7 \%$ of the predicted activity for the non-annealed dosimeters was actually measured. For the reasons outlined in the next paragraph the percentage is even lower for the annealed dosimeters. However, neglecting the annealed dosimeters the percentage does seem to stay rather constant over different reactor powers and chip groups. Therefore either the

same fraction of tritium was lost for all dosimeters during the chemical dissolution or the neutron flux used for the calculation of the predicted value was too high. All the results of the dissolution procedure have so far, however, been reproducible within the uncertainties expected from such a chemical process. Hence, the assumption that the wrong neutron flux was used for the calculations cannot be omitted. In addition it was uncertain whether the recent re-configuration of the TRIGA Mark-II's reactor core may have lead to a change in the neutron flux around the fast pneumatic transfer system used for measurements. Thus, the actual neutron flux within the fast pneumatic transfer system needs to be verified by an independent measurement before a definite answer to this problem can be found.

4.3.2 Comparison between non-annealed and annealed dosimeters

Next the factors measured between the tritium activities of dosimeters irradiated at different reactor powers were compared with the ones expected (Tables 4.3 and 4.4). In general the factors of the non-annealed TLD-600 chips are closer to the expected values than those of the annealed dosimeters. This is also apparent when plotting the measured tritium activities against the reactor power (see figure 4.7). The linear estimate for the correlation with the non-annealed TLD-600 chips shows a very promising R^2 value. Thus it is possible to approximate the reactor power from this correlation if the tritium activity has been measured and the irradiation time is known.

A quadratic function was fit to the data points of the annealed TL dosimeters. As the

Reactor Power [kW]	Aver. Activity non-annealed [Bq/chip]	Aver. Activity annealed [Bq/chip]	Loss through annealing
10	94.2	73.1	19.8%
50	449.8	272.4	41.8%
100	650.8	349.6	49.9%
250	1967.3	810.1	58.6%

Table 4.5: Comparison between the average tritium activity measured for non-annealed and annealed TLD-600 chips irradiated at different reactor powers. The loss caused by the annealing process seems to increase with reactor power.

tritium activity should be zero at zero reactor power the curve was fit in such a way that the function would go through the origin. The deviation of the annealed dosimeters is probably caused by tritium lost during the annealing procedure. It seems that during the heating process some of the tritium is able to diffuse out of the dosimeter crystal and therefore a reduced activity is observed in the LSC measurements. This loss appears to, however, only occur during the first annealing procedure that is performed. This assumption is supported by the fact that the tritium build-up stayed stable over months even though weekly annealing procedures were done (see previous section). Table 4.5 shows a direct comparison of the tritium activity results for annealed and non-annealed chips. The tritium loss seems to increase with reactor power - this fact can also be observed in figure 4.8. This plot compares the functions that were fitted to the data points

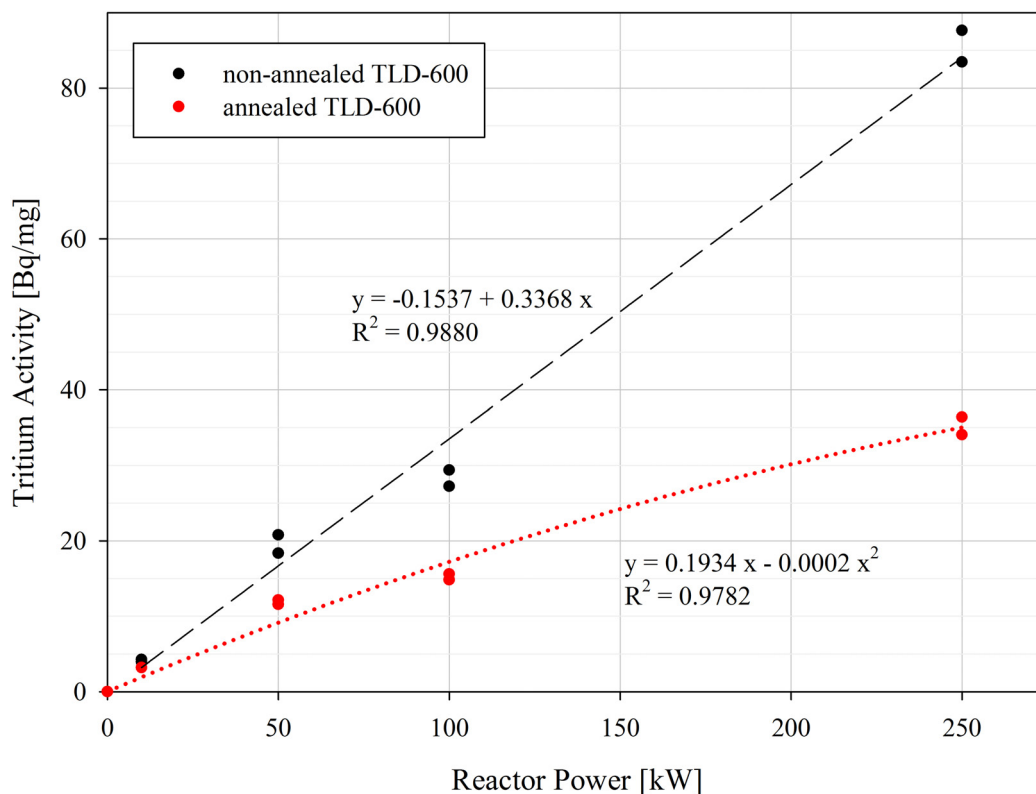


Figure 4.7: Correlation between the tritium activity measured in non-annealed and annealed TLD-600 chips and the corresponding reactor power. A linear approximation was used for the annealed dosimeters. A quadratic function going through the origin was fitted to the data points for the annealed TL chips.

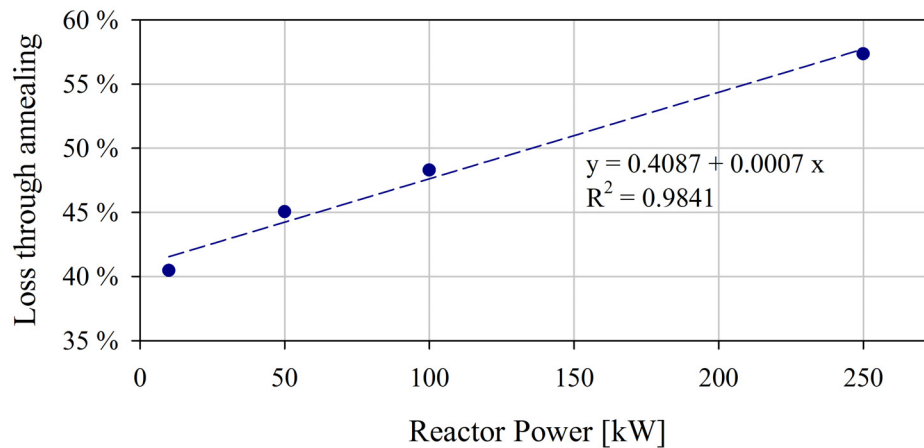


Figure 4.8: The difference between the functions fitted to the data points for non-annealed and annealed TLD-600 chips in figure 4.7. A steady increase with reactor power is visible in the loss of tritium activity through annealing.

in figure 4.7. It shows the percentage that is lost during the annealing process when compared with non-annealed chips. A steady increase of the loss with reactor power can be observed. It is unclear what would cause this effect - therefore more measurement series are necessary to confirm this phenomenon and investigate it further.

4.3.3 Correlation between the LSC and tritium build-up measurements

Table 4.6 gives an overview of the factors found between the measurements for different reactor powers. The LSC measurements of non-annealed TL dosimeters show the best agreement with the expected factors. A remarkable similarity was found between the factors of the LSC measurement of annealed dosimeters and the tritium build-up. This makes sense because an annealing procedure is also performed prior to the tritium build-up measurements. These measurements should however be reproduced with more data points to confirm this good correlation.

Using these results a correlation between the dosage read-out from the secondary TL signal and the tritium activity per chip can be found (see figure 4.9). As the tritium activity is also directly correlated to the reactor power (figure 4.7) estimates between all

Reactor Power [kW]	FACTORS			
	Expected	LSC non-annealed	LSC annealed	Tritium Build-up
10				
50	5.00	4.75	3.73	3.73
100	2.00	1.45	1.28	1.29
250	2.50	3.02	2.32	2.23

Table 4.6: An overview of the factors between the measurement results of dosimeters irradiated at different reactor powers. The non-annealed LSC measurement has the closest correlation with the expected values. An astonishingly good agreement was found between the results from annealed dosimeters measured by LSC and tritium build-up measurements.

three parameters can be made. These estimates are, however, only of a relative kind and cannot be linked to an absolute number for the neutron flux at this time as this parameter still needs to be confirmed.

As no reliable results were obtained from the primary TL measurements no meaningful correlation between the net neutron TL signal and the above parameters was found.

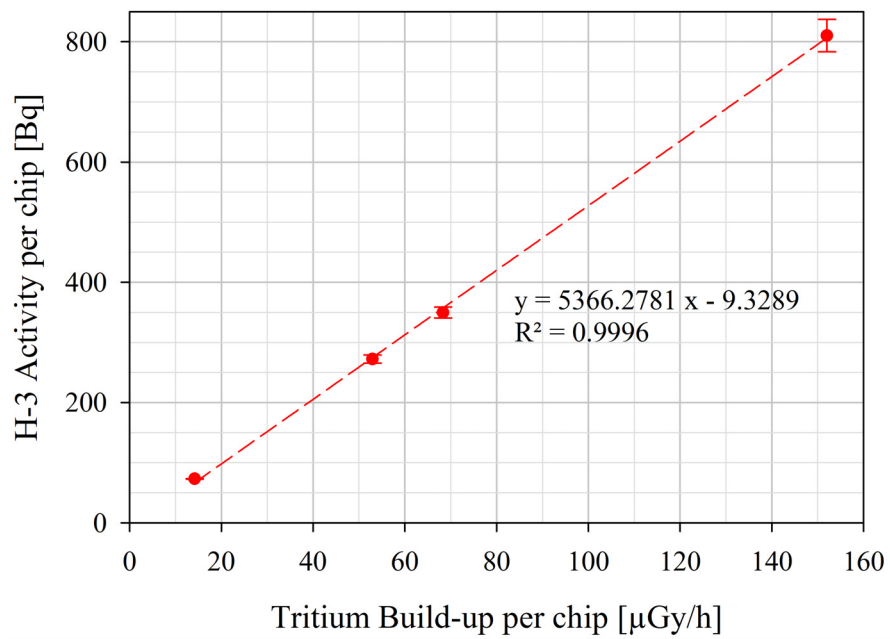
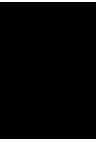


Figure 4.9: Correlation between the tritium activity measured by LSC and the tritium build-up obtained from secondary TL measurements. A linear approximation was fitted to the data points. A surprisingly good correlation was found.



Summary and Future Outlook

The aim of this study was to investigate the use of LiF(Mg,Ti) dosimeters for high-dosage neutron measurements in the mixed radiation field within the TRIGA Mark-II research reactor at the Institute of Atomic and Subatomic Physics, Vienna. For this purpose both TLD-600 (^6LiF) and TLD-700(^7LiF) chips were irradiated within the reactor at different powers and for different irradiation times. In subsequent thermoluminescence measurements first the primary TL signal acquired directly after irradiation was studied. Next the secondary TL signal (tritium build-up) caused by self-irradiation of the chips through tritium produced within the TLD-600 dosimeters during irradiation ($^6\text{Li} (n,\alpha) ^3\text{H}$) was measured in weekly intervals. Finally some of the TLD-600 chips were dissolved and measured in a liquid scintillation analyser. By applying all three of these techniques to the high intensities found within the reactor we aimed to test and find the limits of the respective methods. In addition we aimed to find a correlation between the results of all three techniques.

The influence of several factors had to be accounted for to obtain usable results from thermoluminescence dosimetry. To this end the supra-linear behaviour and saturation effect of both TLD-600 and TLD-700 chips were re-investigated for the particular charge used in this study. In addition repeated reference measurements were done to account for sensitivity loss caused by the high energy dosages inside the reactor. Furthermore we had to find new filter combinations to be able to measure the high light intensities from the TL dosimeters. In the next paragraphs we give a summary of the

results and conclusions from both the preparatory work and the actual implementation of the three measurement techniques.

1. **Supra-linearity and saturation:** Normally both TLD-600 and TLD-700 dosimeters show the same non-linearity at high energy dosages. Due to an anomaly in the glow-curve structure of the TLD-600 dosimeter charge used for this study this effect had to be re-investigated. A comparison of the behaviour of both types of LiF(Mg,Ti) chips showed that the TLD-600 dosimeters were more strongly supra-linear and saturated at higher energy dosages. This fact had to be accounted for in all subsequent TL measurements. In general it seemed that as soon as the neutron flux reached a limit (at around 100 W, 10 s) where the net neutron TL signal could actually be resolved above the reactor background non-linearity effects became significant in the TL measurement as well. Above neutron fluences of around $8 \cdot 10^{12} \text{ n cm}^{-2}\text{s}^{-1}$ (100 kW, 10 s within the fast pneumatic transfer system) primary TL measurements did no longer obtain viable results due to saturation.
2. **Sensitivity loss:** Repeated reference measurements between irradiations showed that especially TLD-600 dosimeters suffered substantial sensitivity loss after exposure to high neutron fluences. The energy dosage accumulated over a dosimeter's lifetime has a direct impact on its sensitivity. The results from continuous monitoring demonstrated the importance of knowing a dosimeter's history. From a neutron fluence of around $8 \cdot 10^9 \text{ n cm}^{-2}\text{s}^{-1}$ upwards dosimeters get damaged and a definite loss of sensitivity can be observed.
3. **Filter attenuation factor:** Several new filter combinations were tested for the measurement of the strong light intensities from dosimeters irradiated with high dosages. Even though new filter attenuation factors were determined this way they had no direct correlation with the strength of the filters that were used. We found that the filter strength was affected by diffuse light reflected off the aluminium wall of the filter housing. While this effect seems to be statistically constant and reproducible it still has an adverse impact on the standard deviation of the thermoluminescence measurements. Thus, the configuration of the filter housing needs to be improved to minimise this systematic error in future measurements.

4. **Primary TL Measurement:** The initial(primary) net neutron TL signal measured directly after irradiation was tested for both its correlation with irradiation time and reactor power/neutron fluence.

A good correlation with time was found for dosimeters irradiated at 1 kW for 10 and 30 seconds respectively. This result does, however, need to be reproduced with more dosimeters and at different reactor powers.

The net neutron TL signal's correlation with reactor power was tested between 10 W and 250 kW. Good results were only obtained for power ranges between 1kW and 10 kW. At lower reactor powers the counting statistics were poor as the neutron signal could barely be resolved above the gamma background inside the reactor. At higher reactor powers supra-linearity and saturation effects became significant and the dosimeter chips turned green as they were severely damaged by the absorbed radiation. At 250 kW the TL signal had saturated completely and was found to be even lower than that of 100 kW. Therefore the primary TL signal seems to generally be a very unreliable source for the measurement of the mixed radiation field within the reactor. Reasonable results can only be acquired between 1 and 10 kW. Even in this range a direct correlation between the neutron flux and the net neutron TL signal was, however, impossible as no neutron calibration was available for the used dosimeters. In addition it was also very difficult to estimate what impact the anomalous glow curve structure of the TLD-600 chips had on these measurements. In the future it would, thus, be prudent to repeat the measurements using a higher number of TL dosimeters from a different charge with a well defined glow curve structure and a known neutron calibration.

5. **Secondary TL Measurement(Tritium Build-up):** The tritium build-up was monitored for different dosimeter groups over the course of several weeks. Here a good correlation was also found between the TL signal and the irradiation time. Again the measurements need to be reproduced with a higher number of dosimeters to confirm this result in the future.

In general the tritium build-up stayed mostly stable even after repeated annealing procedures - only a slight downward trend over time could be observed for all groups.

A comparison of the tritium build-up of dosimeter groups irradiated at different reactor powers showed results similar to the ones for the primary TL measurement. Good correlations could only be obtained in the range of 1 to 10 kW. Due to poor statistics and weak signals the measurements below this range showed sub-optimal results. At higher reactor powers the tritium build-up also showed a deviation from the expected results, the correlation was, however, much better than that of the net neutron TL signal measured directly after irradiation. We assumed that the annealing procedure after the primary TL measurement had an impact on the tritium preserved within the dosimeters. This was confirmed by the LSC measurements of dissolved dosimeter chips. In general more measurements of the tritium build-up at high reactor powers are necessary to confirm the results as we only had a limited number of TLD-600 chips available.

6. **LSC Measurement:** Both non-annealed and annealed dosimeters that had been irradiated at different reactor powers were dissolved for the purpose of LSC. A comparison of the tritium activities within the non-annealed dosimeters with the predicted values showed that only about 13 % of the calculated activity was actually measured. Therefore either the same fraction of tritium was lost during the dissolution of all dosimeters or the neutron flux used for the calculation of the predicted values was too high. As the LSC results seem to be reproducible the assumption that the wrong neutron flux was used for the calculations cannot be omitted. In addition it was uncertain whether the recent re-configuration of the TRIGA Mark-II's reactor core may have lead to a change in the neutron flux around the fast pneumatic transfer system used for measurements. The actual neutron flux within the fast pneumatic transfer system needs to be verified in future measurements to find an answer to this problem.

A comparison between the results for non-annealed and annealed dosimeters showed that a certain amount of tritium is lost during the annealing procedure. This loss seems to increase with reactor power. Why this effect would occur is unclear. Therefore more measurement series are necessary to confirm this phenomenon and investigate it further.

The tritium activity within the non-annealed dosimeters showed the best correla-

tion with the reactor power. The annealed dosimeters' correlation was not as strong due to the tritium lost during annealing. They did, however, show a remarkable correlation with the tritium build-up, which makes sense as an annealing procedure was performed prior to both measurements. In future measurements more dissolved dosimeters are necessary to confirm this strong correlation. A correlation of the LSC measurements with the primary TL signal was not possible as no meaningful results were obtained for the net neutron TL signal at high reactor powers.

In summary it can be stated that in the future

- the impact of the current filter configuration and the possible systematic error connected to it need to be investigated and improved accordingly,
- a charge of TLD-600 dosimeters without an anomalous glow-curve structure and a known neutron calibration needs to be used to be able to accurately determine the actual neutron flux within the fast pneumatic transfer system
- A higher number of TL dosimeters is necessary to be able to reproduce and confirm the results.

In this way a direct and quantitative correlation between the different methods of neutron detection and the neutron fluence within the reactor may be found.

Bibliography

- [1] General Atomic. About TRIGA. Link: <http://www.ga.com/about-triga>, July 2014.
- [2] Thomas Berger. *Dose Assessment in Mixed Radiation Fields*. Dissertation, Atominstitut der Technischen Universität Wien, May 2003.
- [3] Thomas Berger, Michael Hajek, Mamfred Fugger, and Norbert Vana. Efficiency-corrected dose verification with thermoluminescence dosimeters in heavy-ion beams. *Radiation Protection Dosimetry*, 120(1-4):361–364, 2006.
- [4] R. Boyle. *Register of the Royal Society*, 1663.
- [5] B. Burgkhardt and E. Piesch. Estimation of the build-up of zero dose reading in ^6LiF thermoluminescence dosimeters due to neutron produced tritium. *Radiation Protection Dosimetry*, 2:105–107, 1982.
- [6] N. J. Carron. *An Introduction to the Passage of Energetic Particles through Matter*. Taylor & Francis, 2007.
- [7] R. Dierckx. Direct tritium production measurement in irradiated lithium. *Nuclear Instruments and Methods*, 107:397–398, 1973.
- [8] Freeman Dyson. *Disturbing the Universe*. Basic Books, 1979.
- [9] G. F. J. Garlick and M. H. F. Wilkins. Short period phosphorescence and electron traps. *Proceedings of the Royal Society of London. Series A. Mathematical and Physical Sciences*, 184(999):408–433, 1945.
- [10] Charles Kittel. *Introduction to Solid State Physics*. John Wiley & Sons, 8th edition, 2004.

- [11] Marie Skłodowska Curie. *Radio-active Substances*. PhD thesis, Faculté des Sciences de Paris, 1903.
- [12] Marko Mayr. Bestimmung der Messdynamik des Thermolumineszenzdosimeter-Systems TLD-700 LiF:Mg,Ti mit der Messanlage TL-Dat III. Bachelor's thesis, Vienna University of Technology, 2014.
- [13] S.W.S. McKeever. *Thermoluminescence of Solids*. Cambridge Solid State Science Series. Cambridge University Press, 1988.
- [14] John W. McKeever and Michael Schwenk. Reactor flux measurements using thermoluminescent dosimetry. *Nuclear Technology*, 31(2):257–263, November 1976.
- [15] Brookhaven National Laboratory National Nuclear Data Center. Nudat 2.6. Link: <http://www.nndc.bnl.gov/nudat2/>, September 2014.
- [16] The Isotopes Project Home Page. Neutron cross sections from neutron resonance parameters and thermal cross sections. Link: <http://ie.lbl.gov/ngdata/sig.htm>, September 2014.
- [17] W. Pohorecki, P. Bilski, T. Kuc, and B. Ostachowicz. Thermoluminescent method for the measurements of tritium production in neutronics experiments. *Radiation Measurements*, 45:736–738, 2010. Proceedings of the 7th European Conference on Luminescent Detectors and Transformers of Ionizing Radiation (LUMDETR 2009).
- [18] M. Puchalska, P. Bilski, and P. Olko. Thermoluminescence glow peak parameters for LiF:Mg,Ti with modified activator concentration. *Radiation Measurements*, 42(4–5):601 – 604, 2007. Proceedings of the 6th European Conference on Luminescent Detectors and Transformers of Ionizing Radiation (LUMDETR 2006).
- [19] J. T. Randall and M. H. F. Wilkins. Phosphorescence and electron traps. i. the study of trap distributions. *Proceedings of the Royal Society of London. Series A. Mathematical and Physical Sciences*, 184(999):365–389, 1945.
- [20] J. T. Randall and M. H. F. Wilkins. Phosphorescence and electron traps. ii. the interpretation of long-period phosphorescence. *Proceedings of the Royal Society of London. Series A. Mathematical and Physical Sciences*, 184(999):390–407, 1945.

- [21] P. Rinard. *Passive Nondestructive Assay of Nuclear Materials*, chapter 12 - Neutron Interactions with Matter, pages 357–377. U.S. Nuclear Regulatory Commission, March 1991.
- [22] A. Romanyukha, R. Minniti, M. Moscovitch, A.K. Thompson, F. Trompier, R. Colle, A. Sucheta, S.P. Voss, and L.A. Benevides. Effect of neutron irradiation on dosimetric properties of TLD-600H (^6LiF : Mg, Cu, P). *Radiation Measurements*, 46(12):1426–1431, 2011.
- [23] W. Schöner, N. Vana, and M. Fugger. The LET Dependence of LiF:Mg,Ti Dosimeters and its Application for LET Measurements in Mixed Radiation Fields. *Radiation Protection Dosimetry*, 85(1-4):263–266, 1999.
- [24] Johannes H. Sterba. Evaluierung eines Neutronenaktivierungsanalysators. Master's thesis, Institute of Atomic and Subatomic Physics, Vienna University of Technology, May 2004.
- [25] F. Torkzadeh and F. Manouchehri. Thermal neutron fluence measurement in a research reactor using thermoluminescence dosimeter TLD-600. *Journal of Radiological Protection*, 26(1):97, 2006.
- [26] J. Trowbridge and J. E. Burbank. The source of the x-rays. *American Journal of Science*, 5:129–134, 1898.
- [27] N. Vana, R. Erlach, M. Fugger, W. Gratzl, and I. Reichhalter. A computerised {TL} read out system for dating and phototransfer measurements. *International Journal of Radiation Applications and Instrumentation. Part D. Nuclear Tracks and Radiation Measurements*, 14(1–2):181 – 184, 1988.
- [28] Atominstitut Wien. Webpage. Link: <http://ati.tuwien.ac.at/reaktor/>, August 2014.

A.1 Technical Data - TRIGA Mark-II, ATI Vienna

All data taken from:

http://ati.tuwien.ac.at/reactor/technical_data/EN/

REACTOR CORE	
fuel-moderator material	8 wt% uranium, 91 wt% zirconium, 1 wt% hydrogen
uranium enrichment	20% Uran-235
fuel element dimensions	3.75 cm in diameter 72.24 cm in length
cladding	0.76 mm aluminum or 0.51 mm steel
active core volume	max. 49.5 cm diameter, 35.56 cm high
core loading	3 kg of uranium-235

REFLECTOR	
material	graphite with aluminum cladding
radial thickness	30.5 cm
top and bottom thickness	10.2 cm

CONSTRUCTION

reactor shielding construction	heavy and standard concrete 6.55 m high, 6.19 m wide, 8.76 m long
reactor tank	1.98 m in diameter 6.40 m in depth

SHIELDING

radial:	30.5 cm of graphite 45.7 cm of water and at least 206 cm of heavy concrete
vertical:	above the core 4.90 m of water and 10.2 cm graphite underneath the core 61.0 cm water, 10.2 cm graphite and at least 91 cm standard concrete

IRRADIATION DEVICES

No.	Type
5	reflector irradiation tubes
1	central irradiation tube
1	pneumatic transfer system (transfer time 3 s)
1	fast pneumatic transfer system (transfer time 20 ms)
4	neutron beam holes
1	thermal column
1	neutron radiography facility

CONTROL SYSTEM

-	Two boron carbide control rods with electric motor and rack and pinion drive
-	One boron carbide pulse rod with compressed air drive (5 bars)
-	Maximum reactivity insertion rate - time rate of change (excluding pulse operation): 0.04% $\delta k/k$ per second
-	Total rod worth about 4.8% $\delta k/k$.

CHARACTERISTICS IN CONTINUOUS OPERATION

Thermal power output:	250 kW
Fuel element cooling:	natural convection of the tank water below 100 kW,
tank water cooling:	pump circulation cooling above 100 kW heat exchanger
thermal flux:	central irradiation tube: $1 \times 10^{13} \text{ cm}^{-2} \text{ s}^{-1}$ in the irradiation tubes: $1.7 \times 10^{12} \text{ cm}^{-2} \text{ s}^{-1}$
prompt temperature coefficient:	$-1.2 \times 10^{-4} \text{ } \delta k / k ^\circ \text{C}$
mean prompt neutron lifetime:	$6.0 \times 10^{-5} \text{ s}$

CHARACTERISTICS DURING PULSED OPERATION

peak power	250 MW
prompt pulse energy yield	10 MW s
prompt pulse lifetime	40 ms
total energy yield	12 MW s
minimal period	10 ms
maximum reactivity insertion	1.6% $\delta k / k = 2\%$
maximum repetition frequency	12/h
number of fissions during a pulse	3×10^{17}
maximum fuel temperature:	during the pulse 240 °C 9 seconds after the pulse 360 °C

BRIEF STATISTICAL DATA

average during the last 5 years (2014)

power produced (MWh)	300
irradiation experiments	200
beam hole experiments	15
number of reactor pulses	10
number of visitors	2500

A.2 TLD Calibration Data

A.2.1 TLD Set No. 1

Table A.1: Initial calibration results for peak 5 of the first set of TLD-600 dosimeters, filter: 2 x infrared, source: Cs-137 (44h, 1.5 m, 17.23 mGy), date: 19/03/2014

Group	No.	File Name	Peak 5 (220°C) [cts]	Dosage [mGy]	Calibration Factor [cts/mGy]
1	1	Nt(ATI-Kg1-TLD600_M_rest-32.TLG)	10824	17.23	628.21
	2	Nt(ATI-Kg1-TLD600_M_rest-19.TLG)	10982	17.23	637.38
	3	Nt(ATI-Kg1-TLD600_M_rest-13.TLG)	11042	17.23	640.86
2	1	Nt(ATI-Kg1-TLD600_M_rest-16.TLG)	11146	17.23	646.89
	2	Nt(ATI-Kg1-TLD600_M_rest-37.TLG)	11221	17.23	651.25
	3	Nt(ATI-Kg1-TLD600_M_rest-17.TLG)	11260	17.23	653.51
3	1	Nt(ATI-Kg1-TLD600_M_rest-35.TLG)	11310	17.23	656.41
	2	Nt(ATI-Kg1-TLD600_M_rest-07.TLG)	11367	17.23	659.72
	3	Nt(ATI-Kg1-TLD600_M_rest-18.TLG)	11394	17.23	661.29
4	1	Nt(ATI-Kg1-TLD600_M_rest-27.TLG)	11402	17.23	661.75
	2	Nt(ATI-Kg1-TLD600_M_rest-36.TLG)	11406	17.23	661.98
	3	Nt(ATI-Kg1-TLD600_M_rest-08.TLG)	11409	17.23	662.16
5	1	Nt(ATI-Kg1-TLD600_M_rest-01.TLG)	11433	17.23	663.55
	2	Nt(ATI-Kg1-TLD600_M_rest-14.TLG)	11485	17.23	666.57
	3	Nt(ATI-Kg1-TLD600_M_rest-10.TLG)	11498	17.23	667.32
6	1	Nt(ATI-Kg1-TLD600_M_rest-05.TLG)	11608	17.23	673.71
	2	Nt(ATI-Kg1-TLD600_M_rest-06.TLG)	11610	17.23	673.82
	3	Nt(ATI-Kg1-TLD600_M_rest-31.TLG)	11612	17.23	673.94
7	1	Nt(ATI-Kg1-TLD600_M_rest-24.TLG)	11624	17.23	674.64
	2	Nt(ATI-Kg1-TLD600_M_rest-33.TLG)	11647	17.23	675.97
	3	Nt(ATI-Kg1-TLD600_M_rest-28.TLG)	11656	17.23	676.49
8	1	Nt(ATI-Kg1-TLD600_M_rest-25.TLG)	11684	17.23	678.12
	2	Nt(ATI-Kg1-TLD600_M_rest-02.TLG)	11710	17.23	679.63
	3	Nt(ATI-Kg1-TLD600_M_rest-15.TLG)	11725	17.23	680.50
9	1	Nt(ATI-Kg1-TLD600_M_rest-03.TLG)	11781	17.23	683.75
	2	Nt(ATI-Kg1-TLD600_M_rest-26.TLG)	11784	17.23	683.92
	3	Nt(ATI-Kg1-TLD600_M_rest-12.TLG)	11785	17.23	683.98
10	1	Nt(ATI-Kg1-TLD600_M_rest-34.TLG)	11807	17.23	685.26
	2	Nt(ATI-Kg1-TLD600_M_rest-21.TLG)	11849	17.23	687.70
	3	Nt(ATI-Kg1-TLD600_M_rest-11.TLG)	11932	17.23	692.51
11	1	Nt(ATI-Kg1-TLD600_M_rest-04.TLG)	11954	17.23	693.79
	2	Nt(ATI-Kg1-TLD600_M_rest-22.TLG)	11977	17.23	695.12
	3	Nt(ATI-Kg1-TLD600_M_rest-20.TLG)	11985	17.23	695.59
12	1	Nt(ATI-Kg1-TLD600_M_rest-23.TLG)	11986	17.23	695.65
	2	Nt(ATI-Kg1-TLD600_M_rest-09.TLG)	12086	17.23	701.45
	3	Nt(ATI-Kg1-TLD600_M_rest-30.TLG)	12167	17.23	706.15
rest		Nt(ATI-Kg1-TLD600_M_rest-29.TLG)	12983	17.23	753.51

Table A.2: Initial calibration results for peak 5 of the first set of TLD-700 dosimeters, filter: 2 x infrared, source: Cs-137 (44h, 1.5 m, 17.23 mGy), date: 19/03/2014

Group	No.	File Name	Peak 5 (220°C) [cts]	Dosage [mGy]	Calibration Factor [cts/mGy]
1	1	Nt(ATI-Kg1-TLD700_M_rest-09.TLG)	19653	17.23	1140.63
	2	Nt(ATI-Kg1-TLD700_M_rest-05.TLG)	20320	17.23	1179.34
	3	Nt(ATI-Kg1-TLD700_M_rest-12.TLG)	20711	17.23	1202.03
2	1	Nt(ATI-Kg1-TLD700_M_rest-17.TLG)	20764	17.23	1205.11
	2	Nt(ATI-Kg1-TLD700_M_rest-31.TLG)	20771	17.23	1205.51
	3	Nt(ATI-Kg1-TLD700_M_rest-06.TLG)	20885	17.23	1212.13
3	1	Nt(ATI-Kg1-TLD700_M_rest-27.TLG)	20949	17.23	1215.84
	2	Nt(ATI-Kg1-TLD700_M_rest-16.TLG)	21029	17.23	1220.49
	3	Nt(ATI-Kg1-TLD700_M_rest-20.TLG)	21078	17.23	1223.33
4	1	Nt(ATI-Kg1-TLD700_M_rest-32.TLG)	21138	17.23	1226.81
	2	Nt(ATI-Kg1-TLD700_M_rest-29.TLG)	21150	17.23	1227.51
	3	Nt(ATI-Kg1-TLD700_M_rest-24.TLG)	21202	17.23	1230.53
5	1	Nt(ATI-Kg1-TLD700_M_rest-28.TLG)	21491	17.23	1247.30
	2	Nt(ATI-Kg1-TLD700_M_rest-33.TLG)	21499	17.23	1247.77
	3	Nt(ATI-Kg1-TLD700_M_rest-21.TLG)	21522	17.23	1249.10
6	1	Nt(ATI-Kg1-TLD700_M_rest-07.TLG)	21602	17.23	1253.74
	2	Nt(ATI-Kg1-TLD700_M_rest-02.TLG)	21707	17.23	1259.84
	3	Nt(ATI-Kg1-TLD700_M_rest-35.TLG)	21721	17.23	1260.65
7	1	Nt(ATI-Kg1-TLD700_M_rest-34.TLG)	21722	17.23	1260.71
	2	Nt(ATI-Kg1-TLD700_M_rest-22.TLG)	21726	17.23	1260.94
	3	Nt(ATI-Kg1-TLD700_M_rest-10.TLG)	21764	17.23	1263.15
8	1	Nt(ATI-Kg1-TLD700_M_rest-23.TLG)	21835	17.23	1267.27
	2	Nt(ATI-Kg1-TLD700_M_rest-19.TLG)	21855	17.23	1268.43
	3	Nt(ATI-Kg1-TLD700_M_rest-30.TLG)	21887	17.23	1270.28
9	1	Nt(ATI-Kg1-TLD700_M_rest-18.TLG)	21913	17.23	1271.79
	2	Nt(ATI-Kg1-TLD700_M_rest-15.TLG)	21928	17.23	1272.66
	3	Nt(ATI-Kg1-TLD700_M_rest-13.TLG)	21952	17.23	1274.06
10	1	Nt(ATI-Kg1-TLD700_M_rest-11.TLG)	22003	17.23	1277.02
	2	Nt(ATI-Kg1-TLD700_M_rest-04.TLG)	22037	17.23	1278.99
	3	Nt(ATI-Kg1-TLD700_M_rest-26.TLG)	22053	17.23	1279.92
11	1	Nt(ATI-Kg1-TLD700_M_rest-25.TLG)	22065	17.23	1280.62
	2	Nt(ATI-Kg1-TLD700_M_rest-08.TLG)	22170	17.23	1286.71
	3	Nt(ATI-Kg1-TLD700_M_rest-03.TLG)	22205	17.23	1288.74
12	1	Nt(ATI-Kg1-TLD700_M_rest-14.TLG)	22690	17.23	1316.89
	2	Nt(ATI-Kg1-TLD700_M_rest-01.TLG)	23006	17.23	1335.23

A.2.2 TLD Set No. 2

Table A.3: Initial calibration results for peak 5 of the second set of TLD-700 dosimeters, filter: 2 x infrared, source: Cs-137 (69h, 1.5 m, 26.86 mGy), date: 18/06/2014

Chip No.	File Name	Peak 5 (220°C) [cts]	Dosage [mGy]	Calibration Factor [cts/mGy]
620	Nt(ATI-gk1-TLD700-620.TLG)	28,470.00	26.86	1,059.94
624	Nt(ATI-gk1-TLD700-624.TLG)	29,453.00	26.86	1,096.54
626	Nt(ATI-gk1-TLD700-626.TLG)	31,498.00	26.86	1,172.67
627	Nt(ATI-gk1-TLD700-627.TLG)	28,672.00	26.86	1,067.46
632	Nt(ATI-gk1-TLD700-632.TLG)	28,294.00	26.86	1,053.39
639	Nt(ATI-gk1-TLD700-639.TLG)	28,218.00	26.86	1,050.56
641	Nt(ATI-gk1-TLD700-641.TLG)	28,416.00	26.86	1,057.93
646	Nt(ATI-gk1-TLD700-646.TLG)	26,856.00	26.86	999.85
649	Nt(ATI-gk1-TLD700-649.TLG)	28,640.00	26.86	1,066.27
657	Nt(ATI-gk1-TLD700-657.TLG)	29,051.00	26.86	1,081.57
658	Nt(ATI-gk1-TLD700-658.TLG)	30,050.00	26.86	1,118.76
659	Nt(ATI-gk1-TLD700-659.TLG)	30,114.00	26.86	1,121.15
660	Nt(ATI-gk1-TLD700-660.TLG)	29,552.00	26.86	1,100.22
667	Nt(ATI-gk1-TLD700-667.TLG)	28,771.00	26.86	1,071.15
670	Nt(ATI-gk1-TLD700-670.TLG)	29,715.00	26.86	1,106.29
672	Nt(ATI-gk1-TLD700-672.TLG)	28,975.00	26.86	1,078.74
673	Nt(ATI-gk1-TLD700-673.TLG)	29,111.00	26.86	1,083.80
674	Nt(ATI-gk1-TLD700-674.TLG)	29,137.00	26.86	1,084.77
676	Nt(ATI-gk1-TLD700-676.TLG)	25,537.00	26.86	950.74